PHYSIK-DEPARTMENT

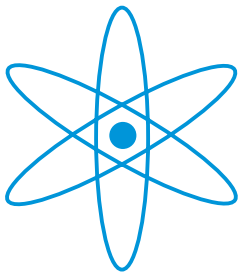

Towards Atom-Photon Entanglement:

State Selective Detection of a Single Atom

Diplomarbeit von
Johannes Vrana

angefertigt unter der Anleitung von
Prof. Dr. Harald Weinfurter
Dr. Martin S. Brandt

TECHNISCHE UNIVERSITÄT
MÜNCHEN

Content

Bestmögliche Kenntnis eines Ganzen schließt nicht bestmögliche Kenntnis seiner Teile ein – und darauf beruht doch der ganze Spuk.

(E. Schrödinger)

Best possible knowledge of a whole does not include best possible knowledge of its parts – and that is what keeps coming back to haunt us.

(Translation by: J.D. Trimmer)

1 Introduction

Quantum mechanics is essential for the understanding of many phenomenons in nature – especially in the atomic and subatomic region. But even for macroscopic objects it has to be assumed that they are made of atoms, ions and electrons. Only by using this assumption it is possible to describe all objects exactly and completely. Therefore quantum mechanics can be seen as the basis for the description of all phenomenons in nature. During the development of this new theory most physicists had and have problems to accept and understand it within the scope of our classical and nonrelativistic everyday experience. Especially one of the most fundamental characteristics of quantum mechanics – the entanglement – resulted in lively discussions.

It is not possible to describe entangled particles independently and it is certainly not possible to describe an entangled state by using classical physical laws. The peculiarity of such states was described in 1935 by Schrödinger (in the same paper in which he introduced the term *entanglement*) in one sentence: "Best possible knowledge of a whole does not include best possible knowledge of its parts – and that is what keeps coming back to haunt us" [3]. This publication of Schrödinger was triggered by the famous paper of Einstein, Podolsky and Rosen [1]. In this paper EPR analyzed the measurement predictions of a two particle system where the particles can not be described independently. They finally argued that quantum mechanics can not be considered complete at least in the view of their requirements for a physical theory, i.e. determinism and locality.
The lively discussions about entangled states were purely philosophical up to 1964. In this year Bell presented an experimentally testable inequality that describes bounds on the so-called local hidden variable theory (proposed to make quantum mechanics complete). This bounds are violated by entangled states. To test quantum mechanics many experiments testing Bell's inequalities have been realized and nearly all experiments have violated the inequalities. The proofs of these violations were up to now not possible beyond all points. A combination of experimental loopholes is still remaining. Nevertheless it is most probable that the quantum mechanical description (entanglement) is correct. So in turn Bell's inequalities are a possibility to test experimentally the entanglement of two (or more) particles.

Due to fascinating new ideas entanglement gained new interest in the whole physical society. By their independent proposals of the simulation of physics by using quantum mechanical systems Feynman [15] and Benioff [16] opened the door in 1982 to the new field of quantum simulators, quantum information processing, quantum computation and quantum cryptography [17]. For all those new ideas entanglement is essential.

The goal of our experiment is to show for the first time explicitly the entanglement of two different quantum mechanical systems – of a single photon and a single atom. Therefore it is necessary to think of a way to generate such an entangled state and how to prove the entanglement in experiments.
We create entanglement between the spin-state of an atom and the polarization of a photon emitted from the atom. To prove the entanglement we have to test Bell's inequality for the quantum numbers of the entangled particles. This means we have to carry out polarization measurements of the single photon and state selective measurements (spin measurements) of the single atom. The challenging part of the verification of the entanglement is the state selective measurement. It consists of a state selective transfer to select the measurement basis and a final state detection. The state selective transfer transfers a chosen superposition of the atomic states (the atomic spin of the two states is different, but with degenerated energy) to a second state distinguishable in energy. For the final state measurement a projection measurement on the two levels (hyperfine states) is carried out.
In the scope of this diploma thesis laser systems for the state selective transfer are set up. This state selective transfer is realized by an adiabatic population transfer process. To estimate the influence of different experimental parameters numerical calculations based on a three level model are carried out. The parameters of the chosen setup fits to the calculated requirements for an adiabatic transfer.
For the hyperfine state measurement of the atom it is necessary to distinguish atoms in two different energetic levels. It is possible to observe fluorescence light from an atom if the wavelength of the light is suitable to an atomic transition. So an idea to detect atoms in a certain energetic level is to observe fluorescence light from atoms in one of the two states. Another possible way is to transfer enough momentum to an atom resonant to an applied light field to kick the atom out of the trap if it is in one particular state and to leave it in the trap, otherwise. By a subsequent detection of the atom it should be possible to distinguish the energetic states. The results from test measurements of those two ideas are presented in this thesis.

Structure of the Thesis

In the theoretical chapter (§2) a description of a theoretical way to describe and test the entanglement of two particles is given. Furthermore interactions between the atom and applied electromagnetic fields are presented (including a description how it is possible to measure atomic populations and how to trap and cool atoms).
In the third chapter I will show in detail the experimental process we want to use to create and test an entangled state between a single atom and a single photon. In the fourth chapter a description of the experimental setup, including vacuum chamber, laser setup and detection optics, is given. Afterwards measurements, carried out to gain some characteristics of the dipole trap, are presented.
In the last two chapters I will present results towards the state selective measurement of the atom. The fifth chapter describes two possible ways for the final hyperfine state detection and an interpretation of the results of the test measurements of the ideas. In the sixth chapter calculations for the state selective transfer are presented (based on the model described in theoretical chapter). Furthermore the set up of the laser system is described.

2 Theory

As we want to create and verify entanglement between an atom and a photon it is necessary to take a theoretic look how it is possible to test the entanglement. Therefore I will explain some quantum mechanical basics including the definition of qubits and entanglement. After this I will switch to the famous paradox proposed by Einstein, Podolsky and Rosen being the fundament for Bell's inequality, which in turn is the basis for the experimental proof of entanglement. In connection with Bell's inequality I will give a short derivation of the formulation of Clauser, Horne, Shimony and Holt being an easy way for an experimentalist to show that two particles are entangled. Furthermore a short outlook on experimental realizations and loopholes is presented.
For the test of the entanglement between an atom and a photon the state of atom has to prepared and measured using laser systems. So in the next part electromagnetic interactions between photons and atoms will be considered. For this I will present a two and a three level atom and its interaction with monochrome light fields. This leads to the well known Rabi oscillations and π-pulse transitions in the first case and to an adiabatic population transfer process between two distinguishable atomic ground states in the second case.
As we have to prepare the state of the atom and as we have to carry out a state selective measurements it is necessary to have a localized single atom. This is possible by trapping and cooling a single atom with laser light. So a description of possible ways is given.

2.1 Quantum Systems

2.1.1 Single Quantum States and Qubits

A qubit is the fundamental computational basis for quantum information processing like the bit for normal computation. It can be described as a two dimensional quantum-mechanical system and so one can write any qubit as a superposition of the two orthogonal basis states $|0\rangle$ and $|1\rangle$:

$$|\psi\rangle = a|0\rangle + b|1\rangle \qquad |a|^2 + |b|^2 = 1 \qquad a, b \in \mathbb{C} \tag{2.1}$$

This state exists in a two dimensional Hilbert space and is given by four real numbers (actually three if we take the normalization in account).

By rewriting those two complex numbers with a global phase ϕ, a relative phase φ and two additional real amplitudes (A, B) we get:

$$|\psi\rangle = e^{i\phi}A|0\rangle + e^{i(\phi+\varphi)}B|1\rangle = e^{i\phi}(A|0\rangle + e^{i\varphi}B|1\rangle) \tag{2.2}$$

But if we neglect the global phase (what is reasonable due to the fact that we can not measure it) and if we remind ourselves of the normalization $A^2 + B^2 = 1$ we see that every qubit can be displayed on the surface of a 3 dimensional sphere – the so-called Bloch sphere. Concerning the polarization of photons this sphere is often called Poincaré sphere.
Any unitary operation results in a rotation of the state vector $|\psi\rangle$ on the Bloch sphere. A measurement of the qubit is a projection to the measurement basis. So (e.g.) if we measure $|\psi\rangle$ in the $|0\rangle, |1\rangle$ basis we get randomly the result $|0\rangle$ with the probability $|a|^2$ and $|1\rangle$ with $|b|^2$.

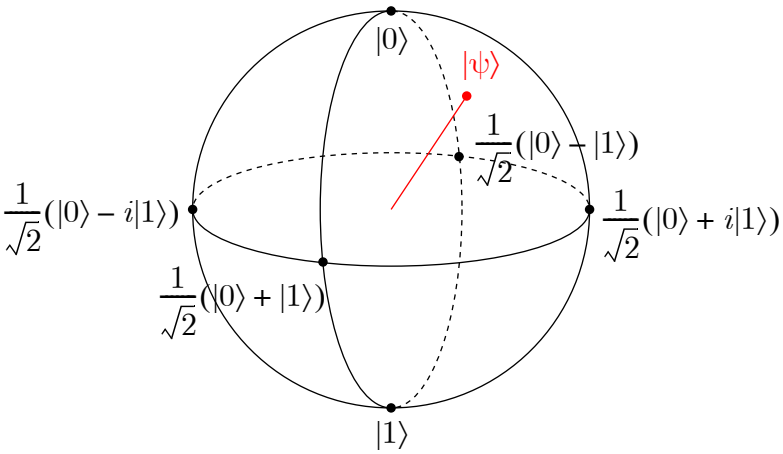

Figure 2.1: The Bloch sphere

Physical realizations of qubits are for example the polarization of photons, atoms with two different atomic states, or other quantum systems with 2 degrees of freedom.

2.1.2 Composite Quantum States

Now let us consider systems composed of several (N) qubits. Then we get a state that can be written as a vector in a 2^N dimensional Hilbert space. Again the probability to measure $|\psi\rangle$ to be in the state $|i\rangle$ is $|a_i|^2$ (e.g. $|i\rangle = |010001110100011\ldots\rangle$).

$$|\psi\rangle = \sum_{i=0}^{2^{N-1}} a_i|i\rangle \qquad \sum_{i=0}^{2^{N-1}} |a_i|^2 = 1 \qquad a_i \in \mathbb{C} \tag{2.3}$$

If we try to separate those wave functions into a product description of single one-qubit wave functions one of the three cases which I will describe below will be the case.

Product States: The wave function can split up into the wave functions of the single qubits. So the wave function of the whole system is a tensor product of the wave functions of each qubit. Two simple examples in two dimensions are:

$$\begin{aligned} |\psi\rangle &= |01\rangle = |0\rangle \otimes |1\rangle \\ |\psi\rangle &= \frac{1}{2}(|00\rangle + |01\rangle + |10\rangle + |11\rangle) = \frac{1}{2}((|0\rangle + |1\rangle) \otimes (|0\rangle + |1\rangle)) \end{aligned} \tag{2.4}$$

Entangled States: The wave function of an entangled state is not separable into wave functions of the single qubits (or multi dimensional quantum mechanical systems).
The most famous example for entangled states consisting of two qubits are the four Bell-States:

$$\begin{aligned} |\psi^+\rangle &= \frac{1}{\sqrt{2}}(|10\rangle + |01\rangle) \\ |\psi^-\rangle &= \frac{1}{\sqrt{2}}(|10\rangle - |01\rangle) \\ |\phi^+\rangle &= \frac{1}{\sqrt{2}}(|11\rangle + |00\rangle) \\ |\phi^-\rangle &= \frac{1}{\sqrt{2}}(|11\rangle - |00\rangle) \end{aligned} \tag{2.5}$$

These Bell-states (the $|\psi^-\rangle$ state is equal to the well-known singlet state and the other three are superpositions of the triplet states) are orthonormal and therefore they span the four dimensional Hilbert space of two qubits. Further the $|\psi^-\rangle$ state is independent of the choice of the basis while the other three change into one another.

Partly Entangled States: This is the most general case. Partly entangled states are a superposition of product and entangled states, we can partly separate out some product states. An example of a superposition of the pure state $|00\rangle$ and the Bell-state $|\psi^+\rangle$ is:

$$|\psi\rangle = \frac{1}{\sqrt{2}}(|00\rangle + |\psi^+\rangle) \tag{2.6}$$

2.2 EPR and the Proof of Entanglement

2.2.1 The Paradox of Einstein, Podolsky and Rosen

During the development of quantum mechanics many physicists refused to accept this new theory and especially one of its most fundamental results – entanglement. Three of the most important critics were Einstein, Podolsky and Rosen [1]. They constructed a paradox to show

the insufficiency of quantum mechanics to describe the physical reality in general. To do this they first defined criteria for a complete physical theory. According to Bohm [4] their requirements are:

1. Every element of physical reality must have a counterpart in a complete physical theory.
2. If, without any way of disturbing the system, we can predict with certainty the value of a physical quantity, then an element of reality exists corresponding to this physical quantity.
3. The world can correctly be analyzed in terms of distinct and separately existing "elements of reality,"
4. Every one of these elements must be a counterpart of a precisely defined mathematical quantity appearing in a complete theory.

Out of these arguments EPR concluded that the quantum mechanical description of physical reality is not complete.

This paradox was advanced afterwards as an argument that quantum mechanics could not be a complete theory but should be supplemented by additional variables. These variables were to restore to the theory causality and locality. So to predetermine measurement results the quantum mechanical theory should be extended by some "local hidden variables" (LHV). Or in other words: the seemingly probabilistic behavior of quantum mechanics is only a result of our inability of not recognizing the local hidden parameters which make the system deterministic and local.

Many people (the first was Bohr [2]) defended quantum mechanics and there were several mathematical attempts to prove LHV wrong but most of them had either mathematical or physical errors (especially the requirement of locality created essential difficulties) [6]. Moreover a hidden variable interpretation of elementary quantum theory has been explicitly constructed, but it had a grossly non-local structure [5].

Schrödinger introduced for the first time the term "entanglement of predictions" [3]. Finally Bohm [4] presented a variation of the EPR "Gedankenexperiment" and Bell derived an inequality which allowed to test the violation of LHV theories [7] based on Bohm's "Gedankenexperiment", which I will present shortly:

A source emits two spin one-half particles (an EPR pair) in a spin-singlet state (that is the $|\psi^-\rangle$ state) in opposite directions. For each of the particles each of the two observers first chooses the measurement basis and than measures the particle. For example they could use Stern-Gerlach-Apparatuses, where the measurement basis is the spatial orientation of the magnetic field (selection of the component of the spins σ) and the measurement is done by detecting which way the particle has taken.

2.2.2 Bell's Inequality

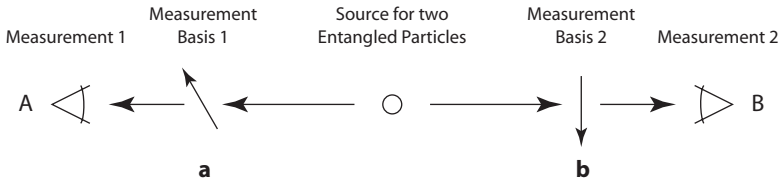

Figure 2.2: Symbolic measurement setup for Bell's inequality with the unity vectors **a** and **b** describing the measurement bases

Each of the two observers measures the selected spin component $\boldsymbol{\sigma}_1\mathbf{a}$ or $\boldsymbol{\sigma}_2\mathbf{b}$ ($\mathbf{a}$, $\mathbf{b}$ are unity vectors describing the measurement bases). For every single measurement they can only get the results $+1$ or -1. So if the two particles were initially in the $|\psi^-\rangle$ state and the observer A gets -1 the observer B we will get with certainty $+1$.
The quantum mechanical two-particle spin expectation value for a singlet state can be calculated by [41]:

$$\begin{aligned} P_{QM}(\mathbf{a},\mathbf{b}) &= \langle\psi^-|\boldsymbol{\sigma}_1\mathbf{a}\otimes\boldsymbol{\sigma}_2\mathbf{b}|\psi^-\rangle \\ &= -\mathbf{a}\mathbf{b} \\ &= -|\mathbf{a}||\mathbf{b}|\cos(\alpha-\beta) \\ &= -\cos(\alpha-\beta) \end{aligned} \tag{2.7}$$

Now let us formulate the LHV idea mathematically. The measurement results *A* and *B* depend on the one hand on the direction of their measurement basis and on the other hand on a set of local hidden variables λ. These hidden variables λ are equal for both particles because the two particles are created in the same physical process. If the measurement stations are well separated (in space-time) from each other the hidden variable λ won't depend on the measurement value of the other detector. To reproduce single particle quantum mechanical results the measurement results of the single particles can only be ± 1, too:

$$A(\mathbf{a},\lambda) = \pm 1,\ B(\mathbf{b},\lambda) = \pm 1 \tag{2.8}$$

Obviously we have $A = 1/A$, $B = 1/B$ and $|A| = |B| = |AB| = 1$.
Further the parameter λ is given by the normalized probability distribution $\rho(\lambda)$ with:

$$\int \rho(\lambda)\, d\lambda = 1 \tag{2.9}$$

So the expectation value for any state should be:

$$P(\mathbf{a},\mathbf{b}) = \int A(\mathbf{a},\lambda)B(\mathbf{b},\lambda)\rho(\lambda)\,d\lambda \tag{2.10}$$

To derive the inequality let us suppose that observer 2 chooses a second measurement basis **c** and let us apply the triangle inequality:

$$\begin{aligned} |P(\mathbf{a},\mathbf{b}) - P(\mathbf{a},\mathbf{c})| &\leq \int |A(\mathbf{b},\lambda)B(\mathbf{b},\lambda) - A(\mathbf{a},\lambda)B(\mathbf{c},\lambda)|\rho(\lambda)\,d\lambda \\ &= \int |A(\mathbf{a},\lambda)B(\mathbf{b},\lambda)|(1 - B(\mathbf{c},\lambda)/B(\mathbf{b},\lambda))\rho(\lambda)\,d\lambda \\ &= \int 1\cdot(1 - B(\mathbf{c},\lambda)B(\mathbf{b},\lambda))\rho(\lambda)\,d\lambda \\ &= 1 - \int B(\mathbf{c},\lambda)B(\mathbf{b},\lambda)\rho(\lambda)\,d\lambda \end{aligned} \tag{2.11}$$

And finally when we want to reproduce the correlation function of the singlet state $|\psi^-\rangle$ where $A(\mathbf{a},\lambda) = -B(\mathbf{a},\lambda)$ we get Bell's inequality:

$$\left|P_{|\psi^-\rangle}(\mathbf{a},\mathbf{b}) - P_{|\psi^-\rangle}(\mathbf{a},\mathbf{c})\right| \leq 1 + P_{|\psi^-\rangle}(\mathbf{b},\mathbf{c}) \tag{2.12}$$

If EPR are right experimental observations have to match the inequality for any choice of the measurement bases **a**, **b**, **c**.
On the other hand it is interesting if the quantum mechanical results P_{QM} fulfill (2.12). If we choose the measurement directions $\alpha = 0°$, $\beta = 45°$ and $\gamma = 90°$ we get:

$$\begin{aligned} \left|P_{QM}(\mathbf{a},\mathbf{b}) - P_{QM}(\mathbf{a},\mathbf{c})\right| &= \left|-\frac{1}{\sqrt{2}} + 0\right| = \frac{1}{\sqrt{2}} \approx 0.707 \\ 1 + P_{QM}(\mathbf{b},\mathbf{c}) &= 1 - \frac{1}{\sqrt{2}} \approx 0.293 \end{aligned} \tag{2.13}$$

So it can be easily seen that the inequality is not fulfilled by P_{QM} (the measurement directions are chosen to maximize this violation). By measurements we can distinguish between quantum mechanics and LHV.

2.2.3 CHSH Formulation of Bells Inequality

The formulation chosen by Bell is good for mathematically proofs, but since the formulation of Clauser, Horne, Shimony and Holt [8] (CHSH) applies directly to our experimental configuration (as both outputs are measured in every basis at the same time) we will use this formulation for the test of the entanglement.

Therefore we choose a fourth measurement direction **d** (in other words: a second direction for observer 2) and again we use the triangle inequality:

$$\begin{aligned} |P(\mathbf{c},\mathbf{d}) + P(\mathbf{c},\mathbf{b})| &\leq \int |A(\mathbf{c},\lambda)B(\mathbf{d},\lambda) + A(\mathbf{c},\lambda)B(\mathbf{b},\lambda)|\rho(\lambda)\,d\lambda \\ &= \int |A(\mathbf{c},\lambda)B(\mathbf{b},\lambda)|(1 + B(\mathbf{d},\lambda)B(\mathbf{b},\lambda))\rho(\lambda)\,d\lambda \\ &= 1 + \int B(\mathbf{d},\lambda)B(\mathbf{b},\lambda)\rho(\lambda)\,d\lambda \end{aligned} \tag{2.14}$$

Now we can rewrite (2.11) and we get this inequality:

$$\begin{aligned} |P(\mathbf{a},\mathbf{b}) - P(\mathbf{a},\mathbf{d})| &\leq 2 - (1 + \int B(\mathbf{d},\lambda)B(\mathbf{b},\lambda)\rho(\lambda)\,d\lambda) \\ &\leq 2 - |P(\mathbf{c},\mathbf{d}) + P(\mathbf{c},\mathbf{b})| \end{aligned} \tag{2.15}$$

For an easier notation we define $S(\mathbf{a}, \mathbf{b}, \mathbf{c}, \mathbf{d})$ and we get the expression:

$$S(\mathbf{a}, \mathbf{b}, \mathbf{c}, \mathbf{d}) := |P(\mathbf{a}, \mathbf{b}) - P(\mathbf{a}, \mathbf{d})| + |P(\mathbf{c}, \mathbf{d}) + P(\mathbf{c}, \mathbf{b})| \tag{2.16}$$

Finally the inequality in the formulation of CHSH can be written as:

$$S(\mathbf{a}, \mathbf{b}, \mathbf{c}, \mathbf{d}) \leq 2 \tag{2.17}$$

For $\alpha = 0°$, $\beta = 45°$, $\gamma = 90°$ and $\delta = 135°$ we get according to a $|\psi^-\rangle$ state:

$$S_{QM}(0°, 45°, 90°, 135°) = \left|-\frac{1}{\sqrt{2}} - \frac{1}{\sqrt{2}}\right| + \left|-\frac{1}{\sqrt{2}} - \frac{1}{\sqrt{2}}\right| = 2\sqrt{2} \tag{2.18}$$

This is the maximum violation of the CHSH formulation of Bell's inequality achievable with an entangled 2-qubit state.

2.2.4 Experiments Testing Bell's Inequality

Another possibility for an experiment testing Bell's inequality is to use polarization entangled photon pairs (e.g. created by a type 2 parametric down conversion [12, 41]) and to perform polarization measurements of both particles. To choose the measurement basis we could use a

combination of lambda plates and for the measurement a polarizing beam splitter with two photo detectors. Here is a symbolic figure for such a kind of setup:

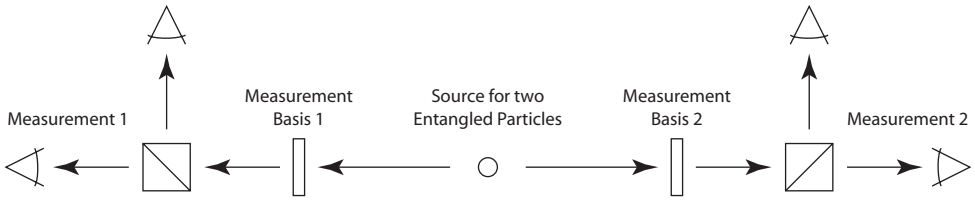

Figure 2.3: Symbolic measurement setup for Bell's inequality

The first experimental realization to test Bell's inequality was done by Freedman and Clauser [9] in 1972 with polarization entangled photons of an atomic cascade. And almost all experiments testing Bell's inequality violated it.
So it is very likely that the assumption of EPR is wrong. But still there are some critics and they pointed out some experimental loopholes which should be closed before making a final inference of quantum mechanics being correct:

1. **Detection loophole:** If the detection efficiency is not perfect it could happen that we detect only those events violating Bell's inequality. Therefore it is possible that a perfect measurement (a measurement of all events) could show other results. To close this loophole experiments with ions and atoms have been made successfully because with those particles it is possible to get detection efficiencies high enough ($> 71\%$ – otherwise $S(0°, 45°, 90°, 135°)$ could be greater then 2 although it would be smaller if we could detect more particles) [14].
2. **Locality loophole:** The space between the two measurement stations has to be large enough so that no classical information can be transferred (at the speed of light) during the whole measurement process. Otherwise it could be possible that the second measurement is predetermined by this information. Experiments with polarized entangled photons over large distances have been made [13] and the results violated Bell's inequality.

Up to now there have been no experiments closing both loopholes at the same time. The ideal configuration for such a proof would be an experiment with entangled particles separated by large distances where their state can be measured with a high detection efficiency.

2.2.5 Proof of Entanglement

The violation of Bell's inequality was shown in many experiments and it is most probable that quantum mechanics is correct.
So in turn we can use the inequality for another purpose. Let's assume we have an experiment and want to show that two particles are entangled. For this purpose we measure $S(0°, 45°, 90°, 135°)$ and if the two particles are in an entangled state (e.g. $|\psi^- \rangle$) we will get a result larger than 2. So by this measurement we can distinguish between entangled states and product states and therefore we can test the entanglement of a state by measuring S.

2.3 Two-Level Problem

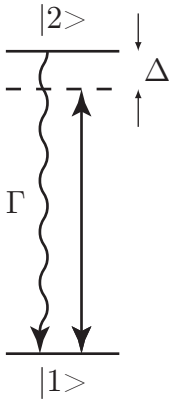

Figure 2.4: The two-level problem

Now it's time to take a closer look on the interaction between an atom and an applied electromagnetic field (light). Let's assume a two-level model for the atom and a classical electromagnetic field driving the transition between the ground state $|1\rangle$ and the excited state $|2\rangle$. The two atomic levels are separated by the energy difference $\hbar\omega$. The wavelength of the light field is ω_L and the light is detuned by $\Delta = \omega_L - \omega$. Further the excited state $|2\rangle$ has a lifetime τ with the natural decay rate $\Gamma = 1/\tau$.
The plane wave electric field (the light) is travelling in z direction with a sufficiently long coherence time. This leads to a time dependent interaction hamiltonian between the atom with the atomic dipole moment $\mathbf{d}$ and the electric field with the field vector $\mathbf{E}(\mathbf{r}, t) = \mathbf{E}_0 \cos(kz - \omega_L t)$.

$$H(t) = -\mathbf{E}(\mathbf{r}, t) \cdot \mathbf{d} = -\mathbf{E}_0 \mathbf{d} \cos(kz - \omega_L t) \tag{2.19}$$

If we define the Rabi frequency

$$\Omega := -\frac{1}{\hbar}\mathbf{E}_0\mathbf{d} = -\frac{E_0}{\hbar}\hat{\mathbf{e}}\mathbf{d} = -\frac{E_0}{\hbar}\langle 2|d|1\rangle \tag{2.20}$$

we finally get this simplified Hamiltonian

$$H(t) = \hbar\Omega \cos(kz - \omega_L t) \tag{2.21}$$

The definition (2.20) shows that the Rabi frequency describes the coupling efficiency between the electric field of the monochromatic light and the atom. By increasing the detuning $|\Delta|$ the frequency of the oscillations is increased to the effective Rabi frequency:

$$\Omega_{eff} = \sqrt{\Omega^2 + \Delta^2} \tag{2.22}$$

The population of the ground state $|1\rangle$ and the population of the excited state $|2\rangle$ ($\left|c_1(t)\right|^2$ and $\left|c_2(t)\right|^2$, respectively) are oscillating with the frequency Ω_{eff}:

$$\begin{aligned} \left|c_2(t)\right|^2 &= \left(\frac{\Omega}{\Omega_{eff}}\right)^2 \sin^2\left(\frac{\Omega_{eff}\cdot t}{2}\right) \\ \left|c_1(t)\right|^2 &= 1-\left|c_2(t)\right|^2 \end{aligned} \tag{2.23}$$

So by increasing the detuning $|\Delta|$ not only the frequency is increased but also the amplitude of the oscillation ($\left|c_2(t)\right|^2$) is decreased as the overlap of the wavelength distribution with the splitting of the atomic energy is decreased.
Up to now we have ignored spontaneous decay. If we include radiative damping into the derivation and if we apply a light field with constant amplitude the excited state population settles at the steady state solution [48]:

$$\left|c_2(t\to\infty)\right|^2 = \frac{(\Omega/\Gamma)^2}{1+4(\Delta/\Gamma)^2+2(\Omega/\Gamma)^2} \tag{2.24}$$

The steady state photon scattering rate (integrated over all directions) is then given by:

$$R_{\mathrm{SC}} = \Gamma\left|c_2(t\to\infty)\right|^2 = \left(\frac{\Gamma}{2}\right)\frac{(I/I_{sat})}{1+4(\Delta/\Gamma)^2+(I/I_{sat})} \tag{2.25}$$

By writing down this expression we have defined the saturation intensity and with the intensity of the light field $I = (1/2)c\varepsilon_0 E_0^2$ we get:

$$I_{sat} := \frac{1}{2}I\left(\frac{\Gamma}{\Omega}\right)^2 = \frac{c\varepsilon_0\Gamma^2\hbar^2}{4(\langle 2|d|1\rangle)^2} \tag{2.26}$$

Equation (2.25) shows that for intensities smaller than the saturation intensity the on-resonance photon scattering rate $R_{\mathrm{SC}}(\Delta = 0)$ increases linearly with I. If I is equal to I_{sat} $R_{\mathrm{SC}}(\Delta = 0)$ reaches half of the maximal possible value. Finally $R_{\mathrm{SC}}(\Delta = 0)$ approximates $\Gamma/2$ asymptotically for large intensities. Therefore the saturation intensity can be seen as the crossing point between a linear increase of the on-resonance photon scattering rate and the saturation of the transition.

As it can be seen from (2.24) the maximal on-resonance value for $\left|c_2(t\to\infty)\right|^2$ is one-half. So for a highly efficient transfer from $|1\rangle$ to $|2\rangle$ we have to choose another way.
If we look at the time dependent development of $\left|c_2\right|^2$ (which can be calculated with the optical Bloch equations [31]) we see a damped oscillation between 0 and 1 settling down to 1/2 for

$t \to \infty$. The maximal possible population probability of the level $|2\rangle$ is reached after the time t:

$$t = \frac{\pi}{\Omega_{eff}} \tag{2.27}$$

And a light pulse with this dependency between duration and Rabi frequency is called a π-pulse. As we have seen this π-pulse is a way to get a good transition efficiency from the ground state $|1\rangle$ to the excited state $|2\rangle$ if $t \ll \tau$ and the detuning $|\Delta|$ is small, too.

2.4 STIRAP (Three-Level Problem)

In the last chapter we have seen how it is possible to transfer populations highly efficient between two atomic states. If we want to realize a transfer between an initial state $|1\rangle$ and a final state $|3\rangle$ and the frequency of the transfer is not accessible with lasers (too small) we have to realize an efficient transfer form a populated level $|1\rangle$ via an intermediate level $|2\rangle$ to the level $|3\rangle$.

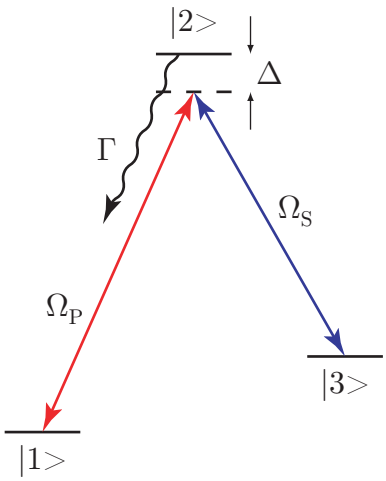

Figure 2.5: A three-level system coupled by two lasers with the Rabi frequencies Ω_P and Ω_S

The first approach to transfer the population from the initial state $|1\rangle$ via an intermediate state $|2\rangle$ to the final state $|3\rangle$ would be to shine in first the pump pulse (Ω_P) on the transition $|1\rangle \to |2\rangle$ and than the Stokes pulse on the $|2\rangle \to |3\rangle$ transition (Ω_S). But this process (including two π-pulses) is very sensitive to various experimental parameters (for example: intensity, detuning and pulse length of Ω_P and Ω_S). Especially decays from the intermediate state $|2\rangle$ are critical.
Another way, less sensitive to the laser parameters, is to use an adiabatic process the so-called stimulated Raman adiabatic passage (STIRAP) [45]. In the STIRAP process the levels $|2\rangle$, $|3\rangle$ are coupled first by the Stokes laser pulse and later by a partially overlapping pump pulse the

initially populated level $|1\rangle$ is emptied. With this sequence it is possible to transfer the population with a high efficiency and without any decay channel from $|1\rangle$ to $|3\rangle$.

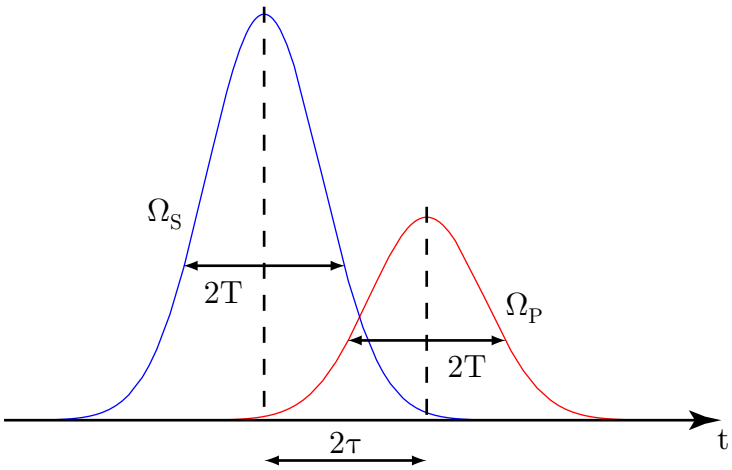

Figure 2.6: A typical STIRAP pulse sequence with two gaussian pulses. Each pulse has a duration of 2·T (at Ω_{max}/e) and the peaks of the pulses are separated by 2·τ.

If we consider a three-level system with no direct coupling between $|1\rangle$ and $|3\rangle$, a detuning of both lasers Δ and a (small) decay rate Γ from $|2\rangle$ we get this Schrödinger equation [47]:

$$i\frac{d}{dt}\begin{bmatrix} c_1(t) \\ c_2(t) \\ c_3(t) \end{bmatrix} = \begin{bmatrix} 0 & \Omega_P(t) & 0 \\ \Omega_P(t) & \Delta - i\Gamma & \Omega_S(t) \\ 0 & \Omega_S(t) & 0 \end{bmatrix} \begin{bmatrix} c_1(t) \\ c_2(t) \\ c_3(t) \end{bmatrix} \tag{2.28}$$

The state vector for the three-level system is:

$$|\psi\rangle = c_1|1\rangle + c_2|2\rangle + c_3|3\rangle \tag{2.29}$$

The initial conditions for this problem are (all population in $|1\rangle$, no population in $|2\rangle$ to $|3\rangle$):

$$|c_1(-\infty)|^2 = 1 \qquad |c_2(-\infty)|^2 = 0 \qquad |c_3(-\infty)|^2 = 0 \tag{2.30}$$

In absence of any decay ($\Gamma = 0$) the three eigenstates ($|+(t)\rangle, |0(t)\rangle, |-(t)\rangle$) of the Hamiltonian in (2.28) can be calculated:

$$\begin{aligned} |+(t)\rangle &= \sin\varphi(t)\sin\vartheta(t)|1\rangle + \cos\varphi(t)|2\rangle + \sin\varphi(t)\cos\vartheta(t)|3\rangle \\ |0(t)\rangle &= \cos\vartheta(t)|1\rangle - \sin\varphi(t)|3\rangle \\ |-(t)\rangle &= \cos\varphi(t)\sin(t)\vartheta|1\rangle - \sin\varphi(t)|2\rangle + \cos\varphi(t)\cos\vartheta(t)|3\rangle \end{aligned} \tag{2.31}$$

with Euler's angles $\vartheta(t)$ and $\varphi(t)$

$$\tan\vartheta(t) = \frac{\Omega_P(t)}{\Omega_S(t)} \qquad \tan 2\varphi(t) = \frac{2\Omega_0(t)}{\Delta} \tag{2.32}$$

and $\Omega_0(t) = \sqrt{\Omega_P^2(t) + \Omega_S^2(t)}$.
If it is possible to stay during the whole process in the $|0(t)\rangle$ eigenstate and the initial state is:

$$|1\rangle = |0(t \to -\infty)\rangle \tag{2.33}$$

the final state will be:

$$|0(t \to \infty)\rangle = |3\rangle \tag{2.34}$$

and no population will be transferred to the excited state $|2\rangle$. So the final populations are:

$$|c_1(\infty)|^2 = 0 \qquad |c_2(\infty)|^2 = 0 \qquad |c_3(\infty)|^2 = 1 \tag{2.35}$$

Up to now we have neglected the decay $\Gamma = 0$. But as we have seen the intermediate level $|2\rangle$ is not populated in any step of the transfer. Therefore a small decay rate $\Gamma \neq 0$ won't disturb the adiabatic transfer process as long as the eigenstates of the hamiltonian are not drastically changed.
The condition to stay in the eigenstate is to stay adiabatic. Nonadiabatic coupling gets small if the rate of change of the mixing angle $\vartheta(t)$ is small compared to the separation of the corresponding eigenvalues [43]. So $|\dot{\vartheta}| \ll \Omega_0$ is necessary to stay adiabatic. This can be rewritten

according to [44] to the condition for adiabacity with the interaction duration T_{interact} of the two pulses:

$$\Omega_0 T_{\text{interact}} \gg 1 \tag{2.36}$$

Results from numerical solutions of the time dependent Schrödinger equation for realistic sets of parameters are presented in chapter 6 showing that the STIRAP process will work in our experiment.

2.5 Atom-Traps

For the experiment we need a single, localized atom which is well separated from the environment. One possibility is to trap the atom [24]. For charged particles like ions it is possible to use the coulomb interaction to build a trap [51, 52] but for neutral particles like atoms this is not possible. Therefore we need another type of interaction to trap the atom.
Some other requirements for the trap results out of the goal of our experiment – the entanglement:

1. All sublevels of the ground state of the atom have to see a binding potential.
2. The interaction used for trapping should not change the atomic state within the measurement time because decoherence should be minimal.
3. The Zeeman levels for one hyperfine level of the atom should be degenerated. This means at least that the energy difference of the Zeeman levels has to be smaller as the natural line width of the transitions. Therefore we have to minimize magnetic fields and can't use magnetic traps [55, 56].

2.5.1 Optical Dipole Traps

The optical dipole trap is the trap we use to capture a single, localized atom and a good description is given in [24, 31]. Dipole forces were first observed in 1962 [58] and in 1986 Chu et al. were finally able to trap atoms with an optical dipole trap [57].
In a dipole trap an oscillating electric field (light) induces an oscillating atomic electric dipole moment that interacts with the light field. This interaction is a function of the detuning of the light and the detuning results in a phase displacement between light and atom. For red detuned light this gives an attractive force. This force can be interpreted as a light shift of the ground state of the atom. If the laser field is spatially inhomogeneous the interaction between the atom and the light varies in space and produces a conservative potential.
The intensity of a strongly focussed gaussian laser beam varies transversely with

$$I(r) = I_0 e^{-2r^2/\omega_0^2} \tag{2.37}$$

where ω_0 is the waist size of the beam. For a red detuned laser beam the ground state light shift is negative at any point, but largest at the point with the greatest intensity – the center of

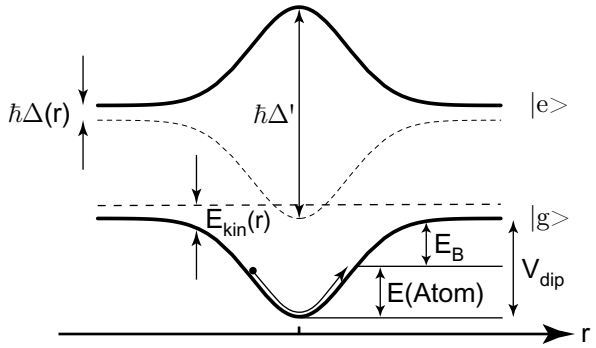

Figure 2.7: Spatial dependency of the ground and excited state levels and of the detuning Δ(r) with a resulting trap depth V_{dip} and kinetic energy $E_{kin}(r)$ of the atom. The final remaining kinetic energy of the atom after cooling into the trap is E(Atom) and so the resulting binding energy is E_B.

the gaussian beam waist. Ground state atoms therefore will experience an attractive force towards the focus given by the gradient of the light shift. For $\Delta \gg \Omega$ this force is:

$$\mathbf{F} \sim -\frac{1}{\Delta}\nabla\left(\left(\frac{\mathbf{E}_0(r)\mathbf{d}}{\hbar}\right)^2\right) = -\frac{1}{\Delta}\nabla(\Omega(r)^2) \sim -\frac{1}{\Delta}\frac{1}{I_{sat}}\nabla(I(r)) \tag{2.38}$$

For the gaussian beam the transverse force at the waist is:

$$\mathrm{F}_t \sim -\frac{1}{\Delta}\,\frac{I}{I_{sat}}\,\frac{r}{\omega_0^2}\,e^{-2r^2/\omega_0^2} \tag{2.39}$$

In the longitudinal direction there is also an attractive force, but it is more complicated and depends on the details of the focussing. It might appear that the trap does not confine in longitudinal direction because of the radiation pressure. But this can be accomplished by a far red detuned dipole laser because the radiation pressure reduces with $1/\Delta^2$ and the dipole force reduces only with $1/\Delta$.
This kind of trap is relatively weak compared e.g. with ion traps (a typical trap depth is of the order of below $k_B \cdot 1$ mK). The trap potential is independent of the magnetic quantum number for a linear polarized laser beam and the scattering rate can be quite low if a far detuned laser beam is used [38].
Due to the attractive force the atom (for example with the kinetic energy $E_{kin}(-\infty)$ far from the trap – see Fig. 2.7) is accelerated towards the center of the trap and after it has passed the center it is decelerated by the same amount and will finally leave the trap with the initial energy $E_{kin}(-\infty)$. This leads to a growth of the kinetic energy $E_{kin}(r)$ within the dipole potential de-

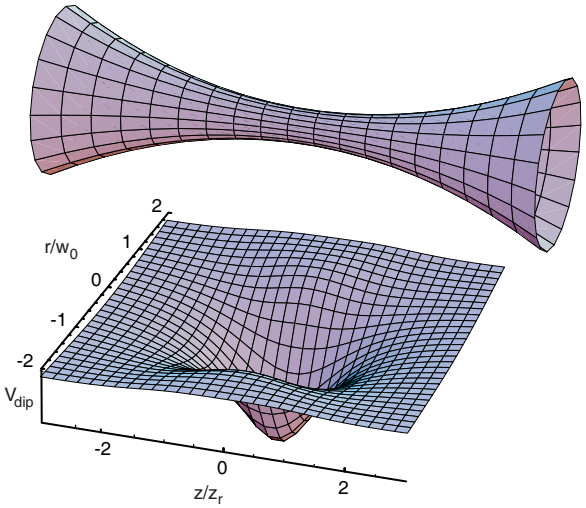

Figure 2.8: The focussed dipole laser beam and the resulting dipole potential

pending on the position because of the attractive potential $V_{dip}(r)$. If the atom in the potential looses some kinetic energy due to cooling the kinetic energy will get:

$$E_{kin}'(r) = E_{kin}(-\infty) + V_{dip}(r) - E_{cool} \tag{2.40}$$

Therefore if $E_{cool} > E_{kin}(-\infty)$ the atom will stay in the trap and will be cooled down further. This will only happen if the initial speed of the atom is slow enough.
In every gas a few atoms are slow enough due to the Maxwell velocity distribution. But this are quite rare cases. So to get more cold atoms near the dipole trap we use the MOT to collect some atoms in the region of the trap center. For some experiments with the single atom the magneto optical trap has to be switched off.

2.5.2 Magneto Optical Trap

The magneto optical trap (MOT) is a radiation pressure trap and uses a combination of optical and magnetic fields [53, 54].
Let us look first at an one dimensional trap. In an inhomogeneous magnetic field applied by two magnetic coils the magnetic field is a linear function of the z-direction (the direction of the laser beam) and is minimal in the trap center. Due to the magnetic field the Zeeman levels are split up differently at different z positions. E.g. for B > 0 the state with $m_f = -1$ will be shifted up, whereas the state with $m_f = +1$ is shifted down.
If two counterpropagating detuned laser beams with opposite circular polarization are applied on the $J \rightarrow J + 1$ transition and the atom is not at $z = 0$ (trap center) one of the Zeeman sub-

levels will be more resonant to the applied light and the atom will experience some force (because of the different radiation pressure of the two beams) to the center of the trap.

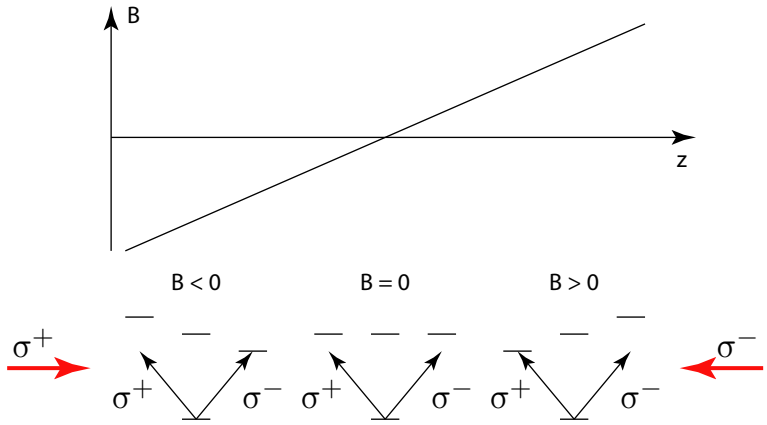

Figure 2.9: Spatially different splittings of the Zeeman levels due to the inhomogeneous magnetic field of the MOT

To get confinement in all 3 dimensions it is necessary to apply 3 pairs of counterpropagating laser beams and an inhomogeneous magnetic field being zero in the trap center. This is possible with a magnetic quadrupole field generated by two antiparallel coils. Further each pair of lasers consists of one left and one right circular polarized laser.

2.6 Laser cooling

As we have seen a very important point for the trapping of atoms is cooling (reducing of the mean kinetic energy).
An easy way to do this is laser cooling. Laser cooling was first purposed by Hänsch and Schawlow [20] in 1975 and first realized by Chu et al. [21] in 1985. In this chapter I will present two different effects resulting in cooling atoms with laser radiation. On the one hand this is the fundamental doppler cooling and on the other hand a form of the polarization gradient cooling which leads to temperatures even below the limit of doppler cooling.

2.6.1 Doppler Cooling

How to reduce the velocity of an atom? If an atom absorbs a photon it will change its momentum by $\Delta\mathbf{p} = \hbar\mathbf{k}$ ($\mathbf{k}$ is the wave vector of the photon) and because the following spontaneous emission happens statistically in all spatial directions this has no effect on the velocity change of the absorption in average. Furthermore if the light is slightly red detuned to the atomic transition the light will be more resonant if the atom moves towards the light source (doppler ef-

fect). So the scattering probability is higher and the atom with velocity **v** will be slowed down in this direction by the force:

$$\mathbf{F} = \hbar\mathbf{k}R_{\mathrm{SC}} = \left(\frac{\Gamma}{2}\right)\frac{(I/I_{sat})}{1+((2\Delta+\mathbf{vk})/\Gamma)^2+(I/I_{sat})} \tag{2.41}$$

If light is applied from both sides, and the atom moves e.g. towards the left, the light from the left beam will be more resonant and the atom will be slowed down in this direction and vice versa. So due to the addition of the two forces the mean velocity of the atom is reduced. But, up to now the atom is only cooled in one dimension. If counterpropagating light fields are applied from all 3 spatial directions the mean kinetic energy is reduced in all spatial dimensions. Doppler cooling is limited by the fact that atoms are heated by spontaneous scattering and for slow atoms the cooling force is too small to reduce the mean kinetic energy further. Therefore these atoms won't be decelerated anymore. With the optimal value for the detuning (which is half of the natural line width of the atom) the lowest temperature (the so-called doppler temperature) can be reached:

$$v_D = \sqrt{\frac{\hbar\Gamma}{2m}} \qquad T_D = \frac{\hbar\Gamma}{2k_B} \tag{2.42}$$

An ensemble of cold atoms (produced by the procedure described above) is called optical molasses [21]. Note that optical molasses are not a trap for neutral atoms because there is no restoring force on atoms that have been displaced from the center. Still, the detainment times of atoms caught in optical molasses can be remarkably long. [31]

2.6.2 Polarization Gradient Cooling

In surprising measurements temperatures below T_D were measured. This is the effect of the so-called polarization gradient cooling introduced by Dalibard and Cohen-Tannoudji [22].
There are two kinds of polarization gradient cooling. One with two counter propagating beams with orthogonal linear polarizations and one with two counter propagating beams with orthogonal circular polarizations. Because in our experiment the MOT laser beams are circularly polarized I will restrict myself to this case.
The electric field of the two circularly polarized beams (σ^+, σ^-) results in a linearly polarized electrical field with constant magnitude in every point. Only the direction of the linear polarization rotates through an angle of 2π over one optical wavelength.
If the atom is at rest we get a constant light shift which is for the $m_f = \pm 1$ ground state levels only $3/4$ of the light shift of the $m_f = 0$ level. Furthermore $9/17$ of the population is in the $m_f = 0$ state and $4/17$ in each of the $|m_f| = 1$ states, as one obtains from the Clebsch-Gordan coefficients.
In the case of two counter propagating beams with orthogonal circular polarizations the atom moves through a region of rotation of the atomic quantization axis due to the electric field and the populations of the $|m_f| = 1$ levels must be optically pumped to follow this. So if the

pumping is not fast enough (movement too fast) the occupation of this levels will lag behind the steady state distribution.
According to [22] the $m_f = 1$ sub state will be populated higher than the $m_f = -1$ sub state if the atoms travels towards the σ^+ laser beam and vice versa, because the $m_f = 1$ sub level scatters σ^+ 6 times better then the $m_f = -1$ sub level according to the Clebsch-Gordan coefficients. And this imbalance in the populations results in a strong damping force.

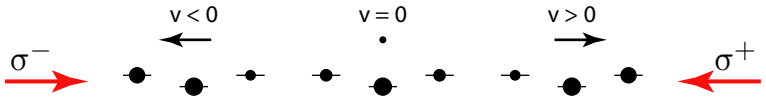

Figure 2.10: Population of the ground states in a rotating linear polarized light field depending on the velocity of the atom

If the movement gets too slow it will be possible for the atom to follow the radiation and no more cooling will happen. With polarization gradient cooling temperatures down to 3 µK were measured [23].

3 Experimental Process

The goal of our experiment is to show the entanglement of two different quantum mechanical systems – of a single photon and a single atom. Therefore it is necessary to think of a way to generate such an entangled state and to prove the entanglement.

We want to create the entanglement between the state of the atom and the polarization of a photon emitted from the atom. This is possible by using a so-called λ-scheme in ^{87}Rb (see Fig. 3.1).

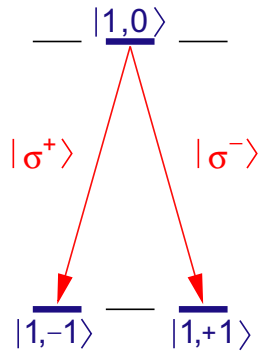

Figure 3.1: The λ-scheme used to entangle the magnetic quantum number of the single atom with the polarization of the single photon

The atom is prepared in the $|F' = 1, m_f = 0\rangle$ excited state. After the lifetime τ of the excited state the atom decays spontaneously to the $|F = 1, \pm 1\rangle$ ground states (degenerated in energy – conservation of the angular momentum forbids the decay to $|0, 0\rangle$) and a $\sigma^{\pm}$ polarized photon is emitted. The simplified atom-photon state after this decay is:

$$|\psi^-\rangle = \frac{1}{\sqrt{2}}(|1,-1\rangle|\sigma^+\rangle - |1,+1\rangle|\sigma^-\rangle) \tag{3.1}$$

So we get entanglement between the atomic magnetic quantum number ($m_f = \pm 1$) of the atom and the polarization of the emitted photon ($\sigma^{\pm}$). After this process the two particles can be spatially separated and the entanglement remains.

To verify that we really have an entangled state, we have to make a measurement of the CHSH formulation of Bell's inequality by calculating $S(\mathbf{a}, \mathbf{b}, \mathbf{c}, \mathbf{d})$ with (2.16). To do this we have to realize polarization measurements of the single photon and state selective measurements of

the single atom. These measurements have to be carried out for each particle in two different measurement bases as seen in §2.2.3.

For the polarization measurement of the single photon we collect it with a microscope objective. The quantum mechanical measurement basis for the photon can be chosen by a combination of λ/2 and λ/4 - plates. To carry out the measurement a polarizing beam splitter (PBS) and two single photon detectors (e.g. avalanche photo diodes (APDs)) are used.
Limited by the NA (numerical aperture) of our objective and losses in fiber, optical components and photo detectors the detection efficiency of the photon is about 0.2 %. So we have to repeat the whole process up to this step until we see a photon correlated to the spontaneous emission creating the entanglement. Only after we have seen such a photon it is reasonable to make the state selective atom measurement.

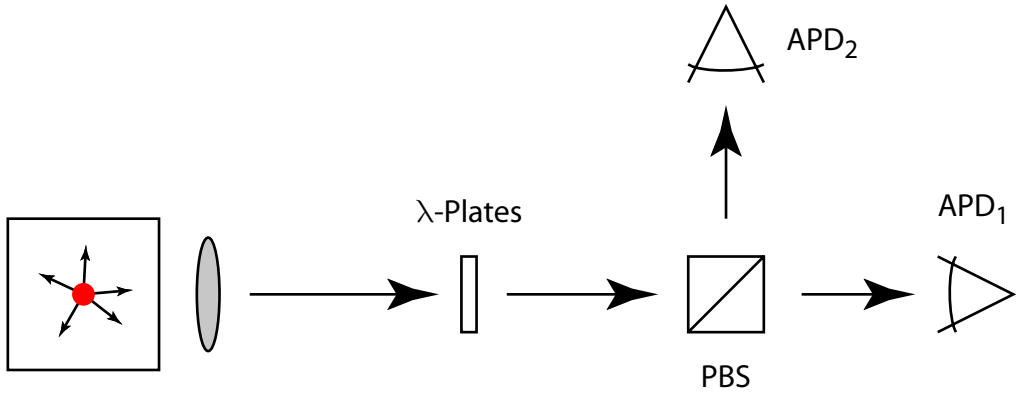

Figure 3.2: Measurement scheme for the photon

For the state selective measurement of the single atom we have to choose the measurement basis and to carry out a projection measurement in the selected basis. To choose the measurement basis of the atom we shine in a probe light polarized in a superposition of σ^+ and σ^- which only excites a certain superposition of $|1,-1\rangle$ and $|1,+1\rangle$ (bright state) while the orthogonal superposition can not couple to the light field (dark state). This is the reversal process to the decay generating the entanglement. E.g. for $\sigma^\pm$ polarized light the $|1,\pm1\rangle$ state will be bright and for V/H polarized light the $|1,+1\rangle \pm |1,-1\rangle$ state.

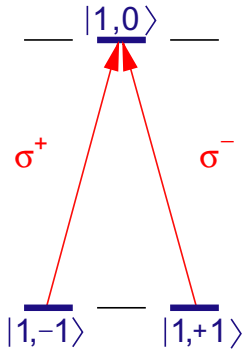

Figure 3.3: Choice of the measurement basis for the atom

After the excitation we have to make a projection measurement of the atomic state (whether the atom is excited to F' = 1 or still in the ground state F = 1). One possibility would be to wait for a decay from F' = 1 to the ground state by looking for the emitted photon of this process. But if we detect no photon we will not know if the atom had been in the F = 1 ground state or if we were just unable to detect the photon because of the limited collection efficiency of our collection optics.
So for a high detection efficiency we have to think of another way to detect the internal atomic state. A good possibility for such a hyperfine state detection scheme for the atom is the closed $F = 2 \rightarrow F' = 3$ transition (this transition is closed because atoms in $F' = 3$ can only decay back to $F = 2$ because of the conservation of the angular momentum (selection rules)). Therefore we have to make a highly efficient transfer from the chosen superposition to the other ground state F = 2. A solution for this transfer is to use the STIRAP process.

In this chapter I will describe in detail all necessary experimental steps for the creation and verification of the entangled state. To prepare and measure the single atom it is necessary first to trap and cool the atom (§3.1). If a single atom is detected in the trap by observation of fluorescence light induced by the cooling beams it has to be prepared to the initial state (§3.2). After the observation (and polarization measurement) of a single photon emitted from the atom we know that an entangled state between the atom and the photon had been created (§3.3). So finally a state selective measurement of the atom has to be carried out (§3.4). For a Bell measurement this procedure has to be repeated several times to get good statistics and in two different measurement bases for each particle. A final scheme summarizing this chapter is presented at the end (§3.5). Several properties concerning ^{87}Rb, including a term scheme of the D line hyperfine transitions, can be found in appendix A.

Since we compensate the external magnetic field we have (nearly) no magnetic field in the trap region so we are free in the choice of the quantization axis of our system. So let us choose for the quantization axis the direction from where we observe fluorescence light coming from the trapped atom. In our case this is the z-direction defined by the position of the atom and the microscope objective. More details on the directions and the corresponding optical polarizations for the atom can be found in appendix B.

3.1 Cooling and Trapping

The first step towards atom-photon entanglement is to get a single atom in a dipole trap. Therefore we shine in a strong (up to 80 mW) far red detuned laser focussed to a small waist (about 3.5 μm) from the positive z direction (the big red beam in Fig. 3.4). Due to this laser we get a dipole force towards the point with the biggest intensity of light. And to catch the atoms within the conservative dipole potential they have to cooled.
This is done with a cooling (CL) and a repump (RP) laser in a 3D configuration. Two cooling beams are applied counterpropagating from the x direction and another two pairs of counterpropagating beams in the z-y plane. The cooling laser is detuned by 4 to 5 line widths to the red of the D_2 transition $F = 2 \rightarrow F' = 3$. This transition between $F = 2$ and $F' = 3$ is closed and therefore ideal for cooling. But there is always some residual probability to excite

a population to $F' = 2$ or $F' = 1$. From $F' = 1, 2$ there is a possibility for the atom to decay to $F = 1$ and so out of the cooling cycle.
To pump the atom back into the cooling cycle the so-called repump laser is used. It is resonant on the $F = 1 \rightarrow F' = 2$ transition and will transfer population from $F = 1$ back into $F = 2$.

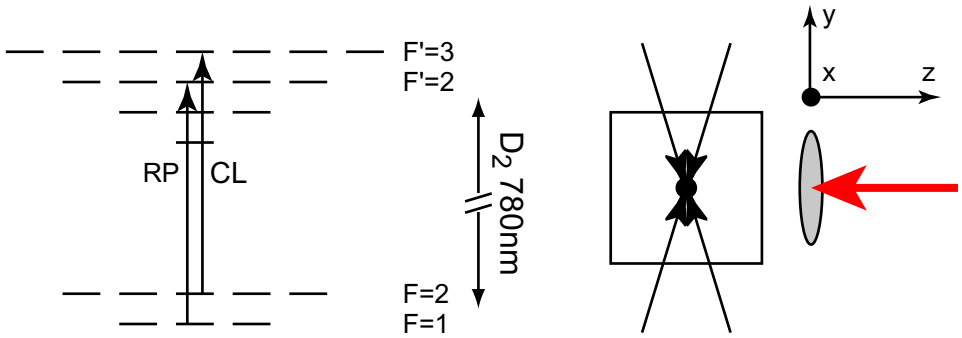

Figure 3.4: Cooling and MOT

Only atoms being slow can be cooled in the dipole potential. Due to the Maxwell velocity distribution it happens in every background gas that a few atoms are cold enough. But this are quite rare cases. So to get more cold atoms near the dipole trap we use the MOT to collect some atoms in the region of the trap center. For the MOT we use the same laser beams as used for cooling and the magnetic quadrupole-field of the MOT is produced by two antiparallel magnetic coils. By this configuration it is possible to collect a cloud of cold atoms (~ 30000) around the dipole trap.

3.2 Preparation of the Initial State

To prepare the atom in the initial state $|\psi_i\rangle = |F' = 1, 0\rangle$ we could pump for example the whole population to $|F = 1, -1\rangle$ and excite it by a σ^+-polarized π-pulse to $|F' = 1, 0\rangle$. But for this scheme σ^+-polarized light has to be applied and this is only possible in z-direction and we would saturate our single photon detectors.
A way without the necessity to excite in z-direction is to prepare the atom by dark state pumping with $H = (1/\sqrt{2})(\sigma^+ + \sigma^-)$ polarized light into the state:

$$\frac{1}{\sqrt{2}}(|1, -1\rangle + |1, +1\rangle) \tag{3.2}$$

For the orthogonal polarization $V = (1/\sqrt{2})(\sigma^+ - \sigma^-)$ polarized light this dark state can be excited and is pumped to $|F' = 1, 0\rangle$. This scheme works without any light in z-direction so it is the process of our choice.

3.2.1 Dark State Pumping

To pump the atom to the $|F = 1, \pm 1\rangle$ state H polarized light is applied on the $F = 1 \rightarrow F' = 1$ transition. By this light any superposition of the F = 1 ground states will be

excited except the superposition of equation (3.2). After a while all population in $F = 1$ will be pumped into the dark state.
But there is also a probability for a decay from the excited state $F' = 1$ to the ground state $F = 2$. Therefore a second laser on the transition $F = 2 \rightarrow F' = 1$ is used to pump the population back.

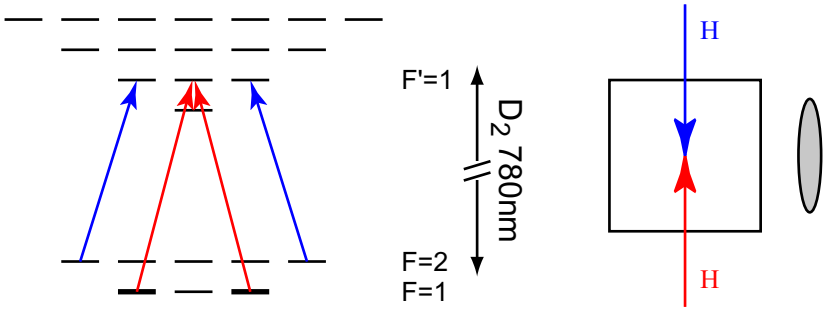

Figure 3.5: Dark state pumping

3.2.2 Excitation to Prepare the Initial State

The state in equation (3.2) is bright for V polarized light (the orthogonal superposition of σ^+ and σ^-). So by shining in a short V polarized π-pulse it is possible to pump the whole population of the atom to $|F' = 1, 0\rangle$. To minimize the coupling of laser light into the detection optics this pulse is applied in x direction. As the spontaneous decay should happen after the excitation the π-pulse should be completed in a time shorter as the lifetime (~25 ns) of the excited state. To do this a maximal pulse duration of a few nanoseconds is necessary.

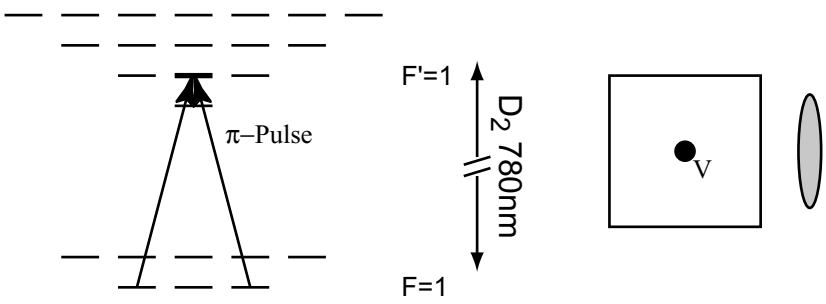

Figure 3.6: Excitation

3.3 Decay and Creation of the Entangled State

The decay is the process creating the entanglement. The atom decays from the initial state $|F' = 1, 0\rangle$ and emits spontaneously a photon conserving the angular momentum. Therefore we get the entangled state (the factor of the terms result from Clebsch-Gordan transition coefficients):

$$\sqrt{\frac{3}{60}}|2,-1\rangle|\omega_2,\sigma^+\rangle + \sqrt{\frac{4}{60}}|2,0\rangle|\omega_2,\pi\rangle + \sqrt{\frac{3}{60}}|2,+1\rangle|\omega_2,\sigma^-\rangle + \\ + \sqrt{\frac{25}{60}}|1,-1\rangle|\omega_1,\sigma^+\rangle - \sqrt{\frac{25}{60}}|1,+1\rangle|\omega_1,\sigma^-\rangle \tag{3.3}$$

Due to the last two terms in equation (3.3) correspond to the $|\psi^-\rangle$ Bell state we want to use these terms as the entangled atom-photon state. To get rid of the other undesirable terms we can make a projection measurement of the photonic or atomic energy (therefore the large probability amplitudes of the desirable terms are an advantage). This can be done in our experiment either by applying a strong laser beam resonant to the transition $F = 2 \rightarrow F' = 3$ to kick out atoms of the trap in the $F = 2$ state or by filtering out the photons with the wrong wavelength by using an etalon. Since the time between the creation and the verification of the entanglement shouldn't be too long (because of decoherence) the second approach is the better one.

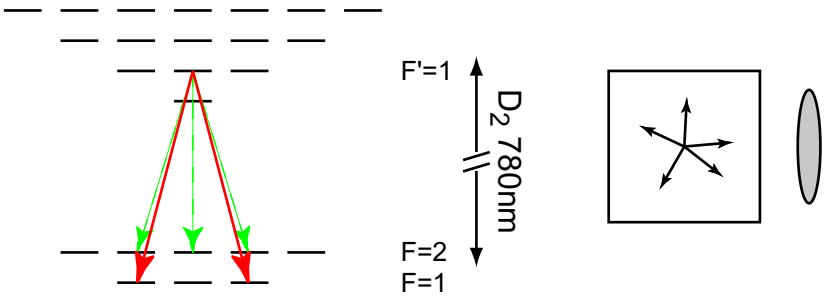

Figure 3.7: Decay resulting in the creation of an atom-photon entangled state

A time dependent relative phase $\Phi(t)$ is the result of the different time evolution of the two atomic states because of residual magnetic fields. This relative phase can be calculated:

$$\Phi(t) = \frac{\Delta E \cdot t}{\hbar} \tag{3.4}$$

Therefore we get the entangled $|\psi^-\rangle$ Bell state:

$$|\psi^-\rangle = \frac{1}{\sqrt{2}}(|1,-1\rangle|\sigma^+\rangle - e^{i\Phi(t)}|1,+1\rangle|\sigma^-\rangle) \tag{3.5}$$

Another possibility to create an entangled atom photon state would be to prepare the atom to the initial state $|F' = 0, 0\rangle$. In this case the spontaneous decay will happen with equal probability to the three Zeeman ground levels and we get this entangled state:

$$\sqrt{\frac{1}{3}}|1,-1\rangle|\omega_1,\sigma^+\rangle + \sqrt{\frac{1}{3}}|1,0\rangle|\omega_1,\pi\rangle + \sqrt{\frac{1}{3}}|1,+1\rangle|\omega_1,\sigma^-\rangle \tag{3.6}$$

To reduce this state to a two qubit Bell state the method of spectrally filtering (mentioned on the last page) is not possible as all photons and atomic states have equal energy. But the different polarizations of the emitted photons enable us to filter spatially. The light from the decay to $|1,0\rangle$ is π polarized and the dipole radiation characteristic of π polarized light is minimal in the direction of the axis of the dipole (in our case the z direction). Therefore the ratio of σ to π polarized light in z direction is about 0.77 % [26] and we can filter out the undesirable photons. But this is only a result of our directed collection (with 4π detection optics we wouldn't be able to filter out the events) and therefore the first approach is the much better one.

Figure 3.8: Another possible way to create atom-photon entanglement

After spatial filtering and taking into account the time developement of the atomic states we get this entangled $|\psi^+\rangle$ Bell state:

$$|\psi^+\rangle = \frac{1}{\sqrt{2}}(|1,-1\rangle|\sigma^+\rangle + e^{i\Phi(t)}|1,+1\rangle|\sigma^-\rangle) \tag{3.7}$$

So by choosing the initial state for the spontaneous decay we can choose wether we want to create a $|\psi^-\rangle$ or $|\psi^+\rangle$ state by changing the frequency of the exciting laser (this is possible in real-time).

3.4 State Selective Detection of the Atom

3.4.1 State Selective Transport by STIRAP

This step is necessary to choose the measurement basis for the atom. Therefore a laser on the transition between $F = 1$ and $F' = 1$ is applied. By choosing the polarization of this laser we choose which superposition of $|1,-1\rangle$ and $|1,+1\rangle$ is bright and can be coupled to $|1,0\rangle$. And as we have to apply several superpositions of σ^+ and σ^- polarized light this has to be done in z direction with the small disadvantage that our photo detectors will be saturated for a short time after this step (about 1 µs [66]). To reduce this effect it is necessary to filter out the light from the state selective transfer and to let fluorescence light and light from the decay through. This is possible by using the D_1 transition for the state selective transfer and an interference filter suppressing light at 795 nm by a factor of about 7,700.
For the final measurement we could use the photon from the decay from $F' = 1$ but as we want the detection of the atom to be highly efficient we use a two photon transition from F = 1 to F = 2 by using the STIRAP technique described in §2.4. Therefore the two photon transition is not very sensitive to several light pulse parameters and we can use the closed transition $F = 2 \rightarrow F' = 3$ to detect the atom.

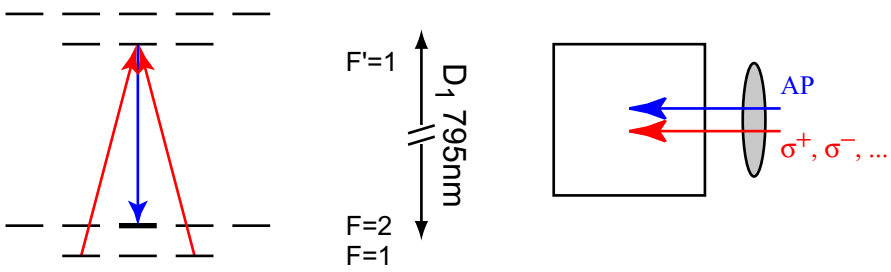

Figure 3.9: State selective transport

As I mentioned in the STIRAP process first the levels $F = 2$ and $F' = 1$ are coupled by a laser pulse and finally the selected superposition of $|1,-1\rangle$ and $|1,+1\rangle$ is emptied by a partially overlapping second laser pulse coupling the levels F = 1 and F' = 1.

3.4.2 Detection of Hyperfine State

For the final measurement we have to distinguish between the atom being in the state F = 2 or in the state F = 1.

Cycling: To decide whether the atom is in F = 2 or F = 1 it is possible to use fluorescence light from the transition $F = 2 \rightarrow F' = 3$. This transition is closed and to prevent any possible excitation to $F' = 2$ (this time we can not use a re-pump laser) we use right circular polarized light. By using right circular polarized light the population of the atom will oscillate between the two states of the closed cycling transition ($|2,2\rangle$ and $|3,3\rangle$).
The fluorescence light we will collect from the cycling process is limited by our collection efficiency. Therefore we have to measure long enough (order of magnitude: 10 ms) to get a good detection efficiency.

We have to use σ^+ polarized light to drive the closed cycling transition. This means that we have to apply the light in z direction and so we would saturate our detector. But as no magnetic field splits the Zeeman levels we can choose the quantization axis free. Therefore we can choose the y direction as quantization axis and shine in the cycling laser from this direction. The only thing we have to be aware of is the fact that the population of all Zeeman sublevels for every hyperfine state are redistributed by changing the quantization axis.
After the state selective transfer the atomic population is in a superposition of the F = 2 states and due to the σ^+ polarized light we will transfer all $F = 2$ populations (after a few scattering events) to higher magnetic quantum numbers (every scattering event increases approximately m_f by one). So finally all population of $F = 2$ will be in the cycling transition and only during the first scattering events there exists a small possibility of a transition to $F' = 2$.

But there are some another points which limit this cycling process:
1. The cycling laser will produce a momentum carry by radiation pressure from one side and this would kick the atom out of the dipole trap. So we have to apply two laser beams with well-balanced intensity in y direction with equal polarization for the atom.
2. By using two beams adjusted in intensity the atom is cooled in this direction but in the other two spatial directions (the x-y plane) we get statistical heating (random walk). As we want the atom to remain during the whole cycling process in the trap (at least) the laser power is limited to minimize the heating.

If it is possible to overcome all those difficulties cycling is a possibility for a hyperfine state detection of the atom. The advantage of this cycling process is that we don't have to wait till another atom is loaded into our dipole trap.

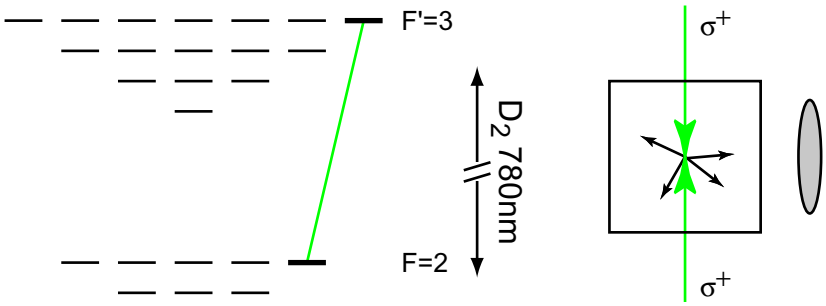

Figure 3.10: Atom detection by using the closed cycling transition

State Selective Kick Out: As the cycling process is fairly critical on several parameters it is reasonable to think of alternative ways for the detection of the hyperfine state.
We take one bright beam resonant to the transition $F = 2 \rightarrow F' = 3$ from one direction. In this case the radiation pressure will kick out atoms being in the $F = 2$ states and those in the $F = 1$ state will remain in the trap. So if we look (by detecting the fluorescence light from cooling and repump laser) whether the atom is still in the trap after this kick out pulse we can distinguish the state of the atom (if there is an atom left it was in the F = 1 ground state if no atom is left it was in the F = 2 ground state). Before repeating this experiment we have to wait for a new atom to be loaded into the trap every time we have kicked the atom out of the trap. Therefore this destructive way of detection leads to longer measurement times. This procedure is easy to implement.

3.5 Experimental Sequence

This flowchart displays the experimental sequence and the time needed for the single steps:

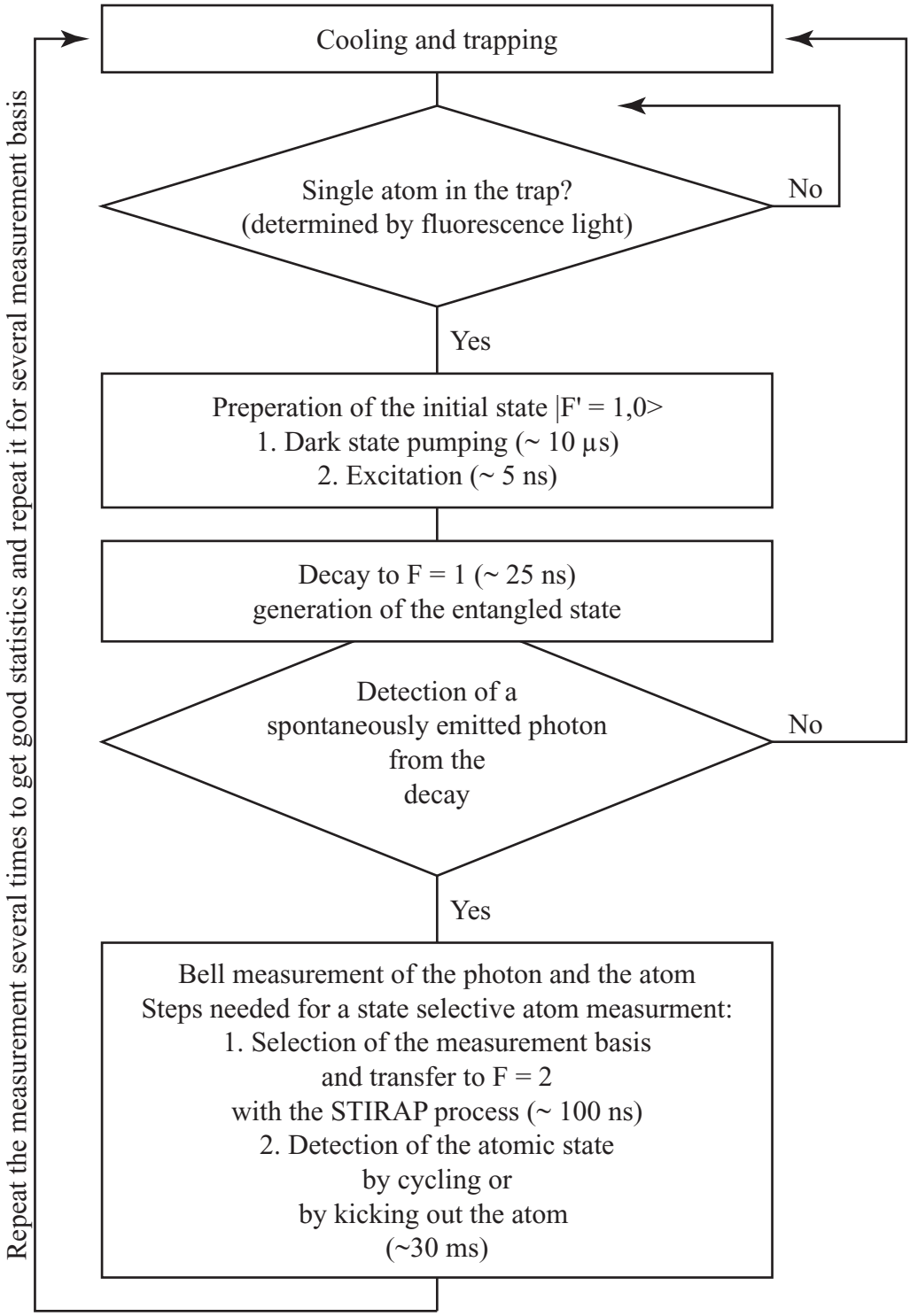

4 Experimental Setup

For the experimental realization of atom-photon entanglement it is essential to have a single localized atom and to apply several laser beams for preparation and detection of internal atomic states. To get localized ^{87}Rb atoms it is necessary to trap them. As we use an optical dipole trap the dipole trap laser and the necessary cooling beams have to be applied. To reduce the probability of scattering events with other undesirable atoms the mean number atoms has to be (nearly) zero. For this purpose we use an ultra high vacuum with built in rubidium dispenser to get a few ^{87}Rb atoms in the trap. To apply the dipole trap laser and to detect fluorescence light (from the atom) from the same direction a confocal microscope is used.
As proposed in the second chapter for the creation of the spin entangled state it is necessary to prepare the atom in an initial state. Furthermore measurements to verify the entanglement in a so-called "Bell-type experiment" have to be carried out. For these preparation and measurement purposes multiple lasers are applied to the atom.
To gain information about important characteristics of the dipole trap (the number of trapped atoms, the lifetime and the mean kinetic energy of the atoms) measurements were performed.

4.1 Vacuum Chamber

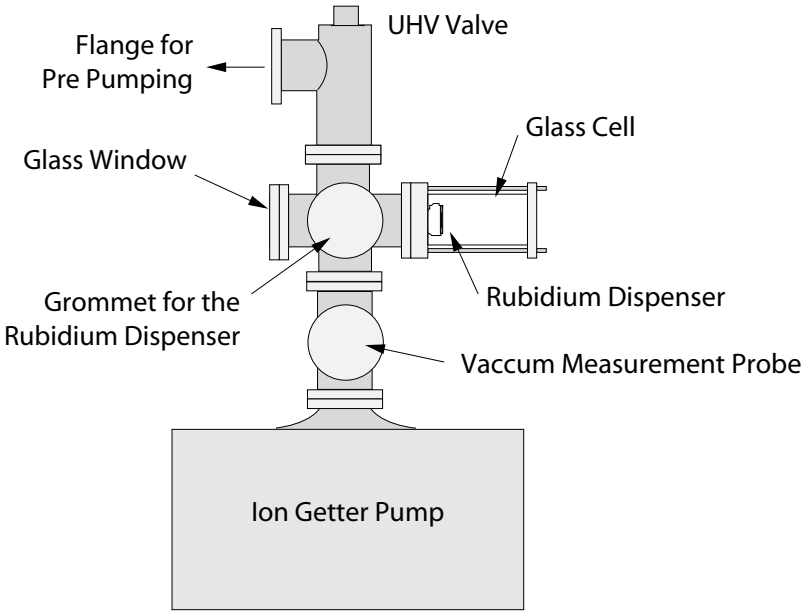

Figure 4.1: Schematic drawing of the vacuum gadget in top view [24]

The vacuum chamber is built with standard ultra high vacuum (UHV) components. The experiment chamber itself is a glass cell (25 x 25 x 70 mm) connected to an ion getter pump sealed

by indium wire. After some pre pumping and heating the pressure in the chamber finally reached a pressure around 10^{-11} mbar (the lower limit of our vacuum measurement probe) with an ion getter pump.
The leak rate for this vacuum system is about $5 \cdot 10^{-11}$ mbar/s due to inner effects like degasifying and about $5 \cdot 10^{-14}$ mbar/s due to real external leaks. With this leak rates a pressure below 10^{-11} mbar with the ion getter pump is reasonable. Further details concerning the vacuum gadget are described in the diploma thesis of Karen Saucke [24].

To get rubidium atoms into the ultra high vacuum there is a rubidium dispenser built in the vacuum system. The dispenser consists of a mixture of RbCr and a reducing agent placed in a tube of stainless steel. If the dispenser is heated by an electrical current of a few ampere to a temperature of a few hundred degrees celsius a fast redox reaction happens and the rubidium atoms are released through a small aperture.

Figure 4.2: The Rubidium dispenser in the vacuum chamber

According to the data given by the manufacturer the release of rubidium starts at a current of about 3 A. Due to the fact that very few atoms in the vacuum chamber are sufficient in our case ($\sim 5 \cdot 10^{-11}$ mbar) the optimal value for the current is about below this lowest operating point (2.5 A). Therefore the lifetime of the rubidium-dispenser is much longer as given by the data sheet and we hope that it is possible to run the experiment for years without exchanging the dispenser.

4.2 The Single-Atom Trap and its Optics

4.2.1 Setup of the Confocal Microscope and the Single-Atom Trap

With the confocal detection arrangement in Fig. 4.3 it is possible to collect light from the atom and to shine in the dipole trap laser at the same time. Since the same objective is used for both purposes the focus of the dipole trap laser can easily be adjusted to the same point as the fluorescing atom.
To separate the incoming dipole trap laser and the outgoing fluorescence light a dichroic mirror is placed in the beam which reflects the trapping laser at 856 nm and transmits light at 780 nm. So fluorescence light from the atom goes straight through the dichroic mirror and is coupled into an optical single mode fiber (used as a spatial filter to suppress stray light from the cooling beams) guiding the light to the detector (an avalanche photo diode (APD)). On the other hand the light coming from the dipole trap laser is reflected by the dichroic mirror and focused into the vacuum chamber by the microscope objective where the dipole trap is established.

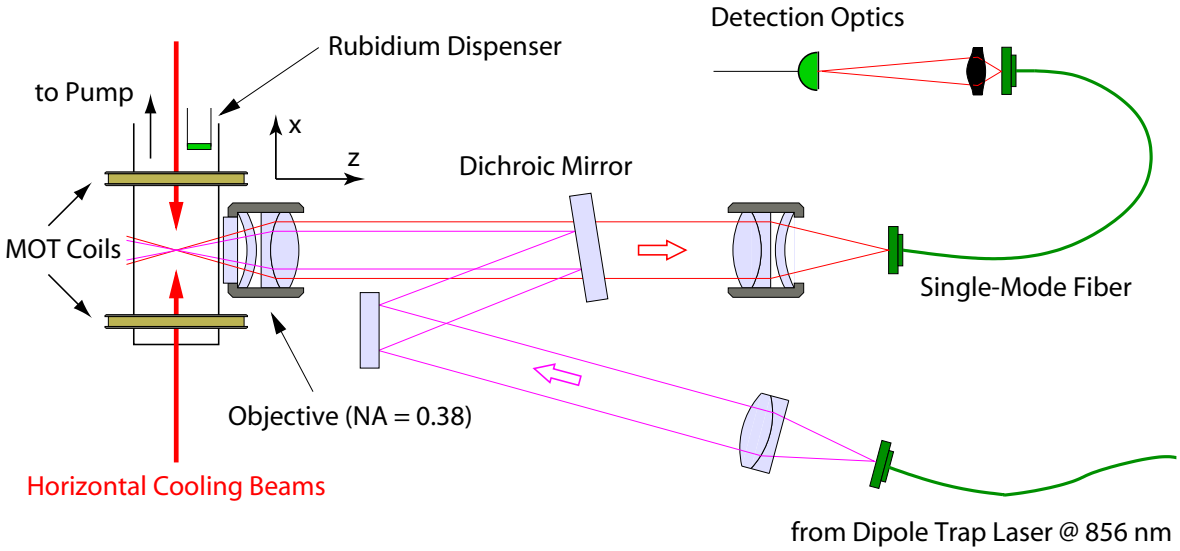

Figure 4.3: The trap setup seen from the top

The intensity of the dipole trap laser has to be large enough to get a sufficiently deep trapping potential and its frequency has to be far red detuned to the D line transitions of ^{87}Rb. Therefore we use a laser diode at 856 nm with a power of 175 mW. Due to losses (fiber, AOM and other optical equipment) we can apply up to 80 mW (about 44 mW correspond to a trap depth of 1 mK) at the position of the dipole trap. To get a localized high intensity we use the objective of the confocal microscope with a numerical aperture of 0.38 and the laser is focussed down to a waist of $3.5 \pm 0.2\ \mu\mathrm{m}$.
To cool atoms into the dipole trap the intersection point of the cooling beams (cooling (CL) and repump laser (RP)) has to overlap with the focus of the dipole trap laser. One pair of the counterpropagating cooling beams is applied in x direction and the other two pairs of beams are applied in the y-z plane with an angle of 17° to the y direction (see Fig. 4.5).

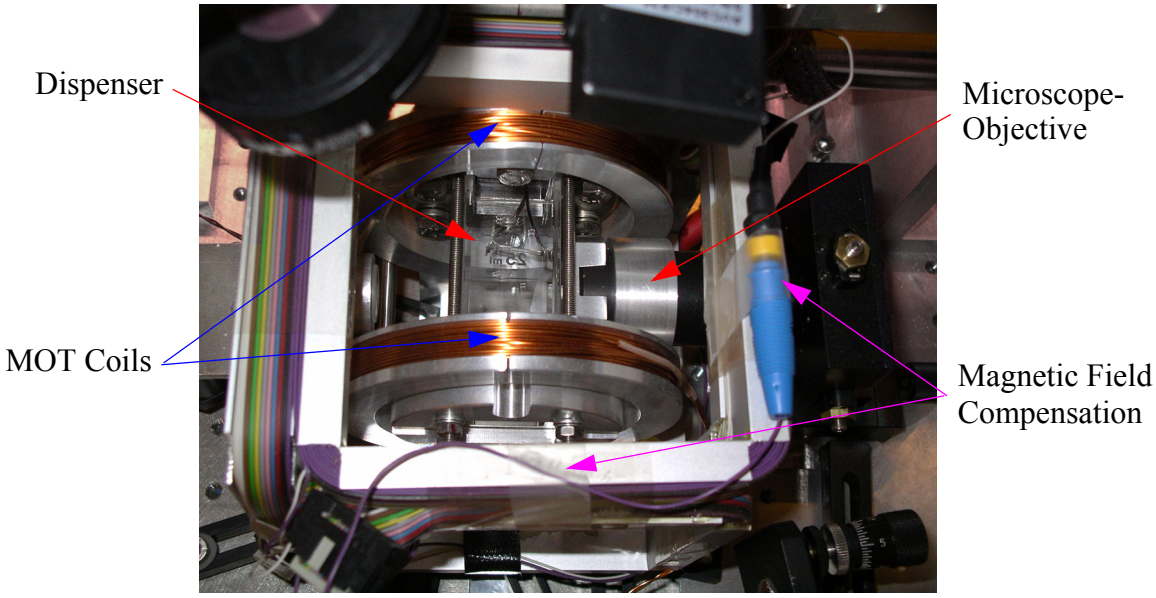

Figure 4.4: A close look on the trap from the top

Both lasers (cooling and repump) have to have a line width clearly smaller than the natural D_2 line width of ^{87}Rb (~ 6 MHz) and their absolute frequency has to be stable within this region, too. Therefore the light for both applications is generated by grating stabilized diode lasers at 780 nm. To lock their absolute frequencies we use saturation spectroscopy for the cooling beam but for the repump laser there is no fitting spectroscopy line. So it is locked relative to a master laser [62]. To switch the CL and the RP on and off both lasers pass an acoustic-optic modulator (AOM). Further details are described in appendix C and D and in the diploma thesis of Karen Saucke [24].

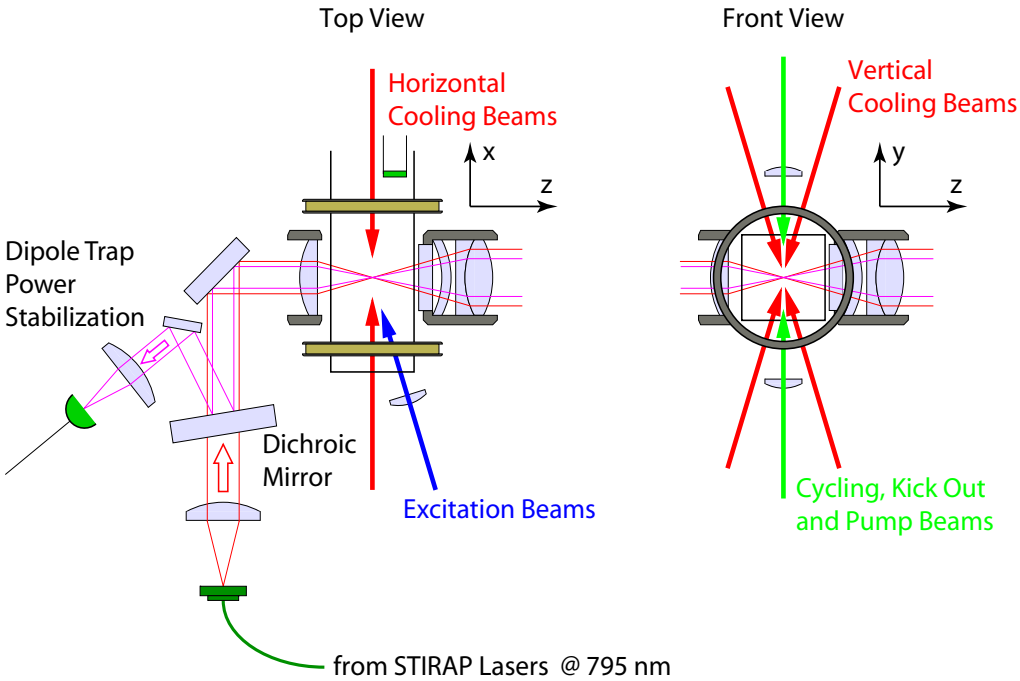

Figure 4.5: Schematic view of the setup with preparation and detection lasers

To provide a reservoir of cold ^{87}Rb atoms (to adjust the loading rate into the dipole trap) we use a shallow magneto optical trap (MOT). The MOT is formed by a magnetic quadrupole field (generated by the MOT coils) and the cooling beams. The optical dipole trap is located in the center of the MOT. By changing the magnetic field gradient of the MOT we can adjust the atomic density in the middle of the trap. Therefore it possible to adjust the loading rate of atoms into the dipole trap (from 0.1 - 0.2 s^{-1}, the MOT coils off, up to 1 atom per second at a magnetic field gradient of 1 G/cm).

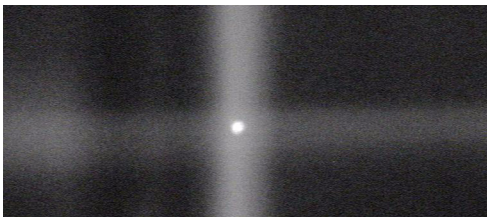

Figure 4.6: After aligning the MOT we observe a small cloud of cold rubidium atoms (the bright spot) and the fluorescence from the background gas in the cooling laser beams for a big magnetic field gradient with a CCD camera.

4.2.2 Setup for the Preparation and Detection Lasers

For the preparation of the initial state for the atom-photon entanglement the two pumping laser beams (for preparing the atom into a superposition of $|1, 1\rangle$ and $|1, -1\rangle$) have to be applied with horizontal and the excitation laser beam (to prepare the atom in the excited state $|F' = 1, 0\rangle$) with vertical polarization. To get H polarization the laser has to be applied out of the y-z plane and for V polarization in the x-z plane. The laser beams are generated from the cooling and repump laser diodes by using AOMs with different frequencies. For high transition probabilities the preparation lasers are focussed into the vacuum chamber. As illustrated in Fig. 4.5 the pumping beams are applied in y direction and the excitation laser is applied at a small angle to the x axis. As the excitation pulse has to be finished in a timescale shorter than the lifetime of the atom in the initial state it is necessary to use a fast optical switching device – the EOM (see appendix D.2).

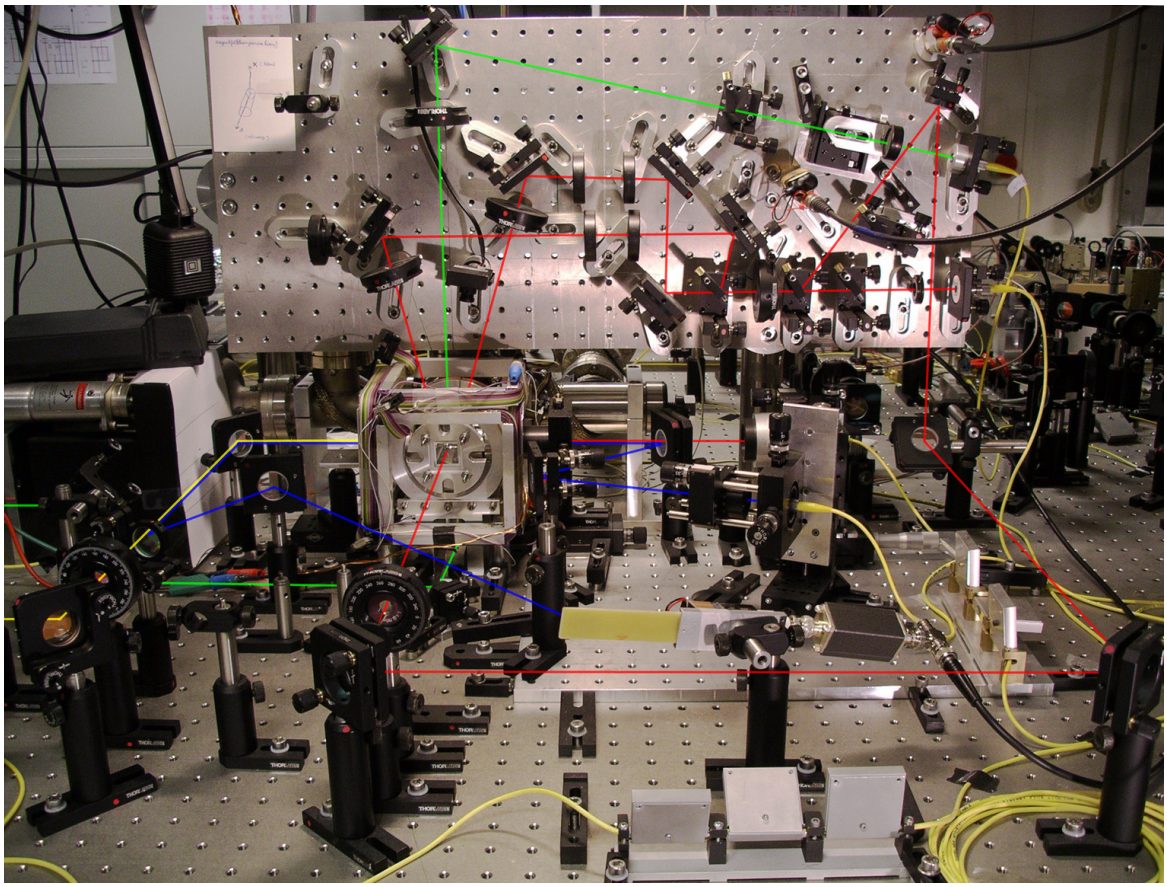

Figure 4.7: A picture of the experimental setup (red: cooling lasers and fluorescence light from the atom, green: cycling, kick out and pump lasers, blue: dipole trap laser and yellow: STIRAP lasers)

To select the atomic measurement basis by using the state selective transfer for the test of Bell's inequality we have to be able to shine in any superposition of σ^+ and σ^- polarization. This is only possible from z direction. The light for the STIRAP lasers has to be resonant to the D_1 lines of ^{87}Rb and as the frequency of the two necessary transitions is separated by

6.8 GHz we have to use two lasers stabilized in frequency by using dopplerfree saturation spectroscopy. Furthermore the intensity of the STIRAP lasers used for this state selective transfer has to be high to run the process adiabatically. For this we use a second objective (f = 40 mm – mounted opposite to the microscope objective) to focus the STIRAP laser beams to a waist of about 10 µm at the position of the atom. Since the same objective is used to collect the light from the dipole trap laser for power stabilization a second dichroic mirror is used to separate the two beams.
For the final state selective measurement on the closed transition between $|F = 2, 2\rangle$ and $|F' = 3, 3\rangle$ (by using the cycling or kick out procedure) the light has to be applied circular polarized in z direction and is generated by the same laser as the CL.

4.3 Characteristics of the Dipole Trap

4.3.1 Fluorescence Light from the Dipole Trap

To load atoms into the dipole trap we switch on the cooling and repump laser of the MOT and measure the fluorescence count rates from the dipole trap. Every time an atom is cooled into the dipole trap we observe an increase of the detected fluorescence count rates from 500 s^{-1} – corresponding to the dark count rate of our detector – to a value of 2200 s^{-1} for a single atom (see Fig. 4.8) by counting (integrating) the events of photo diodes in a certain timebin. Therefore it is possible by choosing the timebins long enough to distinguish between zero, one, or more than one atom in the trap. A blockade mechanism due to two-body collisions assisted by cooling light locks the maximum number of trapped atoms to one [35] for a weak confinement of atoms near the dipole trap. This effect leads to a sub-poissonian occupation statistics of our trap with a maximal duty cycle of one atom to no atom of 0.5.

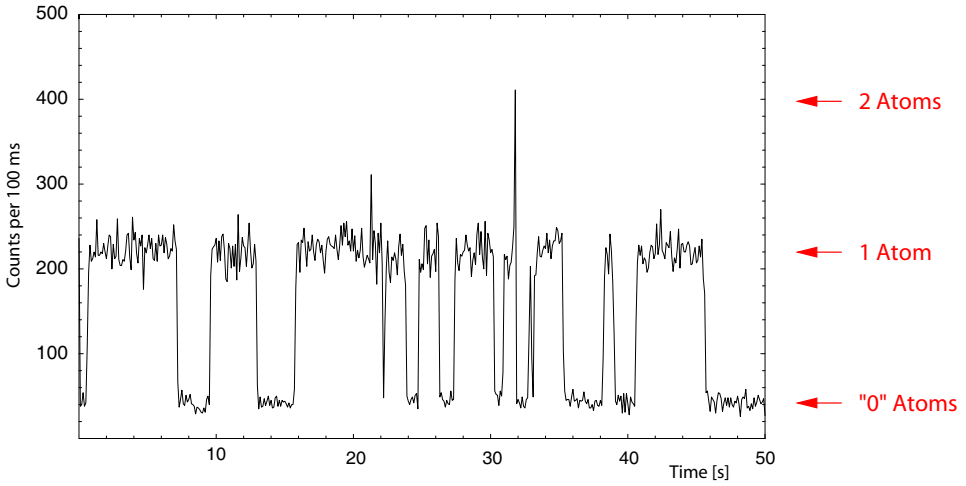

Figure 4.8: Fluorescence countrate for a trapdepth of 0.6 mK integrated over 100 ms and measured with 2 APDs. The “0” atoms count rates are equal to count rates of the background of the APD including background light and real dark counts from the diode. Further “quantized” steps can be seen and we can interpret the first step as scattered light from one atom and the second step could be scattered light from two atoms (1800 counts/s per atom).

By counting the events in certain timebins it is possible for the computer the decide if an atom is in the dipole trap. Therefore the computer is able to start measurements of the single atom if it is in the trap.
By counting the timespans atoms stayed in the trap we were able to observe the maximum lifetime in the presence of cooling light of 2.2 ± 0.2 s.

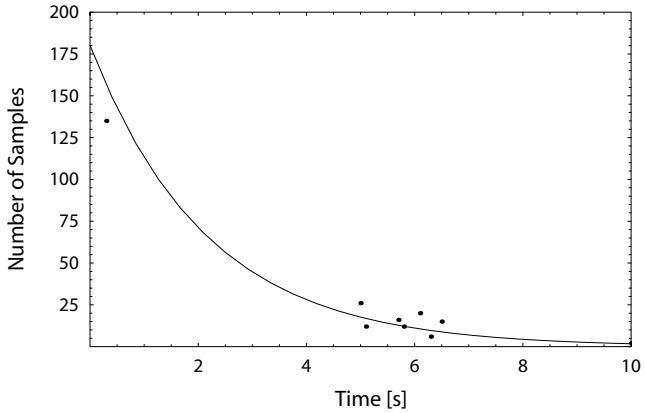

Figure 4.9: The lifetime of the single atom in presence of the cooling light

4.3.2 HBT Measurement to Determine Photon Statistics

To assure that only a single atom was trapped, the second order correlation function $g^{(2)}(\tau)$ of the fluorescence light was measured with a standard Hanbury-Brown-Twiss configuration (Fig. 4.10) by histogramming the differences of detection times $\tau = t_1 - t_2$ of photon pair events. To minimize background contributions the coincidences are only acquired at times we observe fluorescence higher than 1200 s^{-1}. A normalized distribution of time differences τ is equivalent to the second order correlation function as long as τ is much smaller than the mean time difference between two detection events [39].

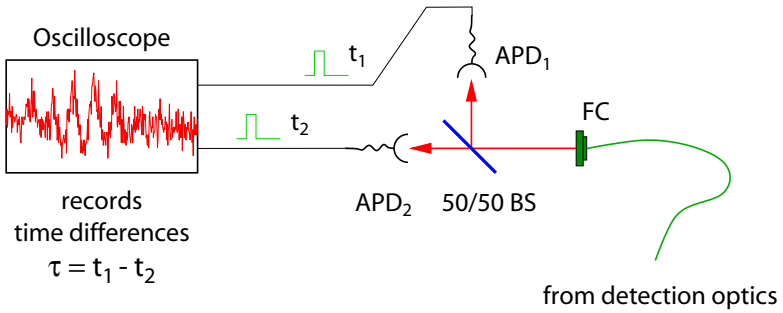

Figure 4.10: The light coming from the detection optics is split up with a 50/50 beamsplitter into two APDs and the time difference between an event in the first and the second APD is measured and histogrammed.

The measured $g^{(2)}(\tau)$ function is displayed in Fig. 4.11 and at the time difference $\tau = 0$ a value corresponding to the dark count rate can be seen. This is a clear sign for photon antibunching. We obtained an uncorrected minimum value $g^{(2)}(0) = 0.52 \pm 0.14$ for a trap depth corresponding to 520 µK and a cooling laser intensity of about 100 mW/cm^2. This value

can be explained only by accidental coincidences due to the dark counts of each detector (300 s^{-1}). Within our experimental errors this is compatible with perfect photon anti-bunching. To get single photons at time t only one source creating a photon by a physical process is allowed and perfect photon anti-bunching is the result of such a real single photon source. Since two (or more) atoms would be able to send out two photons at the same time $g^{(2)}(0)$ would be raised to 0.5. Therefore we have to have a single atom in our trap.

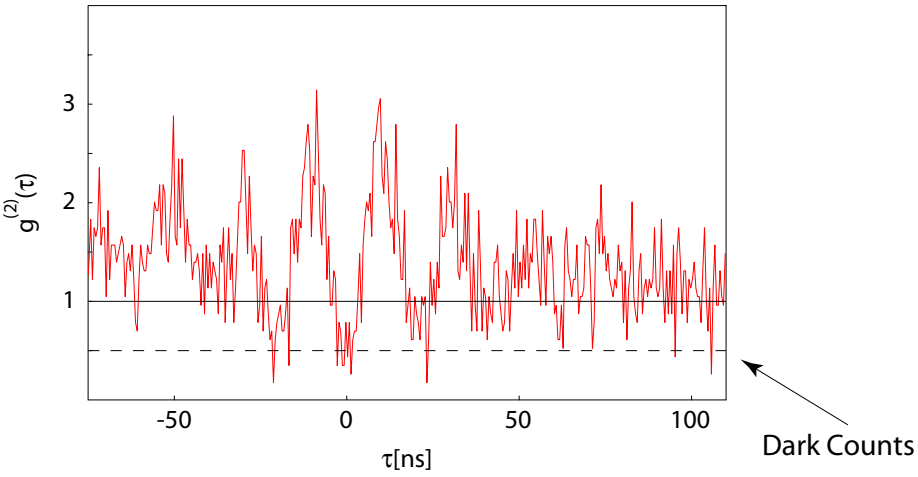

Figure 4.11: HBT signal showing clear photon anti-bunching at τ = 0 and a signature of Rabi oscillations (Ω/2π = 48 MHz) [25]

Due to the coherent interaction of the cooling and repump laser fields with a single atom we observe the signature of Rabi oscillations in $g^{(2)}(\tau)$, which are damped out on a timescale of the excited state lifetime (26.2 ns). Increasing the dipole laser power from 23 mW to 48 mW without changing the laser cooling parameters increases the AC Stark-shift of the atomic levels in the dipole trap laser field. The resulting raise of the detuning of the cooling lasers was observed as the expected increase of the oscillation frequency from 48.5 MHz to 63 MHz.
On a µs timescale the correlation function shows an exponential decay from the asymptotic value around τ = 0 of 1.2 to 1.0 for large τ with a time constant of 1.8 and 2.9 µs, respectively, for the two dipole laser powers. This bunching effect can be explained by the diffusive atomic motion in the intensity-modulated light field of our three-dimensional cooling beam configuration [37]. The three-dimensional modulation of the intensity of the light happens on the scale of the wavelength of the lasers. As the wavelength is about 780 nm we will have several "bright" and "dark points" within the focus of the dipole trap laser (w_0 = 3.5 µm).
An atom in the region of a "bright spots" will emit a second photon with a higher probability. So as the $g^{(2)}(\tau)$ function is measured over a spacelike area corresponding to the mean kinetic energy of the atom in the trap including equal "bright" and "dark points" the $g^{(2)}(\tau)$ will be raised for short timescales.
If an atom happens to be at a bright spot and the second photon is not sent out after a short time the atom will be able to move during this time to a "dark spot". Therefore we will get for a time proportional to the movement of the atom an exponential drop of the $g^{(2)}(\tau)$ function to a value of one corresponding to independent photon detection. So after a time at 1.8 µs the atom will move from a "bright" to a "dark spot" what corresponds to a very roughly estimated mean

kinetic energy (temperature) of the single atom of 160 µK. (Calculated by the simple estimation of the single atom moving half the wavelength in 1.8 µs). Certainly the error for this "temperature" is much too high but as we will see later this estimation isn't so bad either.

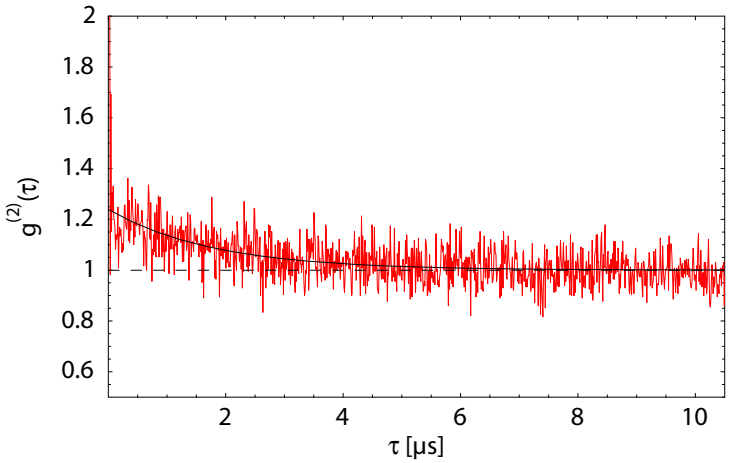

Figure 4.12: Photon pair correlation function on a µs timescale [25]

Our experimental results on the short timescale are incompatible with a simple two-level model, which predicts oscillations of $g^{(2)}(\tau)$ up to a maximum value of 2. In our case we use a weak intensity of the cooling laser (CL) – red detuned to the hyperfine transition $F = 2 \rightarrow F' = 3$ of the D_2 line at 780 nm by 4-5 natural linewidths – and the repump laser (RP) on resonance with the hyperfine transition $F = 1 \rightarrow F' = 2$ (Fig. 4.13). Furthermore, the linearly polarized trapping laser field causes a negative AC Stark-shift of the ground and a positive shift of the excited state hyperfine levels. This significantly increases the probability for excitation of F' = 2 by the cooling laser and leads to a breakdown of the two-level assumption. In order to understand the observed correlation function, we extended the atomic level scheme to all hyperfine levels connected by CL and RP.

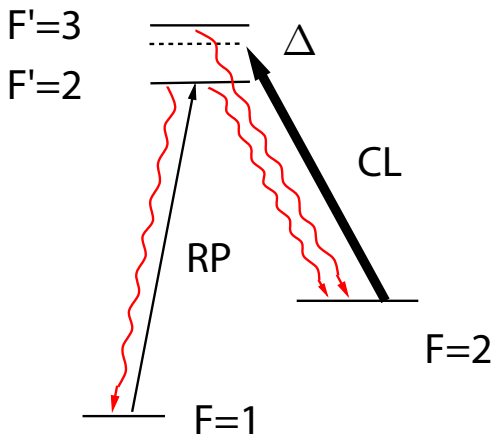

Figure 4.13: Partial level scheme of ^{87}Rb (four-level model) to explain the larger oscillations of the $g^{(2)}(\tau)$ function

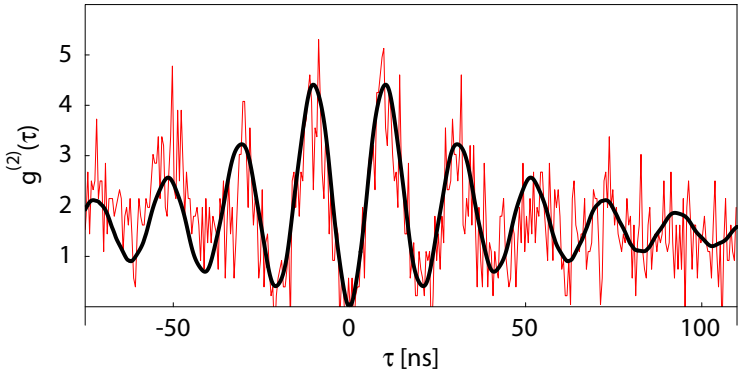

Figure 4.14: Intensity correlation function $g^{(2)}(\tau)$ (background corrected) of the resonance fluorescence from a single atom in the dipole trap. Solid line: fit with only one free parameter which takes into account the detuning of both lasers due to the AC Stark-shift of the atomic levels in the far off-resonant dipole trap laser field.
Experimental parameters: I_{CL} = 103 mW/cm^2, I_{RP} = 11.8 mW/cm^2, $\Delta/2\pi$ = –31 MHz. [25]

4.3.3 Temperature Measurement

Out of the measurement of the $g^{(2)}(\tau)$ function a rough estimation of the mean kinetic energy of the single atom was possible being an interesting parameter of the trap. For its destination we could make a time of flight measurement as done in many experiments concerning macroscopic samples of lasercooled atoms. But with single atoms such measurements would be quite difficult. So we looked for another way by measuring the fluorescence spectrum of the single atom.
The resonance fluorescence spectrum of the atom consists of an inelastic part called the Mollow triplet and the dominating elastic part (for our laser parameters as the intensity of the light is relative weak and as the light is far detuned) which is due to Rayleigh scattering [40]. The spectrum of Rayleigh scattered light is equal to the spectrum of the excitation laser. But due to the movement of the atom we expect some kind of doppler effect leading to an effective broadening of the fluorescence spectrum.

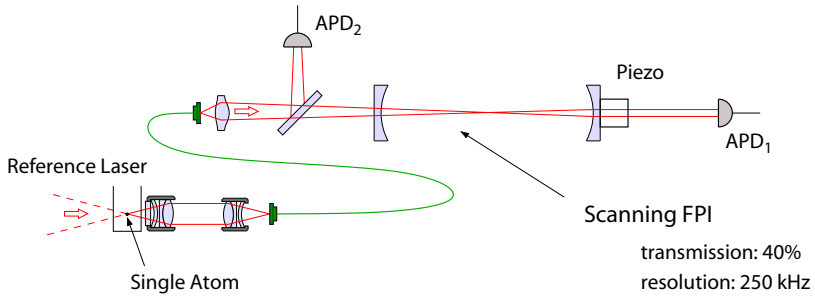

Figure 4.15: Scanning Fabry-Perot interferometer to determine the spectral properties of the emitted fluorescence light

The scattering spectrum is analyzed via a scanning temperature stabilized Fabry-Perot interferometer (FPI) with a frequency resolution of 0.45 MHz (full width half maximum), a transmission of 40 % and a finesse of 370. To check for the presence of an atom inside the trap a

part of the fluorescence light is monitored separately with a reference APD_2. Since the broadening is expected to be a small effect the instrumental function of the spectrometer and the exciting laser line width have to be known accurately. Therefore, we can shine a fraction of the exciting light into the collection optics (see Fig. 4.15). This way, both reference and scattered light are subject to the identical spectrometer instrumental function.
To reduce effects of cavity length drifts, the spectrum of the reference laser – equivalent to our cooling laser – and the light scattered only by the MOT laser beams were measured alternately. For each measurement a compensation of the cavity drift was performed by looking for the maximum transmission of the reference laser. This procedure was repeated many times to acquire a sufficient photon count statistics. With this procedure we obtained the two (normalized) data sets in Fig. 4.16 where we observe a width of 0.94 ± 0.01 MHz and 1.04 ± 0.01 MHz for the laser line and the fluorescence light, respectively. The error bars reflect the statistical error from the individual count rates of each data point. For the reference laser this error is too small to be visible in this graph.

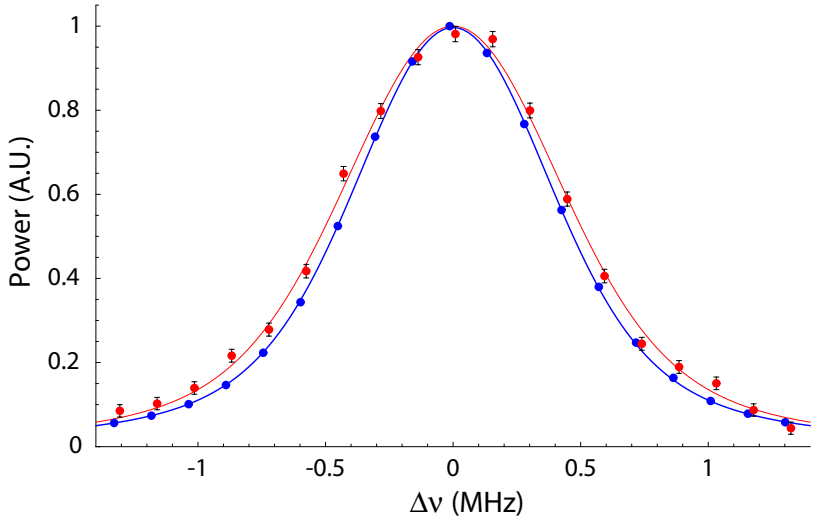

Figure 4.16: The atomic fluorescence and the laser light is analyzed alternating with the same scanning FPI. The spectra exhibit a width of 0.94 MHz and 1.04 MHz (FWHM) for the reference laser (blue) and the fluorescence light (red), respectively. The straight lines are Voigt profile fits to the data [25].

To extract a mean kinetic energy from these spectra, we assume the same stationary Gaussian velocity distribution in all directions. According to this assumption we convolute a Gaussian distribution with the measured reference laser line profile. The resulting function is fitted to the data points of the fluorescence spectrum with the variance of the Gaussian profile being the only free fit parameter [24]. From this fitted variance we directly obtain the mean kinetic energy E_{kin} of a single atom in the dipole trap of

$$\frac{E_{kin}}{k_B} = (110 \pm 15)^{+14}_{-24}\,\mu\mathrm{K} \tag{4.1}$$

with a statistical error of ± 15 μK for a trap depth corresponding to 400 μK. k_B denotes the Boltzmann constant.
The calculation of the mean kinetic energy results in a systematic error of +14/–24 because the cooling beams have different angles relative to the axes defined by the trap and the detection optics. The overall Doppler broadening of the laser line depends on these angles. Therefore, an upper bound for this error is estimated by assuming that the atoms scatter light only from the beams which would give the highest or lowest velocities, respectively. Within the experimental errors, the measured temperature is equal to or smaller than the Doppler temperature of Rubidium (146 μK).
The Doppler broadening of the fluorescence spectrum allowed us to determine the mean kinetic energy of a single atom. A final temperature of 110 μK of our loading process results in an effective line broadening of 4.5 MHz. This broadening is of the same order as the natural linewidth of 6 MHz and should allow the excitation of specific hyperfine levels.

5 Detection of the Hyperfine State

After the generation of the entangled atom-photon state the atom is state selectively transferred in the F = 2 hyperfine state or remains in the F = 1 hyperfine state. For the verification of entanglement the atom has to be measured in this basis. Therefore it is important to distinguish wether the atom is in the F = 1 or F = 2 hyperfine ground state. For this purpose it is necessary to think about possible ways for the detection. These considerations and the measurement results of two possible versions are presented in this chapter.

5.1 Detection of the Atom

To detect the hyperfine ground state F = 1 or F = 2 of a single ^{87}Rb atom with a light field it is reasonable to perform either a measurement of atoms in F = 1 or in F = 2 and to conclude for a negative measurement result that the atom was in the alternative state. Therefore the measurement process is not allowed to transfer any population between the two alternative ground states. So we have to use a closed transition. In ^{87}Rb there exist only two closed transitions: $\mathrm{F} = 2 \rightarrow \mathrm{F'} = 3$ and $\mathrm{F} = 1 \rightarrow \mathrm{F'} = 0$ are possible measurement transitions for the state detection of the atom as the decay to the alternative ground states is forbidden. Nevertheless excitations to F' = 2 and F' = 1 are in both cases not forbidden. Therefore a small and nonzero probability for excitations to undesirable states remains. Such wrong excitations can result in a pumping to the alternative ground state F = 1.
The only way to get a really closed $\mathrm{F} = 2 \rightarrow \mathrm{F'} = 3$ transition is to apply light with right or left circular polarization pumping the population within a few scattering cycles to the Zemann state $|\mathrm{F} = 2, +2\rangle$ or $|\mathrm{F} = 2, -2\rangle$, respectively. For all preceding scattering events the atom will undergo Rabi oscillations between $|\mathrm{F} = 2, \pm 2\rangle$ and $|\mathrm{F'} = 3, \pm 3\rangle$. If we use circular polarization an excitation to F' = 2 or F' = 1 is only possible during the first scattering events. This idea is not working for the $\mathrm{F} = 1 \rightarrow \mathrm{F'} = 0$ transition.
Further the transition $\mathrm{F} = 1 \rightarrow \mathrm{F'} = 0$ couples, depending on the polarization of the light, only a certain Zemann level of the ground state to the excited state and we are only able to detect all population in F = 1 by using light with σ^+, σ^- and π polarization. In addition the splitting of the hyperfine levels F' = 0 and F' = 1 is smaller as the splitting of F' = 2 and F' = 3 and so the probability for a wrong excitation is higher.
Therefore the transition $\mathrm{F} = 2 \rightarrow \mathrm{F'} = 3$ with applied right or left circular polarized light is better suited for our purpose.
As no magnetic field splits the Zeeman levels we can choose the quantization axis freely. Therefore we can shine in circular polarized laser light (driving the transition between $|\mathrm{F} = 2, \pm 2\rangle$ and $|\mathrm{F'} = 3, \pm 3\rangle$) from the y direction and consider this direction as the (new) quantization axis. By changing the quantization axis to the y direction we have to be aware of the fact that the population of all Zeeman sublevels for every hyperfine state are redistributed.

As we have seen the closed transition $F = 2 \rightarrow F' = 3$ is the best way for a state detection of the atom and the obvious idea to use fluorescence light from this closed Rabi oscillations is the first way of detection we have tested – the cycling procedure.
The other way for detection we have tested is to use this resonant transition for an effective way to transfer momentum from the photons to the atom. Therefore atoms resonant to the transition $F = 2 \rightarrow F' = 3$ will gain a big momentum in the direction of the incoming photons and will be kicked out of the trapping potential of the dipole trap. This procedure is similar to the case of a polarizing filter in optics which also removes a part of the photons from the light beam.

5.2 Preparation of the Initial State

To test the state detection the single atom has to be prepared to each of the two possible ground states. This is possible by the sequence of switching the cooling and repump laser off. The repump laser couples the ground state F = 1 to the excited state F' = 2 and the cooling laser couples the ground state F = 2 to the excited states F' = 2 and F' = 3. So by switching off one of the two lasers sooner one ground state will be bright and the other one will be a dark to the remaining light field. Therefore all population will be pumped into the dark state and by this dark state pumping we are able to prepare both initial states.
To prepare the atom to the F = 1 ground state the repump laser beams have to be switched off first and the cooling laser will pump the population to F = 1.

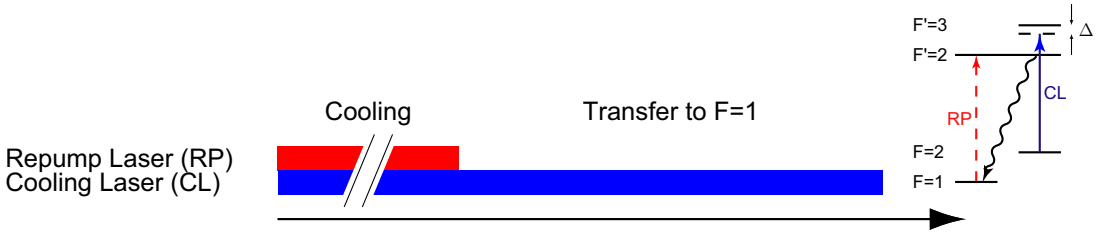

Figure 5.1: Initial preparation of the atom to F = 1

For the preparation of the atom to F = 2 the cooling laser beam has to be switched off first.

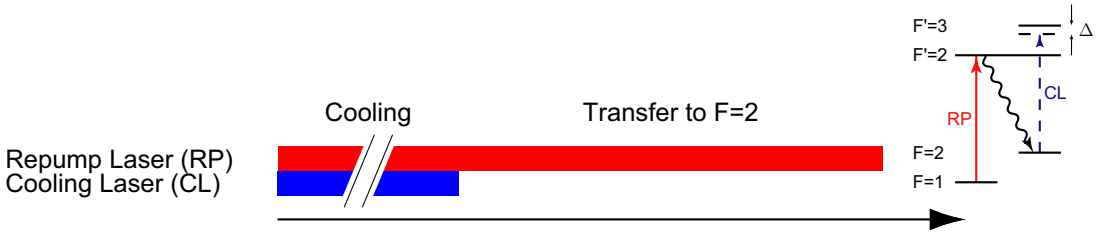

Figure 5.2: Initial preparation of the atom to F = 2

An appropriate timescale for this dark state pumping scheme is limited by the transfer to F = 1 as the off-resonant excitation to F = 2 is not a very probable event. Therefore after a time of about 4 ms we will get a satisfactory preparation efficiency for the preparation of both initial states (for the preparation of F = 1 a time of less than 1 ms would be sufficient, too).

5.3 Cycling

The first scheme tested for the hyperfine state detection of the single atom is detecting the fluorescence light from the cycling laser driving the transition between $|F = 2, 2\rangle$ and $|F' = 3, 3\rangle$ by using right circular polarized light. If fluorescence from this transition is observed the atom is in F = 2 and if not it is in F = 1. As every scattered photon transfers the momentum $\Delta\mathbf{p} = \hbar\mathbf{k}$ to the atom in beam direction it is necessary to reduce the gain of kinetic energy by a second counterpropagating laser beam balanced in intensity. In this configuration only a random walk of the atom in the remaining two dimensions is possible resulting in a statistical heating. Rough estimations have shown that we can scatter about 5000 photons until the kinetic energy of the atom reaches the value of our trap depth (1 mK) by this two dimensional random walk. Due to imperfections of the polarization of the applied laser field there exists also a probability for the excitation to $|F' = 2, 1\rangle$ and therefore the possibility of a spontaneous emission to F = 1. Once this happens the scattering of photons will stop instantaneously because the atom is now in a dark state. If the atom stays in the initial state F = 2 it should emit fluorescence light induced by Rabi oscillations.

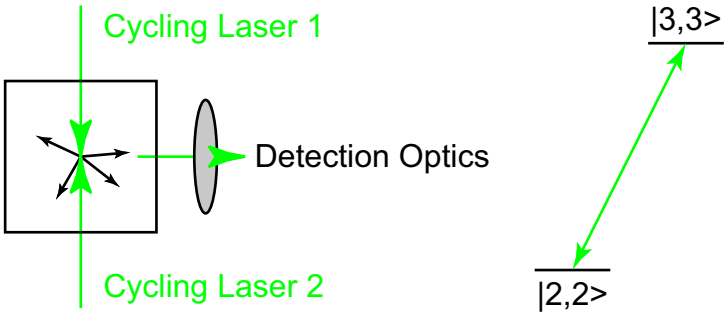

Figure 5.3: Front view of the trap with the cycling lasers applied from top and bottom

To use the cycling process to detect with a high efficiency whether the atom is in the F = 2 state it is necessary to have a good signal to noise ratio or in other words: the case of the atom in F = 2 has to be distinguished well enough from background counts of an atom in F = 1.

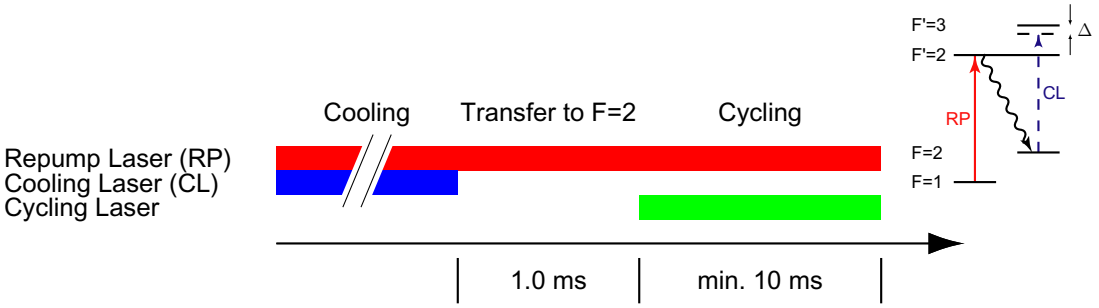

Figure 5.4: Scheme to test the cycling procedure

To get the ideal set of parameters for the cycling process we have to vary six free parameters: duration and detuning of both laser beams and polarization and intensity of each laser beam. To be insensitive to polarization errors in the first set of measurements the repump laser was

also switched on during the cycling process. By this step no possibility of pumping the atom into the F = 1 dark state exists.
To determine the best set of parameters we set the duration and the detuning to a certain value and scanned the intensity of the two beams in a certain reasonable area. For each pair of intensities the fluorescence light and the background light were measured alternatively for about 200 s. After an atom was detected in the trap due to fluorescence light of the cooling beams we switched off the cooling laser and the repump laser prepared the atomic population to F = 2 via dark state pumping. After 1 ms we switched on the cycling lasers (together with the repump laser) measuring the fluorescence counts during this process.
For the measurements a dipole trap about 0.9 mK was chosen (corresponding to a light shift of about 40 MHz). The detuning of the cycling laser was varied between −12 MHz and 6 MHz (for an atom outside of the trap) and the measurement durations were 10.10 ms and 25.25 ms.

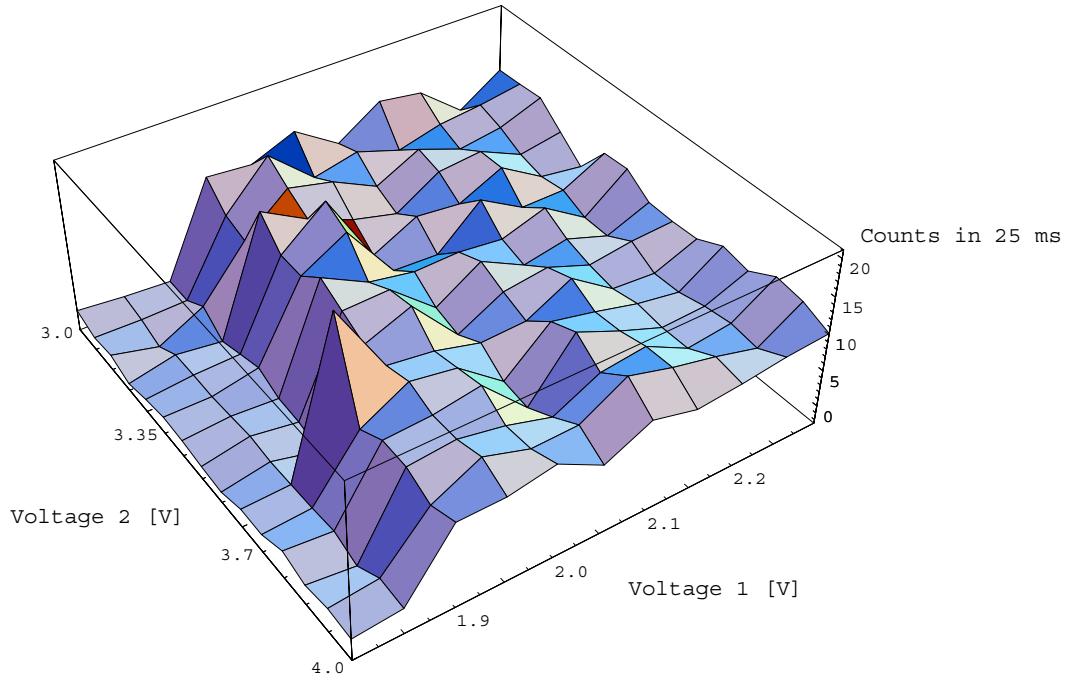

Figure 5.5: Countrate (background corrected) of a cycling test measurment with a duration of 25.25 ms and a detuning of one linewidth (−6 MHz) for each laser. The two voltages correspond to the amplitude of the sound wave propagating through the crystal of the AOM. Therefore they are proportional to the intensity of the lasers.

The highest countrate we obtained with this measurment was about s = 8 counts in 25.25 ms with a background countrate of about b = 12 counts for a duration of 25.25 ms and a detuning of one linewidth (−6 MHz) for each laser.

In our experiment we have to distinguish the total countrate being a result of fluorescence including dark counts or only of dark counts. To get a value for the minimal observation time (the time we have to drive the cycling transition) let us consider the worst cases: background counts are understood as fluorescence counts or vice versa. According to the poissonian statistics the standard deviation σ of the background counts b and the fluorescence counts s + b is

$\sqrt{b}$ and $\sqrt{s+b}$, respectively. For the experiment we have to define a fixed number of counts to distinguish the two cases. This limit has to be smaller as s + b – n σ and bigger as b + n σ to decide between fluorescence and background by n standard deviations.

$$\frac{s}{n} \geq \sqrt{b} + \sqrt{s+b} \tag{5.1}$$

In our experiment we observed 8 signal counts and about 12 background counts in 25.25 ms. This corresponds to an one σ decision – a proof with a detection efficiency of 68.3 %. So in 37.7 % of the cases we could have a fluorescing atom not being detected or vice versa. Furthermore we also observe a decrease in the lifetime of the atom in the trap from about 1 to 2 seconds (20 measurement cycles) without cycling lasers to 0.240 to 0.360 ms (4 to 6 measurement cycles) during the cycling process. To get a measurement with a detection efficiency of more than 95.5 % at least a 2 σ separation of the detected counts is necessary. With the measured count rates this would correspond to measurment times of more than 100 ms and would also result in further heating leading to a decrease of lifetime.

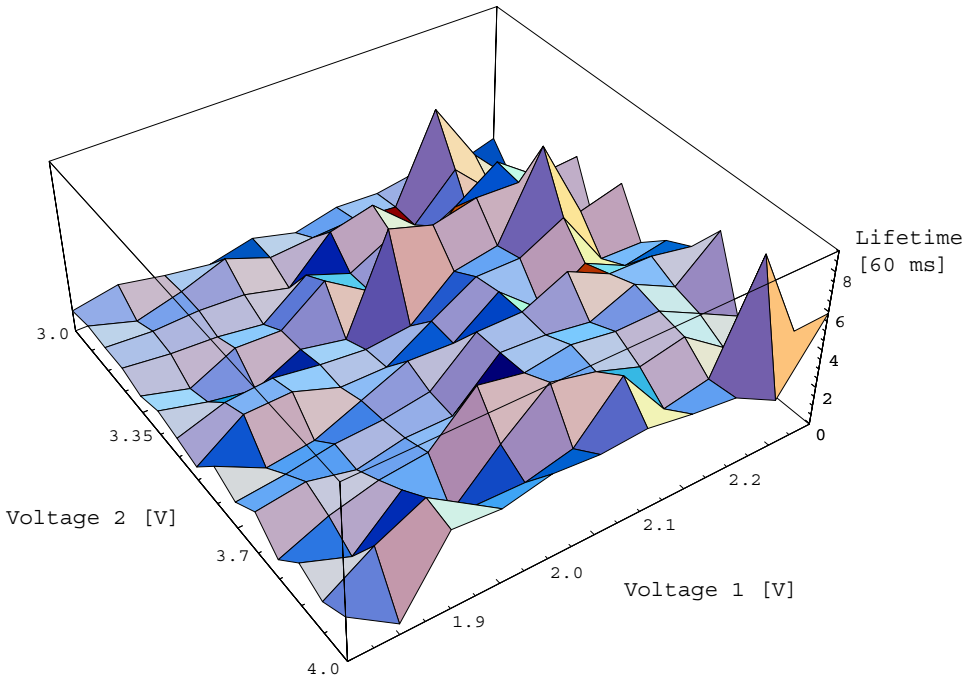

Figure 5.6: Lifetime of the atom in a cycling test measurment with a duration of 25.25 ms and detuning of one linewidth (–6 MHz) for each laser

The results of the measurements to test cycling for the hyperfine state detection of single atoms have shown that we are able to realize a 1 σ proof in 25.25 ms in the ideal case of no possible decay to F = 1 during cycling. For a more satisfactory 2 or 3 σ proof a longer measurement time would be needed (minimally 100 ms or 225 ms, respectively). But as the lifetime of the atom in the trap drops even in the 1 σ case to about 5 measurement cycles the atom will be most probable heated out of the trap after a longer cycling procedure.

5.4 State Selective Kick Out

The second scheme tested for the hyperfine state detection of the single atom is the "state selective kick out". By this process the atom is kicked out of the trap by a strong laser beam depending on the hyperfine state. For this procedure we use the closed transition between $|F = 2, 2\rangle$ and $|F' = 3, 3\rangle$ for an effective way to transfer the momentum of the photon to the atom without the possibility of a decay in the undesirable other hyperfine ground state. Every time a photon is scattered it will transfer the momentum $\Delta\mathbf{p} = \hbar\mathbf{k}$ in the direction of the incoming beam and the following spontaneous emission is isotropic and can therefore be neglected. So a laser with strong intensity and applied from one direction will transfer enough momentum to kick out resonant atoms of the dipole trap. Atoms in the state $F = 2$ will be kicked out while atoms in $F = 1$ ground state will scatter no photons and will remain in the trap.

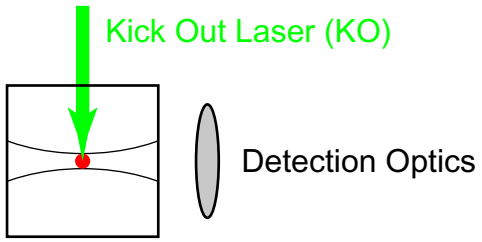

Figure 5.7: Front view of the trap with the kick out laser applied from the top

To test this detection scheme we prepared the atom either to the initial state F = 1 or to F = 2. After the preparation we applied for 0.24 ms the kick out laser and cooling and repump laser were switched on again and we looked for 55.7 ms for fluorescence light from the atom. If the atom was in F = 1 the atom will survive the laser pulse and can be observed in the dipole trap by fluorescence of the cooling light.

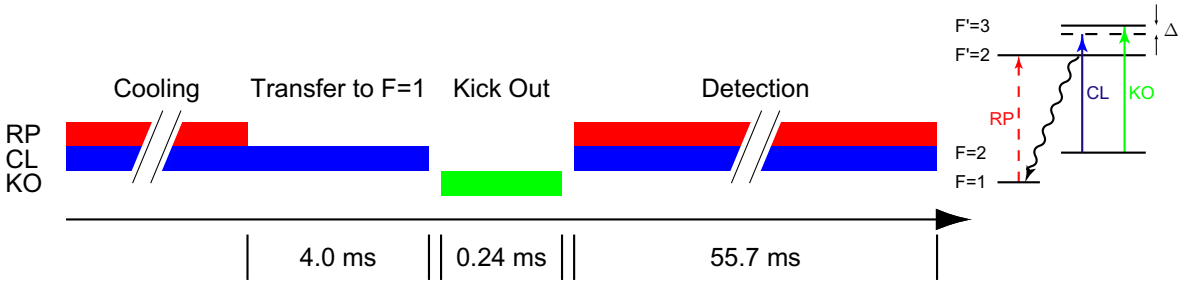

Figure 5.8: Transfer scheme to F = 1 and subsequent kick out laser pulse and atom detection

For the preparation of the initial state F = 1 the cooling laser is switched off 4 ms later than the repump laser and the kick out laser pulse is applied for 0.24 ms. The experiment was repeated many times and the fluorescence counts from the detection were histogrammed.
We see a big peak at high counts (about 100) equivalent to the countrates of a single atom in the trap and a small peak at low counts (about 40) corresponding to the background count rate.

The peak of kicked out atoms (at low countrates) is most probable an effect of the bad efficiency of the pumping process to F = 1 using the cooling laser.

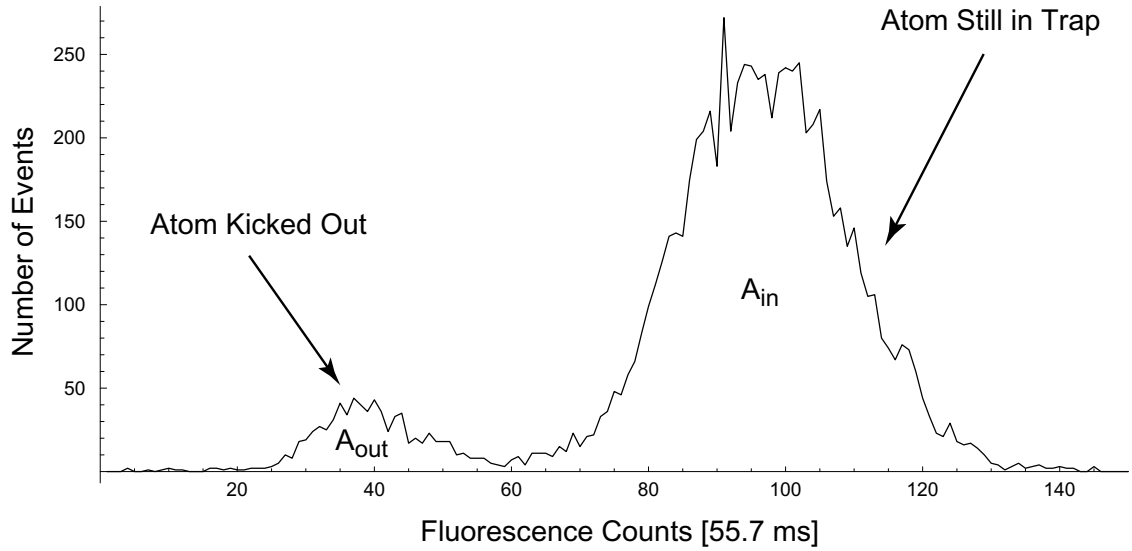

Figure 5.9: Histogram of the fluorescence counts for the preparation of atoms to F = 1 from the cooling light after the kick out laser was applied

By summation over the single peaks (A_{in} is the number of events the atom stayed in the trap and A_{out} the number of events the atoms was kicked out of the trap) the preparation and detection efficiency is calculated:

$$\frac{A_{in}}{A_{in} + A_{out}} = 85.9\ \% \tag{5.2}$$

To prepare the atom to F = 2 the repump laser is running 4.0 ms longer as the cooling laser. After this preparation of the initial state the same detection scheme is used as before.

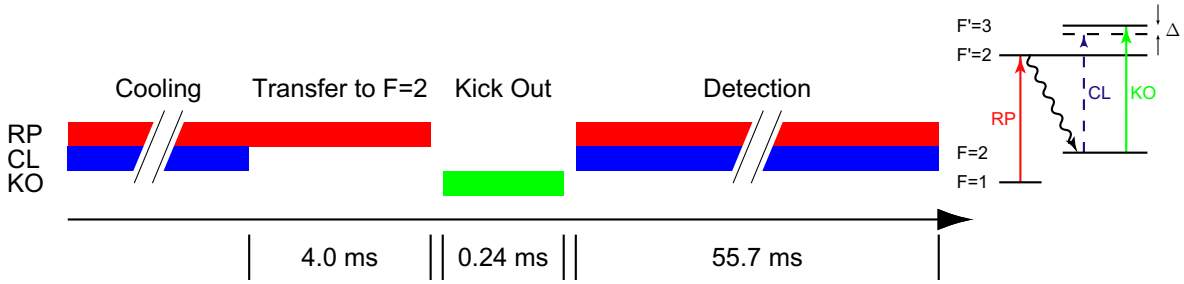

Figure 5.10: Transfer scheme to F = 2 and subsequent kick out laser pulse and atom detection

The result of this measurement is again displayed by histogramming the fluorescence counts after detection. The events corresponding to the single atom still in the trap after the process

can not be explained by a bad preparation efficiency as the preparation to F = 2 should be very effective. Possible explanations for this effect could be relaxations to the other ground state level or a limited efficiency of the kick out pulse (to short pulse duration or polarization errors).

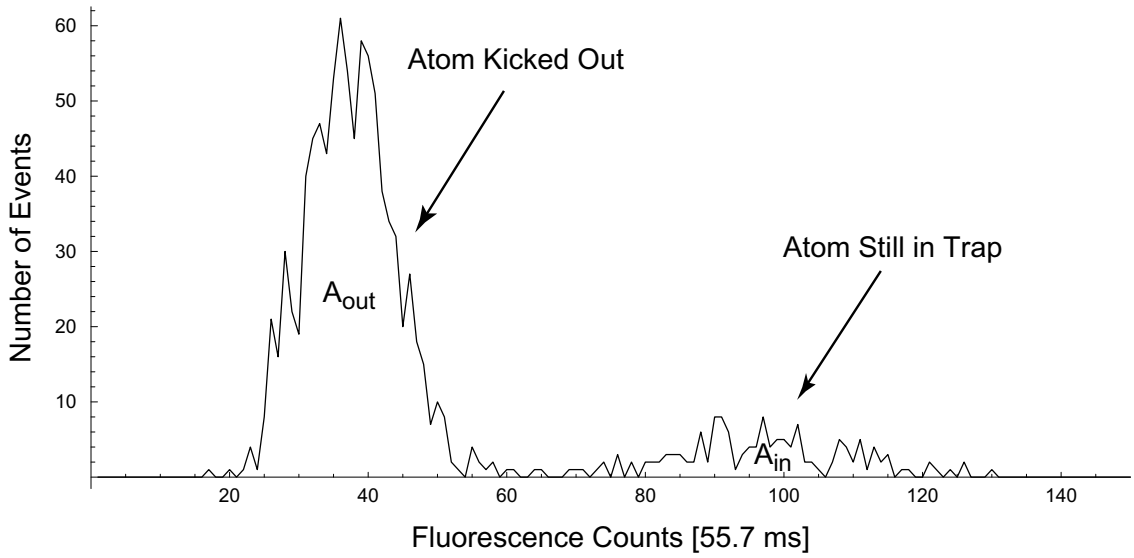

Figure 5.11: Histogram of the fluorescence counts of atoms prepared to F = 2

Again by summation over the single peaks the preparation and detection efficiency is calculated:

$$\frac{A_{out}}{A_{in} + A_{out}} = 90.5\ \% \tag{5.3}$$

5.5 Conclusion

In the perfect case without any possibility of pumping the atom into the F = 1 dark state (because of the repump laser) we were able to perform a state detection via cycling with a detection efficiency of about 68 %. By increasing the duration of the cycling pulse the detection efficiency would be increased but the average lifetime of the atom in the trap would be decreased. To distinguish the signal (fluorescence) count rate from the background by 2 standard deviations a cycling pulse length of 100 ms would be necessary. At the same time the atomic lifetime in the trap would drop to 1 to 2 measurment cycles.
This results with an absence of decays into the F = 1 dark state were achieved to gain the best settings for the power and detuning of the lasers and to estimate the countrates. But in a test without the repump laser we were not able to distinguish between signal and background counts although the polarization of the lasers was adjusted well. Therefore it becomes clear that the polarization of the two cycling beams is a very critical parameter.

In first test measurement of the state selective kick out of a single atom we were able to obtain a preparation and detection efficiency better than 85 %. In this measurment scheme we kicked out atoms in F = 2 and atoms in F = 1 remained in the trap.
Cycling would be a method to detect the atomic state but only with a much better adjustment of the polarization and an increase of the collection efficiency. This could be realized by using a collection optics with a bigger solid angle or by reduction of the dark counts by using better photo detectors. In contrast to cycling the state selective kick out is a quite easy and efficient way for the hyperfine state detection of a single atom.

6 State Selective Transfer via STIRAP

To choose the quantum mechanical measurement basis for the Bell-type experiment we have to select a superposition of the states $|1, \pm 1\rangle$ and to transfer the population of this superposition to F = 2. We want to realize this state selective transfer by the STIRAP process. This process is realized by a sequence of two laser pulses, the Stokes pulse with the Rabi frequency $\Omega_S(t)$ and the pump pulse with the Rabi frequency $\Omega_P(t)$. The first one couples the states F = 2 and F' = 1 and the second one (partially overlapping in time) empties the selected superposition of the F = 1 states.

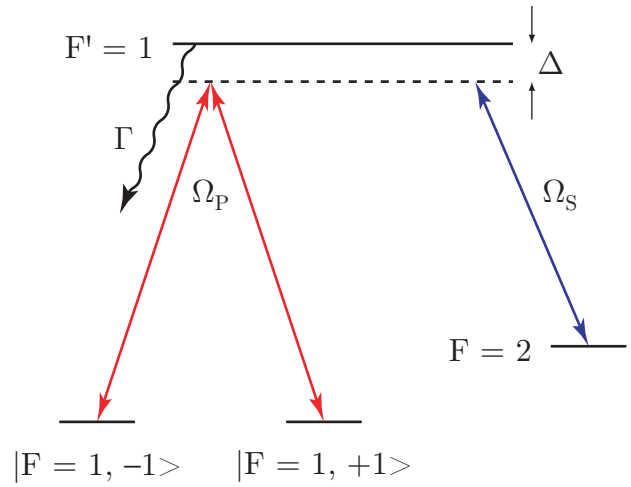

Figure 6.1: The STIRAP process with the Stokes and pump laser to transfer a selected superposition of the states $|1, \pm 1\rangle$ to F = 2. The transferred population will be in a superposition of all Zeeman sublevels depending on the polarization of the Stokes pulse.

As the light of the STIRAP lasers has to be applied in z direction (the direction to observe fluorescence light from the trap) we would saturate the photo diodes by using light with a wavelength corresponding to the D_2 transitions of ^{87}Rb. Therefore we use for the STIRAP process light with a wavelength corresponding to the D_1 transitions at 795 nm which can be reduced by interference filters.
In this chapter I will present numerical solutions of the timedependent three level Schrödinger equation (2.28) to estimate the experimental parameters (intensities, pulse durations, ...) and first steps towards the experiment.

6.1 Numerical Solution of the Timedependent Schrödinger Equation

To get knowledge about the conditions for the adiabacity of the STIRAP process the timedependent Schrödinger equation (2.28) has to be solved. This allows to calculate the time development of the population probability of the three states $|c_{F=1}(t)|^2$, $|c_{F'=1}(t)|^2$, $|c_{F=2}(t)|^2$. In our case $|c_{F=1}(t)|^2$ is the probability to find the atom in the initial ground state F = 1 at time t, $|c_{F'=1}(t)|^2$ for the excited state F' = 1 and $|c_{F=2}(t)|^2$ for the destination ground state F = 2.
For certain time evolutions of the two STIRAP beams $\Omega_S(t)$ and $\Omega_P(t)$ (e.g. for the artificial model described by a function defined in steps – the model is presented in [46]) it is possible to get an analytical solution. But even for an exponential decay of the first pulse and an exponential raise of the second one it is necessary to switch to a numerical solution.
Fast switching times of our AOM should result in a laser pulse of approximately gaussian form. So to get realistic results we have realized the simulations by two gaussian laser pulses:

$$\begin{aligned} \Omega_S(t) &= \Omega(I_S)\exp\left(-\left(\frac{(t-\tau)}{T}\right)^2\right) \\ \Omega_P(t) &= \Omega(I_P)\exp\left(-\left(\frac{(t+\tau)}{T}\right)^2\right) \end{aligned} \tag{6.1}$$

with the Rabi frequencies $\Omega(I_S)$, $\Omega(I_P)$ defined by (2.26).
For example for two gaussian STIRAP pulses with a pulse duration T = 20 ns, separated by a relative pulse postponement τ = 10 ns, with a power P = 1 mW, focussed down to a waist of w_0 = 10 µm and the natural decay rate of ^{87}Rb we calculated the following plot of the population probabilities.

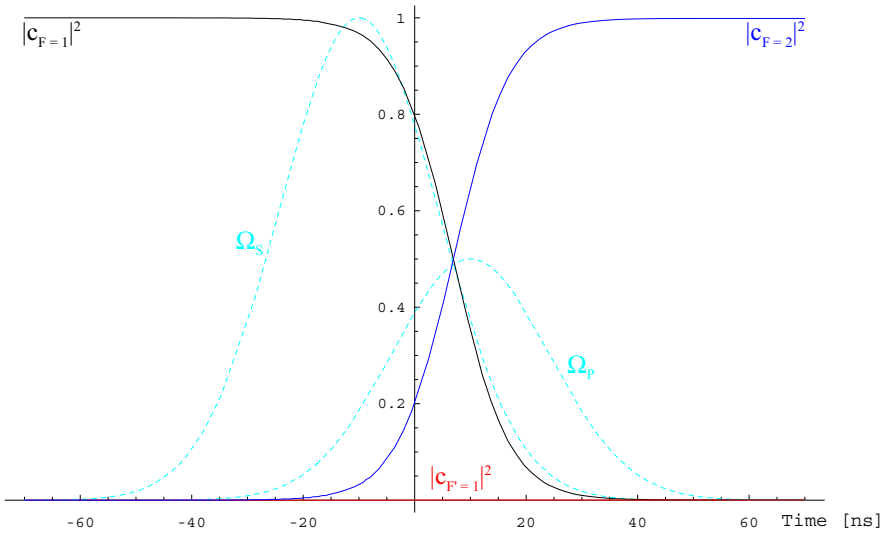

Figure 6.2: The time developement of the population probabilities of the states |F = 1>, |F' = 1> and |F = 2> for a nearly ideal adiabatic case. For illustration purposes the two normalized gaussian STIRAP pulses are shown in the same figure.

As it can be seen $|c_{F=2}(t)|^2$ reaches a value of one after the process and $|c_{F'=1}(t)|^2$ is nearly zero during the whole process. This is exactly we want to get. With $|c_{F'=1}(t)|^2 = 0$ during the whole process we won't have any possible decay channel and all population is transferred to the final state.
What is the result in the case of a nonadiabatic following. To give an example for this case, too, I calculated the Schrödinger equation with nearly the same conditions. Only the waist of the beam was increased to $w_0 = 200$ µm resulting in a reduction of the intensity by a factor of 400.

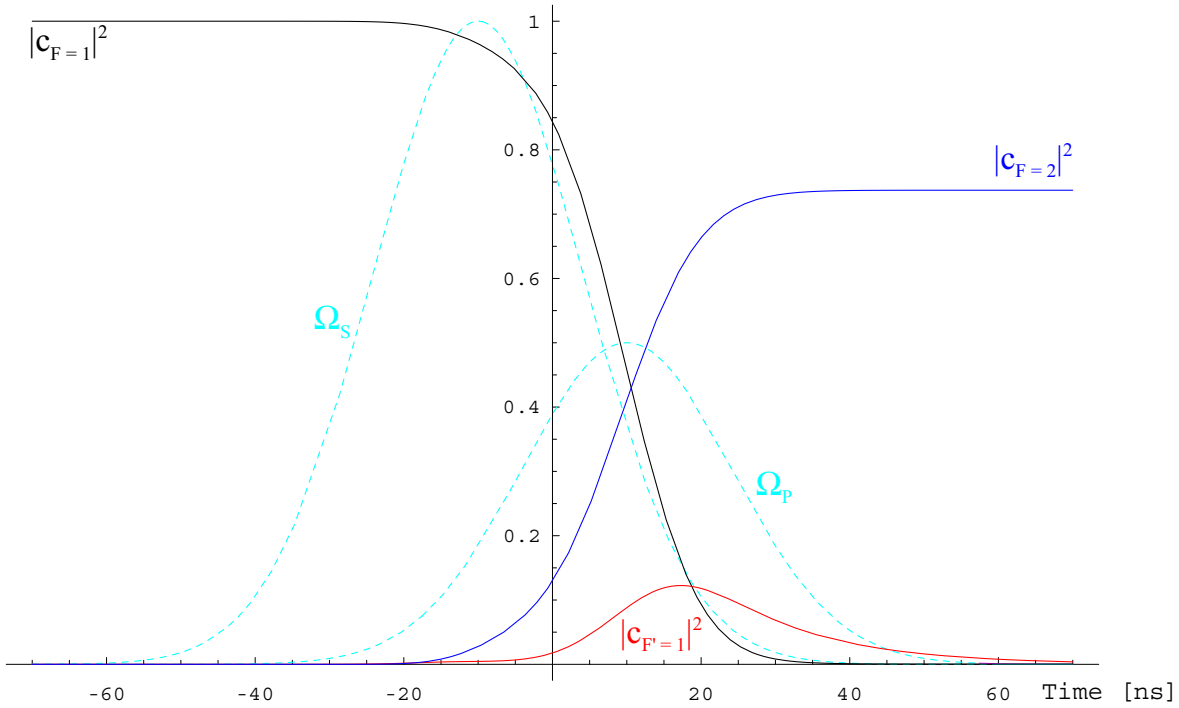

Figure 6.3: The time developement of the populations of the states |F = 1>, |F' = 1> and |F = 2> for a nonadiabatic case with a waist of $w_0 = 200$ µm. For illustration purposes the two normalized gaussian STIRAP pulses are shown in the same figure.

After the process the sum of the populations is less than 1 because for simplification all decays happen to a fourth level not coupled to any laser fields. This time $|F' = 1\rangle$ is populated during the process and a some decay is possible. Therefore $|c_{F=2}(t \to \infty)|^2$ is only about 67 %.

To determine the effect of the different parameters I have calculated $|c_{F=2}(t \to \infty)|^2$ for a great deal of cases. In each plot one parameter is varied and for the rest of the parameters we have chosen reasonable values: a power of P = 1 mW for each lasers, focussed down to a waist of $w_0 = 10$ µm, a detuning $\Delta = 0$, the natural decay rate of the excited state $|F' = 1\rangle$, a relative time delay $\tau = 0.6$ T (which should give the maximal efficiency). Each calculation was done for different pulse durations T = 10, 20, 50, 100, 200 and 500 ns.

The relative time delay between the two laser pulses is one of the values easily accessible in experiment. But we have to know how big it should be and how critical this parameter is to some time jitter.

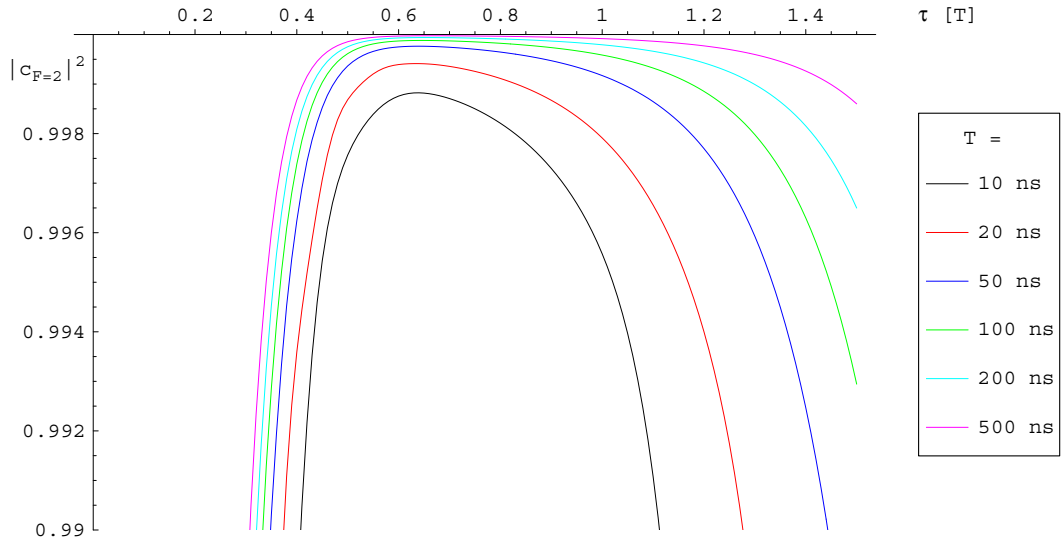

Figure 6.4: Dependence of the transfer efficiency on the relative time delay of the STIRAP pulses ($P_S = P_P = 1$ mW, $w_0 = 10$ µm, $\Delta = 0$)

As it can be seen the postponement should be greater then 0.5 T or better 0.6 T and smaller as 1 T. In our experiment we have observed a time jitter of τ of about 2 ns. This results for T = 10 ns and 20 ns (which will be the most probable values in our experiment) in a jitter of about 10 % and 5 %, respectively. So for $\tau = 0.7$ T the transfer efficiency will be good enough (better then 99 %).
In Fig. 6.5 I have varied the power of the Stokes laser pulse. For powers greater than 0.2 mW the transfer efficiency reaches a level better than 99.8 %.

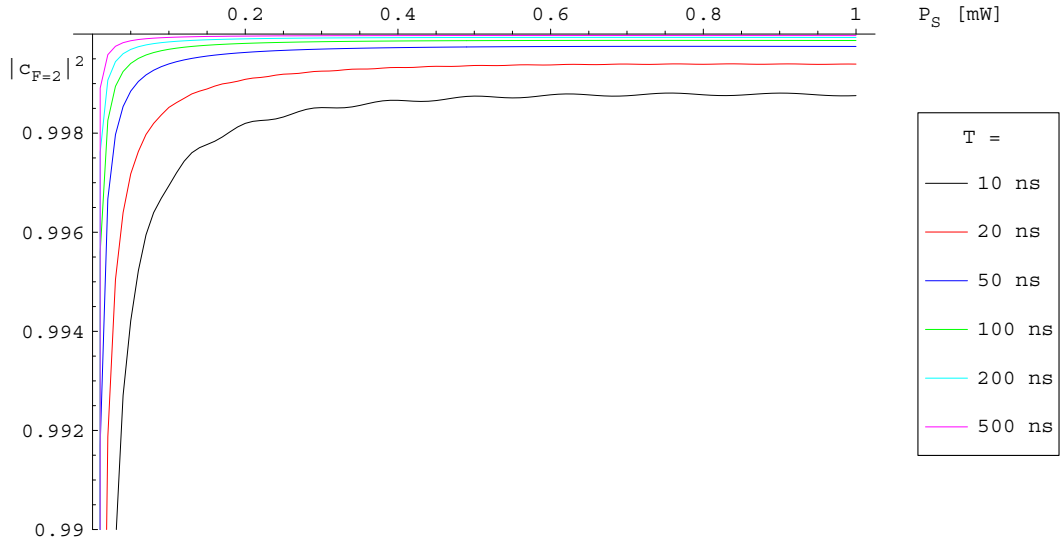

Figure 6.5: Dependence of the transfer efficiency on the power of the Stokes laser ($P_P = 1$ mW, $w_0 = 10$ µm, $\Delta = 0$, $\tau = 0.6$ T)

Fig. 6.6 shows the transfer efficiency dependent on the power of the pump laser. The dependency looks different compared to the case of the Stokes laser. But this is only a result of the different saturation intensities of the two transitions. Therefore we need a bigger power for the pump laser.

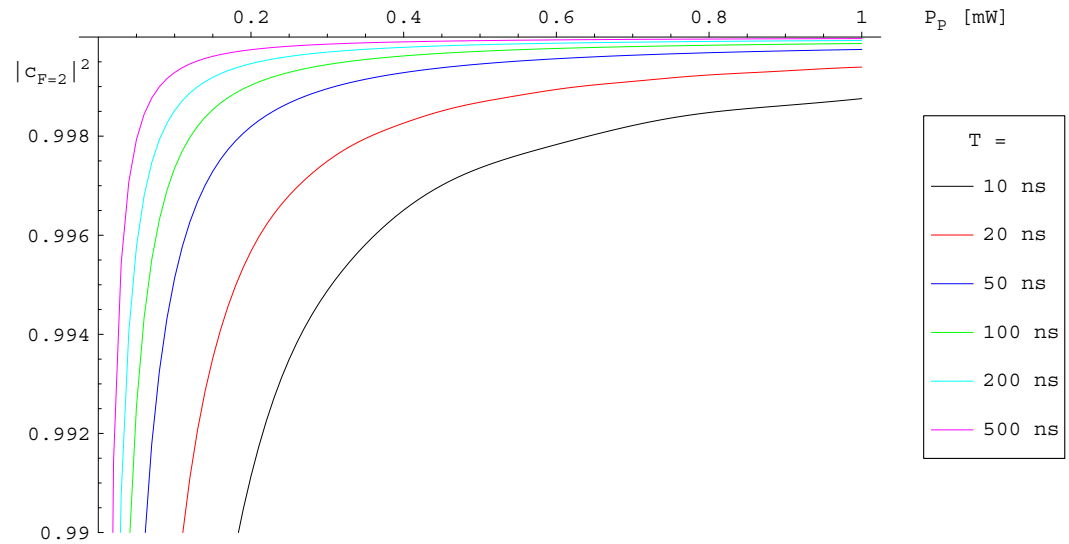

Figure 6.6: Dependence of the transfer efficiency on the power of the pump laser (P_S = 1 mW, w_0 = 10 µm, Δ = 0, τ = 0.5 T)

The next varied parameter, the waist w_0, depends on the optics we use to focus the beams and together with the power it sets the intensity of the lasers. And it is the most critical parameter (this is the only plot between 95 and 100 %).
Most probable the waist will be in a region between 10 and 50 µm and for T = 10 ns the transfer efficiency will be better as 95 %.

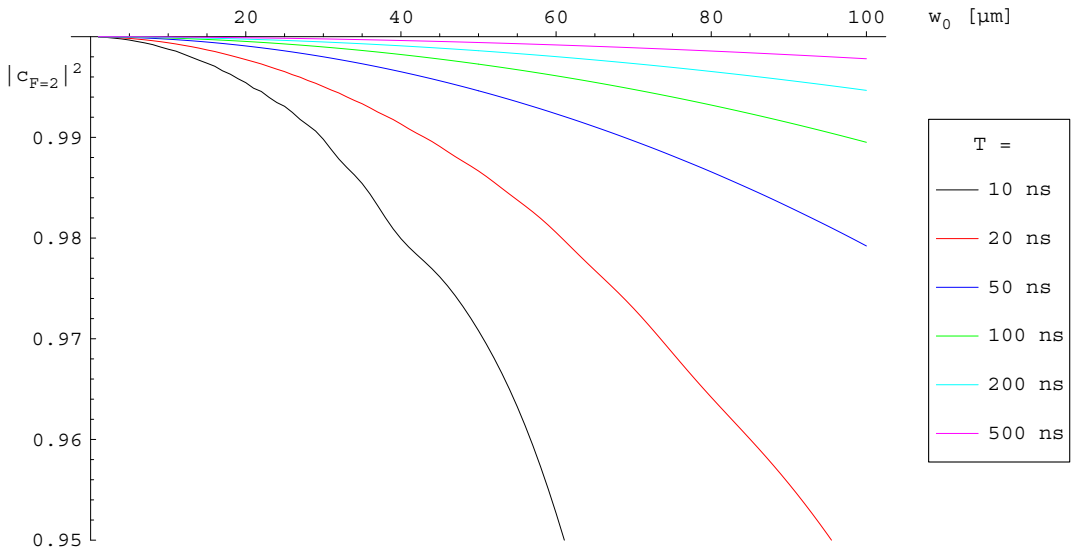

Figure 6.7: Dependence of the transfer efficiency on the waist of the two lasers ($P_S = P_P$ = 1 mW, Δ = 0, τ = 0.6 T)

The transition efficiency is further nearly independent of a small joint detuning of both lasers relative to the F' = 1 excited state. This is important for our experiment because the atom sees a detuning depending on the position in the trap due to the spatial variation of the light shift of the dipole trap. So it is not possible to shine in light exactly on resonance. The transfer efficiencies form calculations for $\tau = 0.6$ T showed nearly no dependency on the detuning. As the time delay jitters I have calculated the transfer efficiencies for a time delay of $\tau = 0.5$ T, too. Those results are presented in Fig. 6.8.

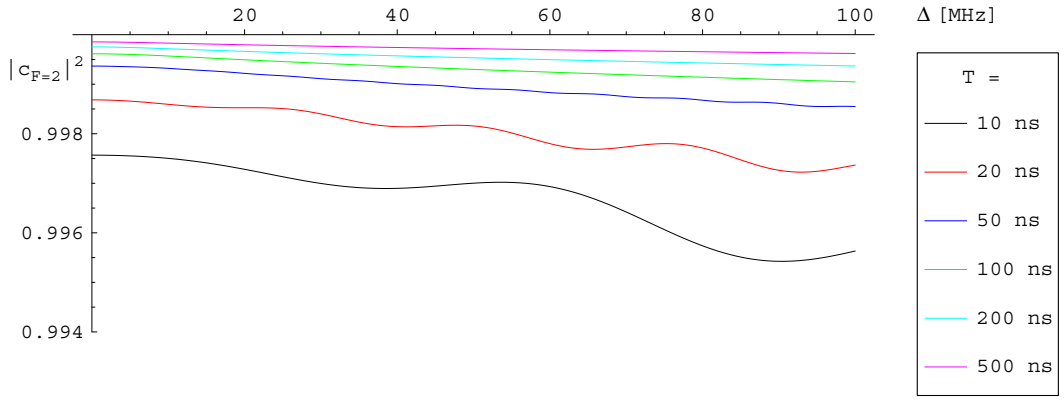

Figure 6.8: Dependence of the transfer efficiency on the detuning of the two lasers ($P_S = P_P = 1$ mW, $w_0 = 10$ µm, $\tau = 0.5$ T – for $\tau = 0.6$ T nearly no dependency on the detuning could be seen)

Finally the dependency on the pulse duration of the two lasers.

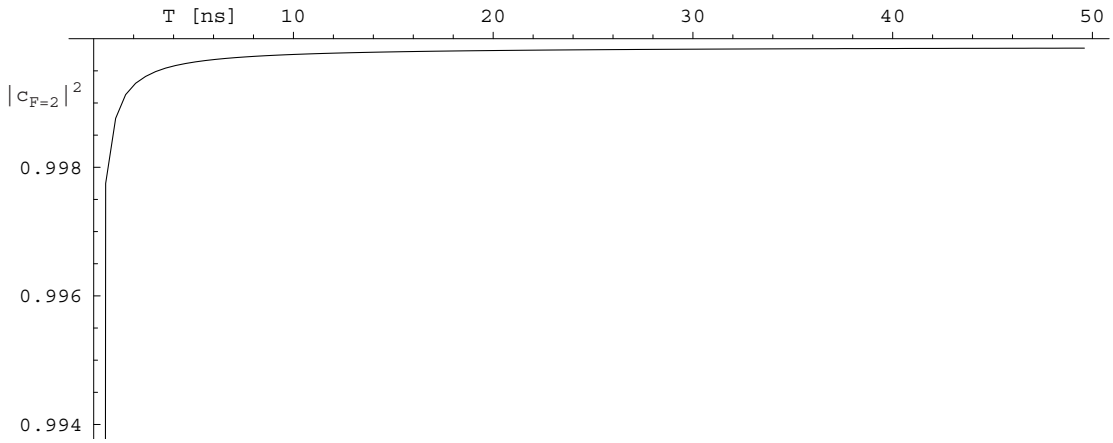

Figure 6.9: Dependence of the transfer efficiency on the pulse duration of the two laser ($P_S = P_P = 1$ mW, $w_0 = 10$ µm, $\Delta = 0$, $\tau = 0.6$ T)

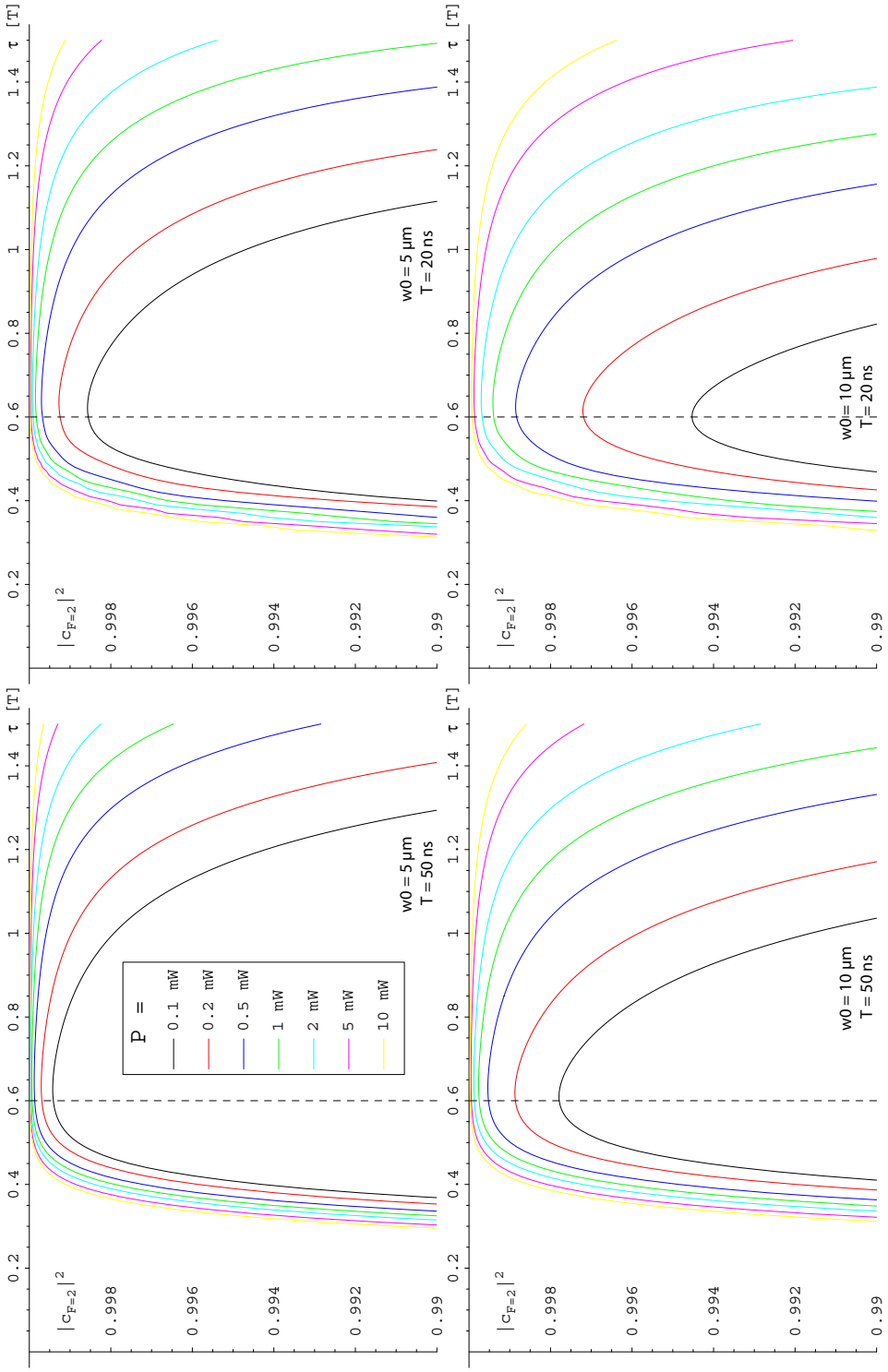

Figure 6.10: Dependence of the transfer efficiency on the relative pulse postponement of the STIRAP pulses for several laser powers. The pulse duration for the two lower plots is T = 50 ns and for the two upper plots T = 20 ns. And the waist is for the two plots on the left side w_0 = 5 µm and for the other two plots w_0 = 10 µm. The rest of the parameters is chosen as usual. ($P_S = P_P$, $\Delta = 0$, $\tau = 0.5$ T)

6.2 Experimental Realization

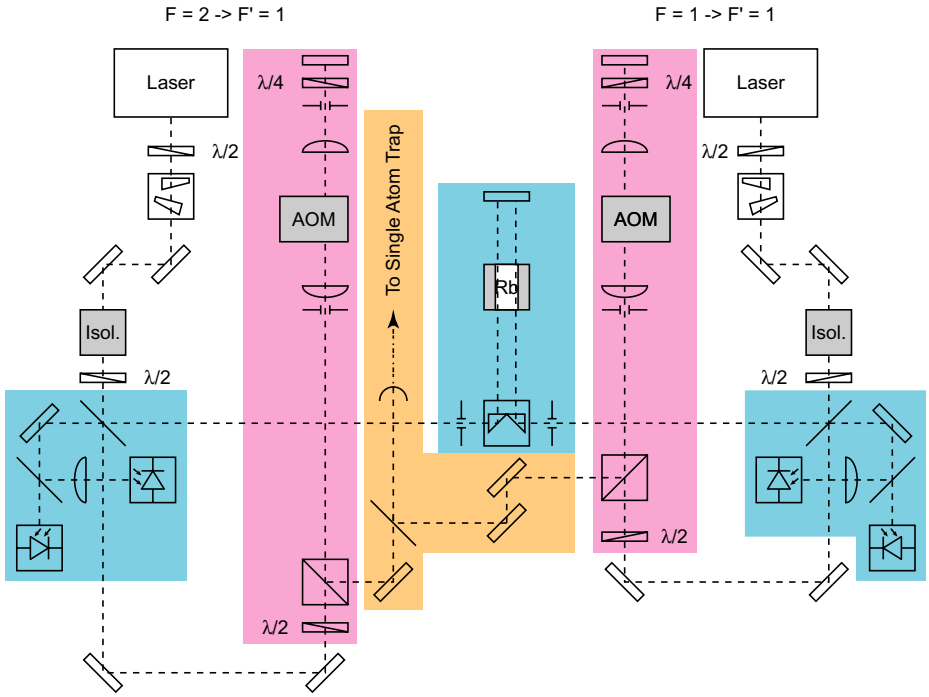

Figure 6.11: A schematic drawing of the two STIRAP laser setup with spectroscopy, AOMs and coupling into the fiber

The light for the STIRAP process is generated by two grating stabilized laser diodes – one for the Stokes pulse ($F = 2 \rightarrow F' = 1$) and one for the pump pulse ($F = 1 \rightarrow F' = 1$). The beam profile of both lasers is shaped from elliptical to round by a pair of anamorphic prisms. To reduce backreflections from the fiber the light passes an optical isolator. To stabilize the laser frequency a small amount of the light is split for spectroscopy.
For switching on and off the laser light and to adjust the detuning to the atomic levels we use an AOM in double-pass configuration. The light from the AOM of both STIRAP lasers is overlapped at a beam splitter to couple both into one single mode fiber with a coupling efficiency of about 60 % for each laser (about 2.5 mW laser power of the Stokes laser and about 6 mW of the pump laser). Fig. E.1 is a picture of this STIRAP laser setup.
To lead the STIRAP beams to the single atom we use a standard fiber coupler and the objective mounted opposite to the microscope objective (see Fig. 4.5). By this it should be possible to realize a focus with a waist of about 10µm.

The time dependent relative phase $\Phi(t)$ of the entangled atom-photon state is the result of the time evolution of the two atomic states because of residual magnetic fields. The magnetic field compensation around the glass cell (see Fig. 4.4) should result in a residual magnetic field below 20 mGauss at the center of the dipole trap. Therefore the relative phase between the two terms of the entangled state will oscillate with a cycle time of 35 µs. As the entangled state should not change during the STIRAP process the process should be finished in a time less then 1 % of the oscillation time. Further the relative phase of STIRAP lasers is not stabilized

(this is actually necessary for the STIRAP process but it would require additionally costly electronics). The relative phase of two lasers is stable on timescales corresponding to their coherence time. Due to this fact the STIRAP process should be faster than the coherence time of the lasers of about 250 ns. On the other hand the process has to be adiabatic and as the power of the laser diodes is limited the duration of the pulses has to be longer than 10 ns. Therefore the reasonable timescale for the duration of one laser pulse is between 10 and 100 ns.
To generate the optical pulses we triggered two tunable delays (with an adjustable delay time and pulse duration) by one pulse of a process control unit (called "Spieluhr" – with minimal time steps of 20 ns) to suppress jitter between the two pulses (1-2 ns remaining) and to fine adjust the pulse duration and the relative pulse postponement. By using the tunable delays and by slightly disaligning the forward and backward beams of the AOMs we were able to generate "gaussian pulse shapes" (20 - 30 ns long) and to overlap the pulses.

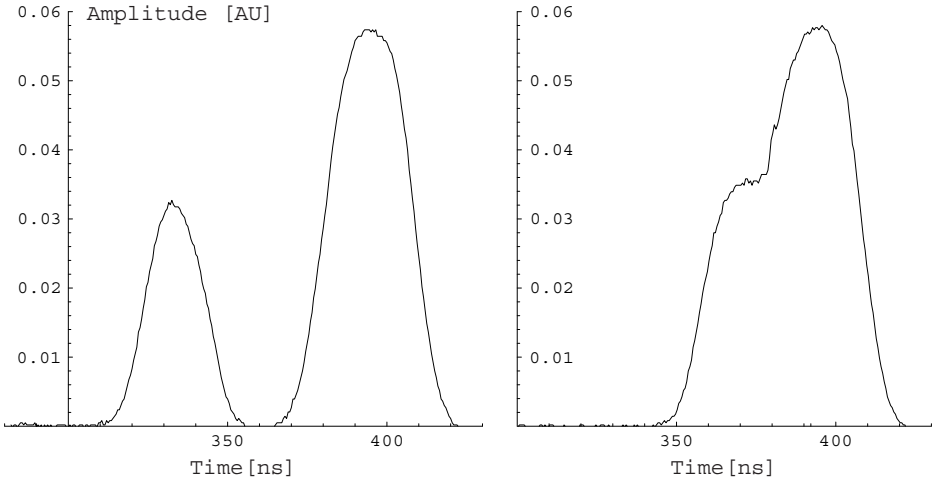

Figure 6.12: The optical signal of the two STIRAP pulses created with AOMs, overlapped by a beam splitter, and optimized for a "gaussian shape" of the intensity. In the first plot they are separated in time and in second plot the second pulse is partially overlapping in time with the first one.

7 Conclusion & Outlook

To measure the amount of entanglement of the spin state of a single atom and the polarization of a spontaneously emitted single photon it is necessary to test the violation of a Bell's inequality. Therefore a correlation measurement of the polarization of the photon and of the atomic spin-state is necessary. The measurement of the atomic state consists of two parts. To choose the measurement basis of the atom a state selective transfer is carried out and for the projection measurement on the chosen basis the hyperfine ground state of the atom has to be detected.

To select the measurement basis of the atom for the Bell measurement it is necessary to transfer a chosen superposition of the states $|F = 1, m_f = -1\rangle$ and $|F = 1, m_f = 1\rangle$ to $F = 2$. The orthogonal state will remain in $F = 1$. This is possible by using an adiabtaic two photon transfer process – the so-called STIRAP technique. In the framework of this diploma thesis a laser system for this state selective transfer was set up and to get insight into the adiabaticity (depending on nonperfect experimental parameters) of this two-photon raman process I performed analytical and numerical calculations. For this purpose I solved optical Bloch equations in the case of two short laser pulses with realistic parameters. As the parameters of the laser pulses (intensity, pulse length, ...) fit to the calculated requirements for an adiabatic transfer it should be possible to use this technique.

For the final state measurement it is necessary to distinguish the atom in the two different hyperfine ground states $F = 1$ and $F = 2$. Our solution to this problem is directly connected to the existence of the closed transition between $|F = 2, m_f = 2\rangle$ and $|F' = 3, m_{f'} = 3\rangle$. On the one hand we tried to distinguish the two hyperfine ground states directly by observing fluorescence light from this closed transition for atoms in the ground state $F = 2$. On the other hand we used the transition for an effective way to transfer momentum to the atom from one direction. After a few cycles a resonant atom in $F = 2$ gains sufficient kinetic energy to be kicked out of the trap while an atom in $F = 1$ stays in the trap after this laser pulse and can be observed.
With the second method it was possible to gain a detection efficiency of about 90 % in first test measurements. For directly observing the fluorescence it seems to be necessary to improve the collection efficiency of the fluorescence light. Therefore the so-called "state selective kick out" process will be used in the experiment.

Using the STIRAPs to choose the measurement basis and the state selective kick out process for the projection measurement it should be possible to realize the state selective measurement of the single atom. For the next steps towards the final experiment it will be necessary to test

the state selective transfer and the preparation of the initial state experimentally. As the necessary equipment is already built up those steps should be (hopefully) finished soon and the entanglement will be shown.

In the future it should be possible by quantum teleportation to transfer the state of an independent photon to the atom. This is possible by a Bell-state measurement of the two photons after which the photonic state will be teleported to the atom. Such experiments can be seen as a proof of principle for quantum information processing if it is assumed that quantum information is transferred by photons and stored and processed in atoms.
Given a second entangled atom-photon pair a Bell-state measurement on the two emitted photons can be used to create an entangled atom-atom pair (entanglement swapping). As the two photons can easily be transported the two atoms can be spatially separated. Further the detection efficiency of the atomic state is high.
In the same way it should be possible to entangle "our" atom with every "particle" (qubit) by entanglement swapping of the two emitted photons (e.g. by entanglement swapping with an entangled photon - quantum dot system).
As the detection efficiency is bigger than 71 % and the two atoms (experiments) can be separated spatially well enough (to be sure that no classical information can be transmitted during the measurement) it is possible to realize a loophole-free test of Bell's inequality. For the realization of this experiment the second setup creating an entangled atom-photon pair could e.g. be placed in Garching and a single mode fiber could be laid to Munich (another possibility would be to use the optical free space communication system developed in the group of Harald Weinfurter). As the distance is about 15 km the test of Bell's inequality of the two atoms has to be finished in a time shorter than 50 μs.

Appendix

Content

A Rubidium and Atom-Physics

Rubidium was discovered in 1861 and is named because of its bright red spectroscopic lines from the Latin word “rubidius” (meaning “dark red” or “deepest red”). There are 24 isotopes of rubidium known, but naturally occurring rubidium is made up by only two of those: $^{85}\mathrm{Rb}$ (72,17 %) with a nuclear spin $I = 5/2$ and the radioactive $^{87}\mathrm{Rb}$ (27,83 %) with $I = 3/2$. The nuclear lifetime of $^{87}\mathrm{Rb}$ is about $4.88 \cdot 10^{10}\,\mathrm{years}$ (approximately 3 times the age of the universe) and it decays to the stable $^{87}\mathrm{Sr}$ by a β^--decay. Due to this lifetime it’s effectively stable.
Rubidium is a silvery-white metallic element and belongs to alkali metal group with one valence electron. It is highly reactive and has a melting point at about 39°C.

A.1 Rubidium in Atom Optics

All alkali metal group atoms are suitable for experiments because of their strong transitions in the range of visible and infrared light. First experiments were done with Sodium atoms due to their D line transition at 589 nm which is easily accessible [49]. Today Cesium (895 and 852 nm) [50] and Rubidium 87 [48] are more important because their near infrared D line transitions are accessible with standard laser diodes.
$^{87}\mathrm{Rb}$ has its D_1 line ($5^2\mathrm{S}_{1/2} \rightarrow 5^2\mathrm{P}_{1/2}$) at 795 nm and the D_2 line ($5^2\mathrm{S}_{1/2} \rightarrow 5^2\mathrm{P}_{3/2}$) at 780 nm. Especially 780 nm is a standard wavelength for multimedia consumer electronics which is a great profit for experiments due to the really cheap price of the lasers.
The D line transitions are the components of a fine structure doublet like in all alkali atoms. The fine structure is the result of the coupling between the orbital angular momentum of the valence electron $\mathbf{L}$ and its spin angular momentum $\mathbf{S}$. Each of those transitions has additionally a hyper fine structure. This is a result of the coupling between the total electron angular momentum $\mathbf{J} = \mathbf{L} + \mathbf{S}$ with the total nuclear angular momentum $\mathbf{I}$ and leads to the total atomic angular momentum $\mathbf{F} = \mathbf{J} + \mathbf{I}$.

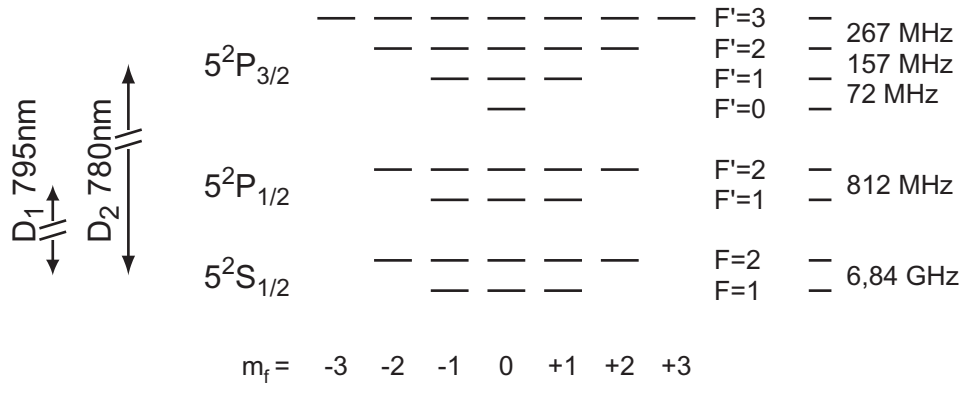

Figure A.1: Energy diagram of ^{87}Rb including hyperfine splitting and Zeeman sublevels

For the ground state $\mathrm{L} = 0$, $\mathrm{S} = 1/2$ and so $\mathrm{J} = 1/2$ (=> $5^2\mathrm{S}_{1/2}$) and for the excited states $\mathrm{L} = 1$, $\mathrm{S} = 1/2$ and therefore $\mathrm{J} = 1/2$ (=> $5^2\mathrm{P}_{1/2}$) for D_1 or $3/2$ (=> $5^2\mathrm{P}_{3/2}$) for D_2.

Due to $I = 3/2$ in ^{87}Rb F is either 1 or 2 for the ground state; for the excited state of the D_2 line F can take any of the values 0, 1, 2 or 3 and or the excited state of the D_1 line it can be again 1 or 2.
Each of that hyper fine energy levels has again several $(2 \cdot F+1)$ Zeeman sublevels. These levels result from the angular distribution of the electron wave function or from the orientation of the total spin of Rb and are described by the atomic magnetic quantum number m_f. If there is no external magnetic field those Zeeman levels are degenerate. (Fig. A.1)

A.2 Selection Rules

In each emission or absorption of a photon the angular momentum has to be conserved by the atom. The projection of the angular momentum of the photon to the z axis (quantization axis) is $0, \pm 1$ and has to be accomplished by the projection of the angular momentum of the atom to the z axis. So we get this transition rules (as well described in the textbooks [30, 31]) which have to be fulfilled all during emission or absorption of a photon:

$$\begin{aligned} \Delta L &= \pm 1 \\ \Delta J &= 0, \pm 1 \\ \Delta F &= 0, \pm 1 \end{aligned} \tag{A.1}$$

As $\Delta L \neq 0$ the transitions $J = 0 \rightarrow J' = 0$ and $F = 0 \rightarrow F' = 0$ are forbidden. Dependent on the polarizations (see Fig. B.1) of the light (defined in the system of the atom) m_f has some restriction for transitions, too. For π polarization:

$$\begin{aligned} \Delta m_f &= 0 \\ m_f &= 0, \Delta F \neq 0 \end{aligned} \tag{A.2}$$

for σ^+ absorption:

$$\Delta m_f = 1 \tag{A.3}$$

and for σ^- absorption:

$$\Delta m_f = -1 \tag{A.4}$$

A.3 Some Numbers Concerning Rubidium

Finally some numbers of the physical properties of ^{87}Rb [48]:

Atomic Number	Z	37
Total Nucleons	Z+N	87
Relative Natural Abundance		27.83(2) %
Nuclear Lifetime	τ_n	4.88×10^{10} yr
Atomic Mass	m	86.909 180 520(15) u $1.443\ 160\ 60(11) \times 10^{-25}$ kg
Density at 25°C	ρ_m	1.53 g/cm^3
Melting Point	T_M	39.31°C
Boiling Point	T_B	688°C
Vapor Pressure at 25°C	P_V	3.0×10^{-7} torr
Nuclear Spin	I	3/2

Some optical properties from the ^{87}Rb D_2 transition:

Frequency	ω_0	$2\pi \cdot 384.230\ 484\ 468\ 5\ (62)$ THz
Transition Energy	$\hbar\omega_0$	1.589 049 439(58) eV
Wavelength (Vacuum)	λ	780.241 209 686(13) nm
Wavelength (Air)	λ_{air}	780.032 00 nm
Lifetime	τ	26.24(4) ns
Decay Rate/ Natural Line Width (FWHM)	Γ	$38.11(6) \times 10^6$ s^{-1} $2\pi \cdot 6.065(9)$ MHz
Recoil Velocity	v_r	5.8845 mm/s
Recoil Temperature	T_r	361.96 nK
Doppler Shift	$\Delta\omega_d(v_{atom}=v_r)$	$2\pi \cdot 7.5419$ kHz
Doppler Temperature	T_D	146 µK

And some optical properties from the ^{87}Rb D_1 transition:

Frequency	ω_0	$2\pi \cdot 377.107\,463\,5(4)$ THz
Transition Energy	$\hbar\omega_0$	1.559 590 99(6) eV
Wavelength (Vacuum)	λ	794.978 850 9(8) nm
Wavelength (Air)	λ_{air}	794.765 69 nm
Lifetime	τ	27.70(4) ns
Decay Rate/ Natural Line Width (FWHM)	Γ	$36.10(5) \times 10^6$ s^{-1} $2\pi \cdot 5.746(8)$ MHz
Recoil Velocity	v_r	5.7754 mm/s
Recoil Temperature	T_r	348.66 nK
Doppler Shift	$\Delta\omega_d(v_{atom}=v_r)$	$2\pi \cdot 7.2649$ kHz

B Polarization Directions

For the atom a complete description of the electric field vector in 3 dimensions is given by two circular and one linear polarization (see Fig. B.1). The two circular polarizations (named σ^+ and σ^-) are perpendicular to the quantization axis and the linear polarization (named π) is parallel to the direction of the quantization axis. All other polarizations are superpositions of the three – e.g. H and V linear polarized light:

$$\begin{aligned} H &= \frac{1}{\sqrt{2}}(\sigma^+ + \sigma^-) \\ V &= \frac{1}{\sqrt{2}}(\sigma^+ - \sigma^-) \end{aligned} \tag{B.1}$$

In the z direction it is possible to apply σ^+, σ^-, H and V polarized light, in the y direction H and π and finally V and π in the x direction. But it is not possible to shine in π polarized light in the z direction because the electric field vector is always perpendicular to the direction of the propagation. On the other hand it is not possible to apply σ^+ and σ^- polarized light from the x or y direction since they are superpositions of H and V.

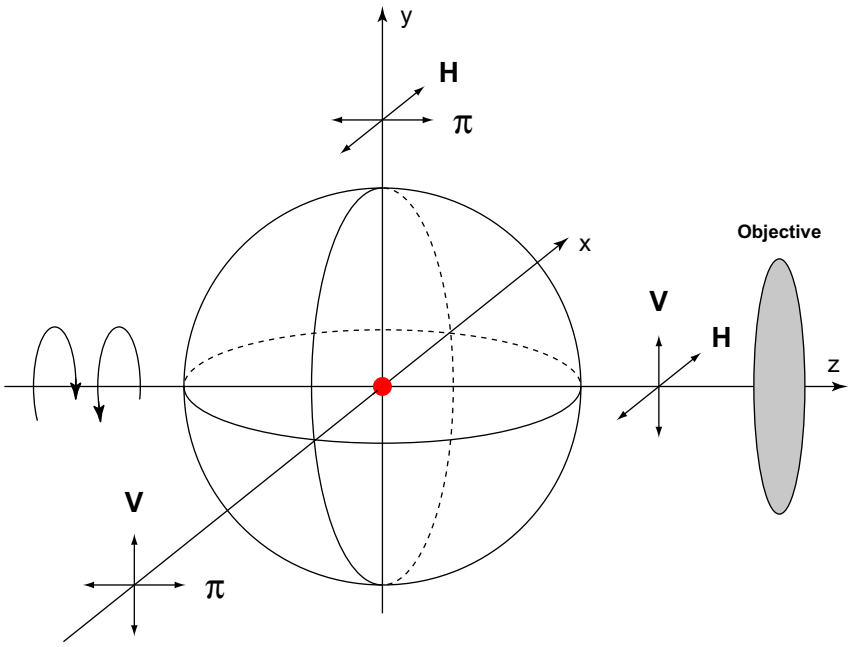

Figure B.1: The naming of polarizations of light applied to the atom

C Dopplerfree Saturation Spectroscopy

C.1 Grating Stabilized Diode Lasers

The lasers running on the D line transitions and are made out of single mode laser diodes and they all have to run at an exact and adjustable wavelength. Therefore a holographic reflection grating is placed in the beam (at an angle of about 45°). Using the "Littrow configuration" the first diffraction maximum is reflected back into the laser diode and the zero order maximum is diffracted by an angel of about 90° (this is the light used in the experiment). With this setup a second external resonator is build up with a relative small free spectral range due to its length. This reduces the line width of the laser from about 20 MHz to 0.68 MHz (compared to the natural linewidth of about 6 MHz). This external resonator can be scanned over several hundred MHz by a piezo mounted behind the reflection grating. This setup allows stable usage of all lasers with a laser linewidth one order of magnitude below the natural linewidth. The output power is due to losses to the backreflected beam about 40%.

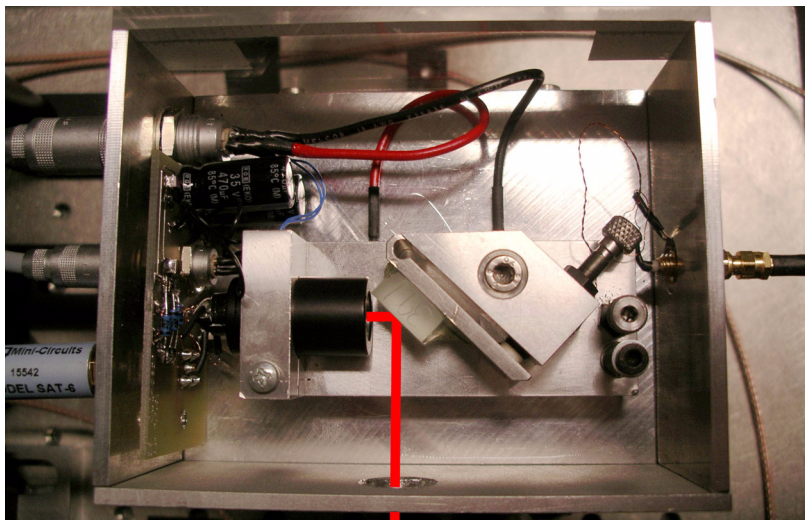

Figure C.1: A picture of the grating stabilized laser

To get rid of temperature fluctuations the whole laser setup including laser diode, collimation lens, adjustable holographic reflection grating and the temperature sensor is mounted on an aluminium block which can be cooled and heated by a Peltier element. Therefore the temperature of the laser setup can be kept constant by a PID (proportional, integral and differential) regulation [61].

C.2 Saturation Spectroscopy

Due to the grating stabilization the lasers are running at a sharp wavelength and some larger wavelength drifts are compensated by the temperature stabilization. But we want the lasers (cooling, preparation, STIRAP and detection) to run for several hours at a certain wavelength. For this purpose we have to lock our laser via dopplerfree RF saturation spectroscopy at suit-

able hyperfine transitions.

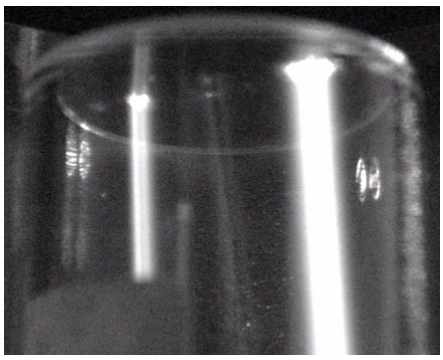

Figure C.2: Resonant fluorescence light of the two STIRAP lasers in the spectroscopy cell filled with rubidium gas. The weaker lines in the middle of the photo are caused by multiple reflections inside the glass cell.

To lock the laser we can not use absorption of resonant light in a cell filled with rubidium vapor because the temperature of the rubidium atoms in the trap is about 300 K resulting in a doppler broadening of the velocity of about 500 MHz. Due to this broadening we won't be able to distinguish between different hyperfine transitions.
To realize a dopplerfree saturation spectroscopy we have to choose only atoms of a certain velocity class. Therefore a small amount of the laser light is separated from the laser beam and runs two times on the same path through a cell with rubidium vapor. The first time the light passes through this gas atoms at $v = 0$ will be excited if the light is resonant to an atomic transition. So if the reflected beam passes a second time the atoms will still be in the excited state and they can't absorb the light anymore. So the total absorption is reduced. Finally if we look with a photo diode to the light passing through the cell (the blue curve in Fig. C.5, C.6 and C.4) we will see every resonant transition as a peak (called Lamb-dip).

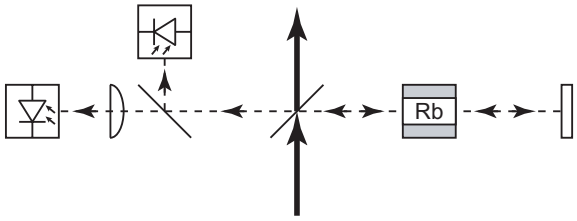

Figure C.3: Scheme for the dopplerfree saturation spectroscopy including two photo diodes. One is used for a direct observation of the spectroscopy signal and the second fast photo diode (marked by an objective to focus the beam on the diode) is used to generate the spectroscopy signal for the regulation of the tilt of the grating.

Furthermore transmission peaks can be seen at the cross-over (CO) frequency $\omega = (\omega_1 + \omega_2)/2$ (ω_1 and ω_2 are frequencies of allowed ^{87}Rb hyperfine transitions). The saturation signal of the CO lines is a result of atoms with the velocity $v = (\omega_1 - \omega)/k \neq 0$ which are resonant to the doppler shifted frequency ω_1 and therefore are excited. Light passing back the same way is now resonant to the same atoms with the relative velocity $-v$.
To lock the laser to an atomic transition frequency and to get a better ratio between the signal

and the noise a “lock in” type technique is used. Therefore the amplitude of the laser current is modulated with a weak RF-Signal (f_{mod} = 15 MHz) leading to optical sidebands beside the laser frequency ($f_{laser} \pm f_{mod}$). The demodulator multiplies the input signal ($f_{laser} \pm f_{mod}$ measured by a fast photo diode) and the reference signal (f_{mod}) and we get the sum and the difference frequencies as the result. By scanning the laser frequency (via tilting of the grating with a piezo) over an atomic resonance a relative phaseshift between the carrier and the sidebands is introduced. This phaseshift can be monitored directly in the DC part of the mixed RF spectroscopy signal. In contrast to the ordinary saturation signal this signal is the derivation with a reduced signal to noise ratio and it can be used to lock the laser at the center of an atomic transition. By applying this signal directly to the piezo small drifts will be automatically readjusted by tilting the grating.
In the following you can see the doppler free spectroscopy signal (blue) and the spectroscopy signal generated by the “lock in” unit (used for stabilization) (green) for both $^{87}\mathrm{Rb}\ \mathrm{D}_1$ transitions (Fig. C.4), for the $^{87}\mathrm{Rb}\ \mathrm{D}_2$ transitions $\mathrm{F} = 1 \rightarrow \mathrm{F'} = 0, 1, 2$ (Fig. C.5) and $\mathrm{F} = 2 \rightarrow \mathrm{F'} = 1, 2, 3$ (Fig. C.6). All lasers have to be locked to a cross-over line (which is marked in all four cases) as by combining these frequencies with the detuning induced by the used acoustic-optic modulators (AOMs) all necessary optical wavelengths can be produced.

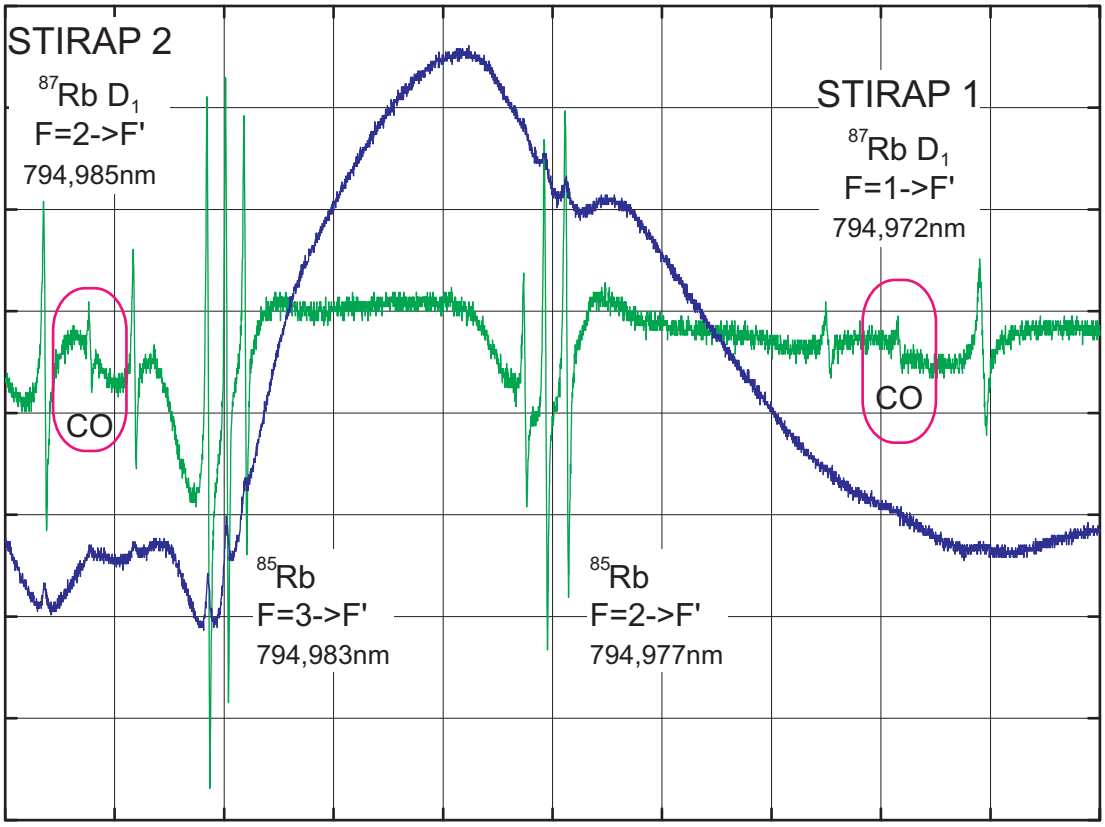

Figure C.4: The spectroscopy signal (blue) and the signal used for stabilization (green) at about 795 nm including the two $^{87}\mathrm{Rb}\ \mathrm{D}_1$ lines needed for STIRAP. The prominent line-triplets are generated by $^{85}\mathrm{Rb}$ because we use a natural mixture of Rb isotopes in our spectroscopy cell with 72,17 % of $^{85}\mathrm{Rb}$.

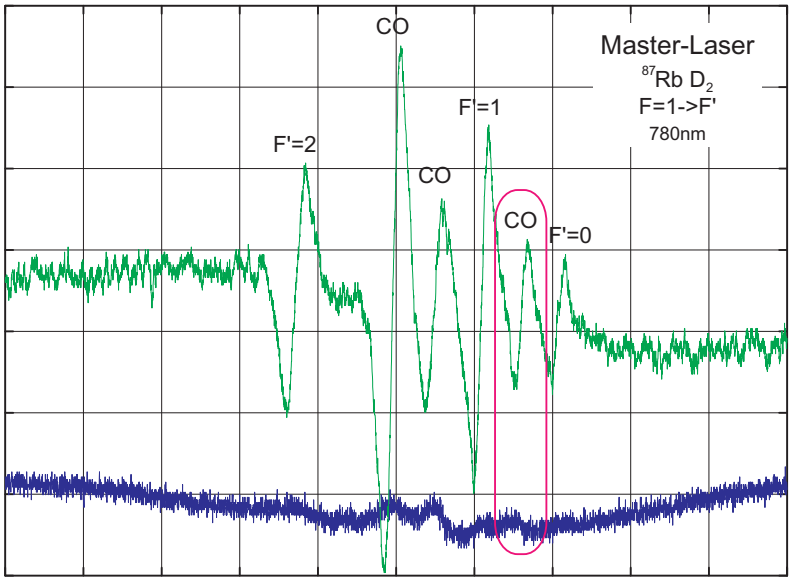

Figure C.5: Spectroscopy signal (blue) and signal used for stabilization (green) from the ^{87}Rb D_2 F = 1 → F' = 0, 1, 2 lines at 780 nm.

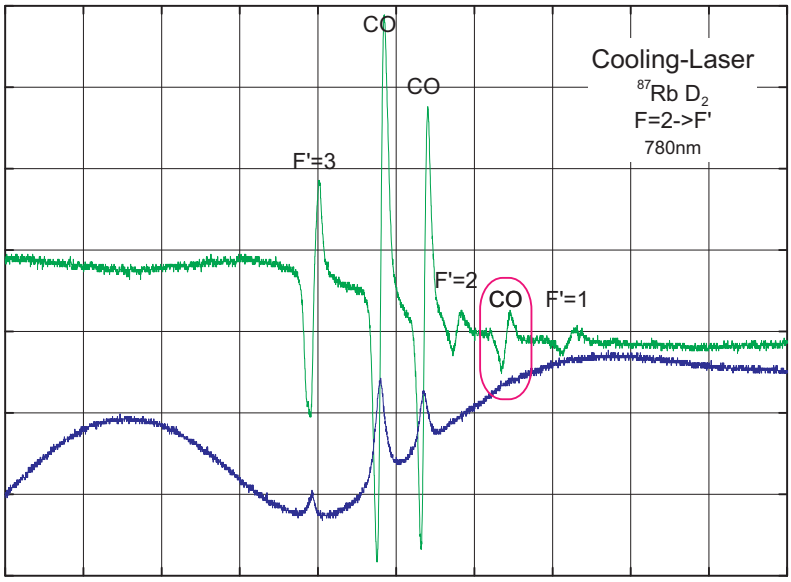

Figure C.6: Spectroscopy signal (blue) and signal used for stabilization (green) from the ^{87}Rb D_2 F = 2 → F' = 1, 2, 3 lines at 780 nm.

C.3 Measurement of the Linewidth and the Drift of a Locked Laser

To measure the line width of our STIRAP lasers we superposed the light of both STIRAP lasers on a fast photo diode (bandwidth about 650 MHz). The result is a beat signal which can be displayed directly with a spectrum analyzer.
The spectral distribution of the beat signal of two independent lasers can be used to deduce the linewidth of both lasers. The spreading of the frequencies is the convolution of the spreading of the single laser beams:

$$I_{beat}(\lambda) = I_1(\lambda) * I_2(\lambda) \tag{C.1}$$

So if we assume a gaussian profile for the spreading of the frequencies of each laser we should get a gaussian profile for the beat signal, too. And this profile is spread by a factor of $\sqrt{2}$ regarding to the single profiles if we assume both lasers to have the same linewidth.
As the full width at half maximum of the interference signal is about 960 kHz the single lasers have a line width of about 680 kHz.

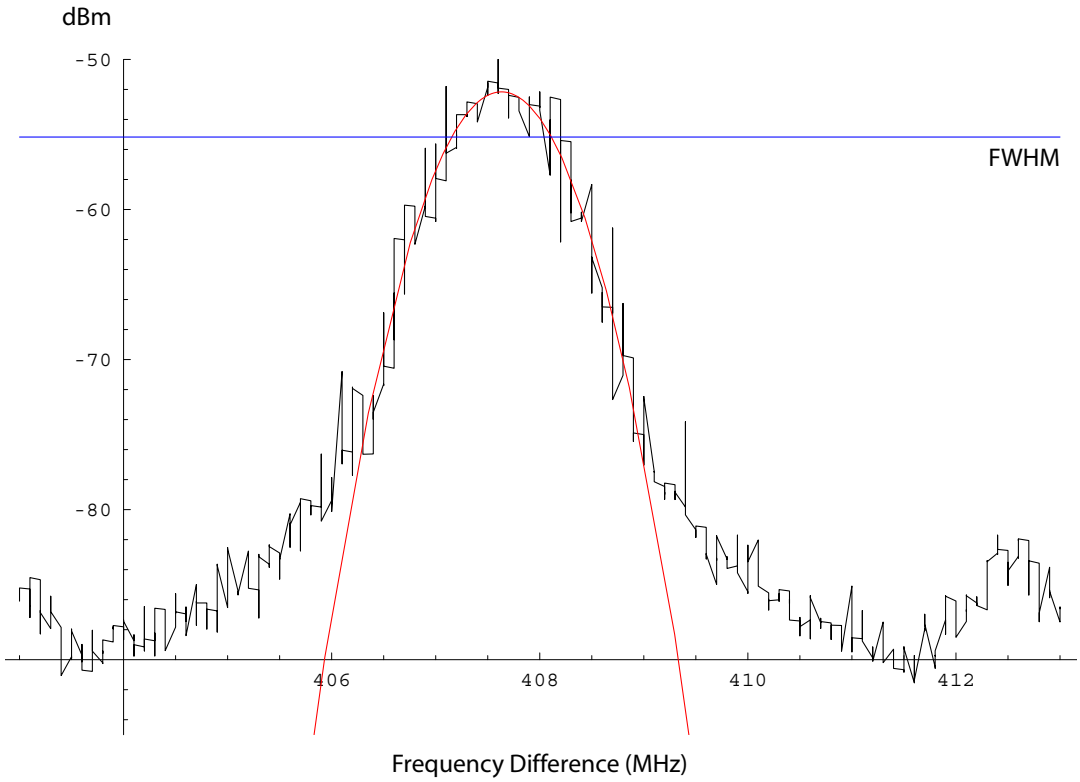

Figure C.7: The beat signal of the two STIRAP lasers including a fitted gaussian profile (red) based on values in a reasonable area (406.4 to 409 MHz).

To measure (Fig. C.8) the time development of the frequency difference of two individually locked lasers (in this example the two STIRAPs) is displayed. Long-term variations of about 2 MHz can be observed with a short time variation on the order of 0.2 MHz.

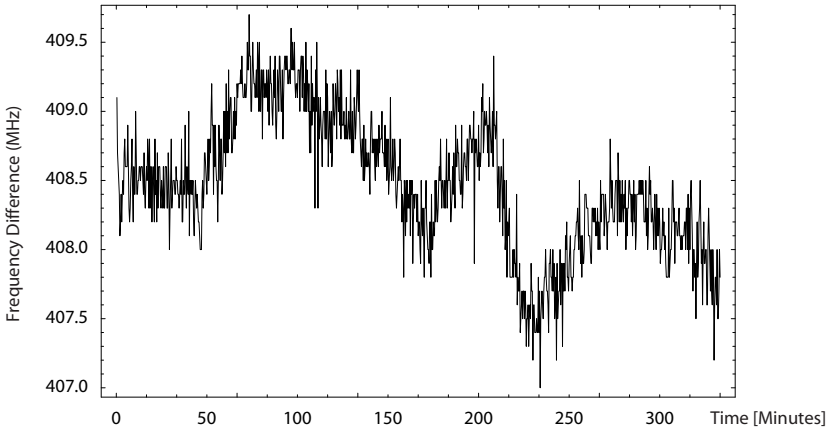

Figure C.8: Temporal variation of the frequency difference of the two STIRAP lasers measured by recording their beat signal

D Optical Modulators

D.1 Acoustic-Optic Modulator (AOM)

For our experiment it is necessary to switch and detune several laser beams independently. For this purpose we use acoustic-optic modulators in double-pass configuration.

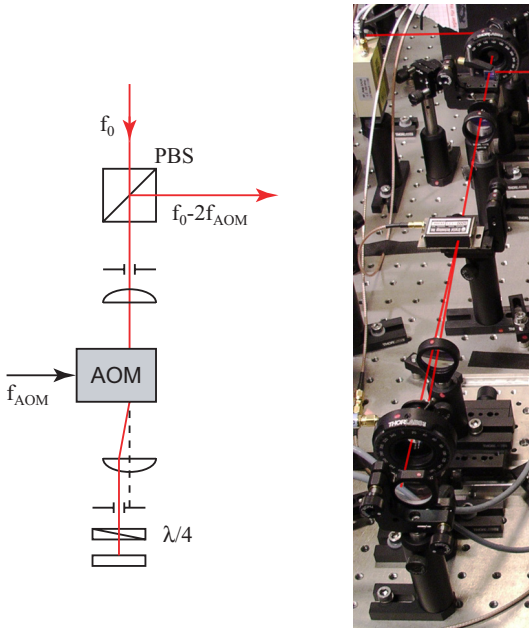

Figure D.1: An AOM in double-pass configuration.

An AOM consists of a crystal with a spatial variation in the density because of a sound wave with the frequency f_{AOM} (generated by an oscillating piezo) propagating through the crystal. The density variations generate a diffraction pattern with the lattice parameter $d = c/(2f_{\mathrm{AOM}})$ where c is the speed of the sound wave propagating in the AOM. If the piezo is switched on by applying a RF pulse after a short time (~ 0.5 µs – this is the time the sound wave needs to propagate to the interaction region with the light) a diffraction pattern of the incoming light beam is generated behind the AOM.
If now all light except the first order of the diffraction pattern is blocked with an iris we can switch on and off this beam. Further the frequency of the first diffraction pattern of this beam is shifted by the frequency of the travelling sound wave (f_{AOM}) to $f = f_0 \pm f_{\mathrm{AOM}}$ according to a deflection of the incoming light beam in the direction of the sound wave or against it.
To switch the AOM fast it is placed in the focus of a symmetric telescope. A small waist leads to a fast switching time. Due to this the diffracted beam is redirected parallel after the second lens to the incoming beam. If a $\lambda/4$ plate is placed in this beam and the beam is reflected by a mirror in itself it passes a second time through the same AOM and the frequency is therefore shifted to $f = f_0 \pm 2f_{\mathrm{AOM}}$. And because the incoming, for example horizontal polarized, beam passes two times the $\lambda/4$ plate the polarization gets vertical and can be splitted off the incoming beam by a polarizing beam splitter. At this point we have an AOM in double pass

configuration. The great advantage of a double pass AOM is the independency of the diffraction angle on the modulation frequency of the AOM because this angle is balanced exactly by the second pass.

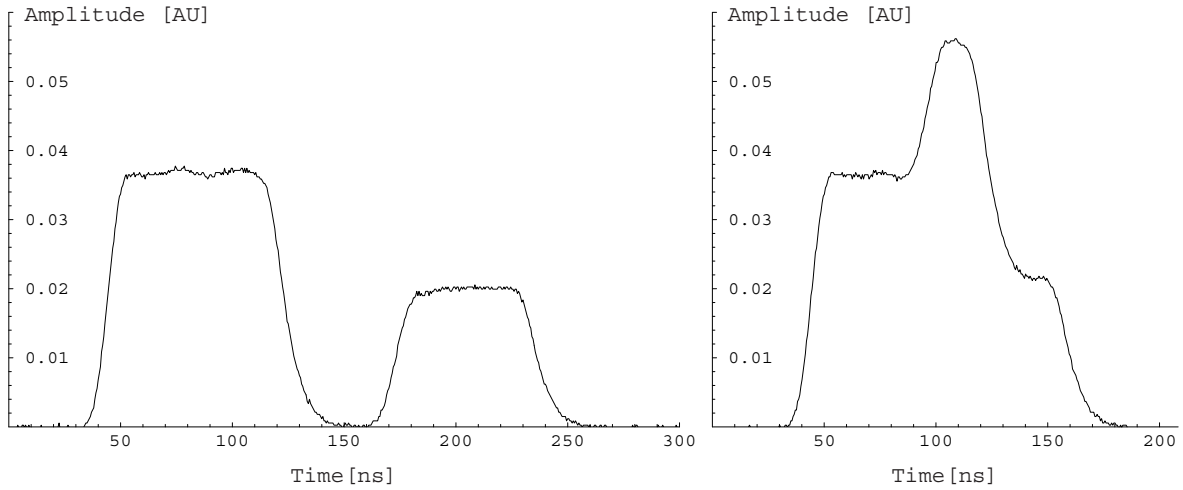

Figure D.2: The optical signal of two pulses created with AOMs, overlapped by a beam splitter, and optimized for fast raising and trailing. In the first plot they are separated in time and in second plot the second pulse is partially overlapping in time with the first one. The raising time for a single pulse is about 10 ns and the trailing time about 20 ns

D.2 Electro-optical Modulator (EOM)

The π-pulse to excite the population of the atom into the initial state before the decay has to be finished in a time of about 5 ns. This can't be done by an AOM (this can be seen in Fig. D.2) so we need a faster switching device.
One possibility is to use the linear electro-optic effect (the so-called Pockels effect) where a birefringence is induced in an optical medium due to an external electric field. Polar materials (e.g. ferroelectrical crystals) are showing the linear electro-optic effect.

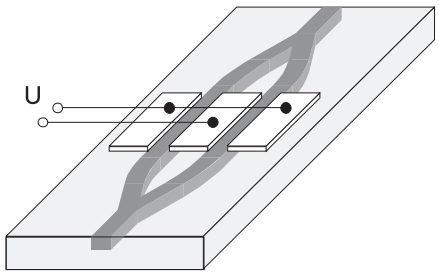

Figure D.3: Scheme of the integrated Mach-Zender amplitude modulator [65]

This Pockels effect can be used to change the phase of light passing the optical material in dependence of the applied electrical voltage. So to realize a modulator for the intensity of the light this electro-optical phase modulator is integrated into both arm of an integrated Mach-Zender interferometer (MZI). By changing the applied voltage on the modulators the relative

phase of the light in both arms can be changed leading to a change in the interference at the output of the device. The use of two phase modulators reduces the temperature dependence of the device. The small dimensions of the integrated MZI allows the use of relative small switching voltages of about 5 V.
Such an integrated modulator was characterized with light at 780 nm. First a measurement of the bandwidth of the modulator in the HF region was made with a fast photo diode (bandwidth 1.4 GHz) between 10 and 1000 MHz. The 3dB point is at about 800 MHz.

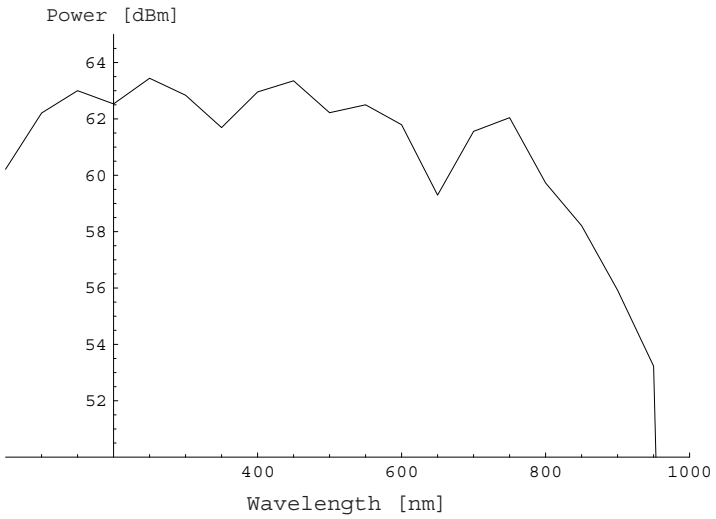

Figure D.4: Frequency response of the EOM after subtraction of the background of the photo diode

The smallest raising time possible with this device is about 1.2 ns. This corresponds very well with the measured frequency of the 3dB point of the MZI. Therefore this integrated electro-optical modulator is fast enough to switch the light of the π-pulse.

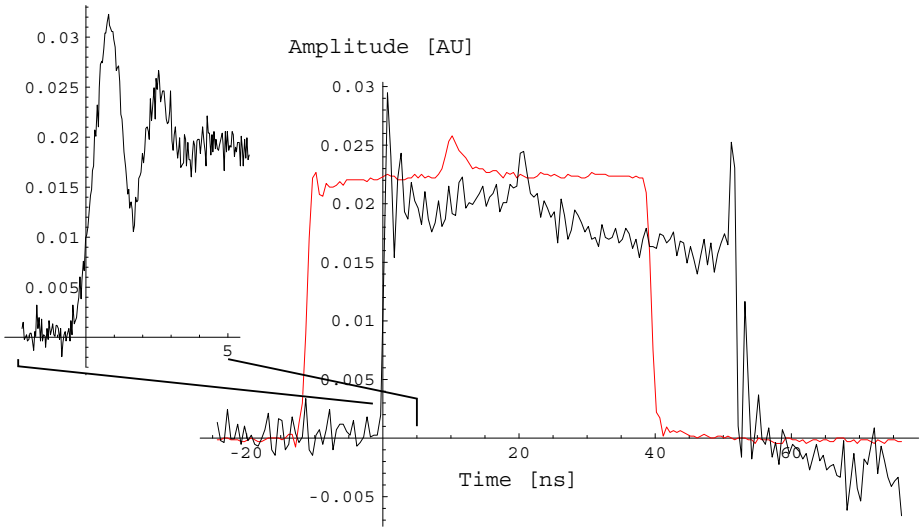

Figure D.5: Optical signal of the AOM (and a section enlargement of the raising edge) driven by an electrical signal (red)

E Pictures of the Experimental Setup

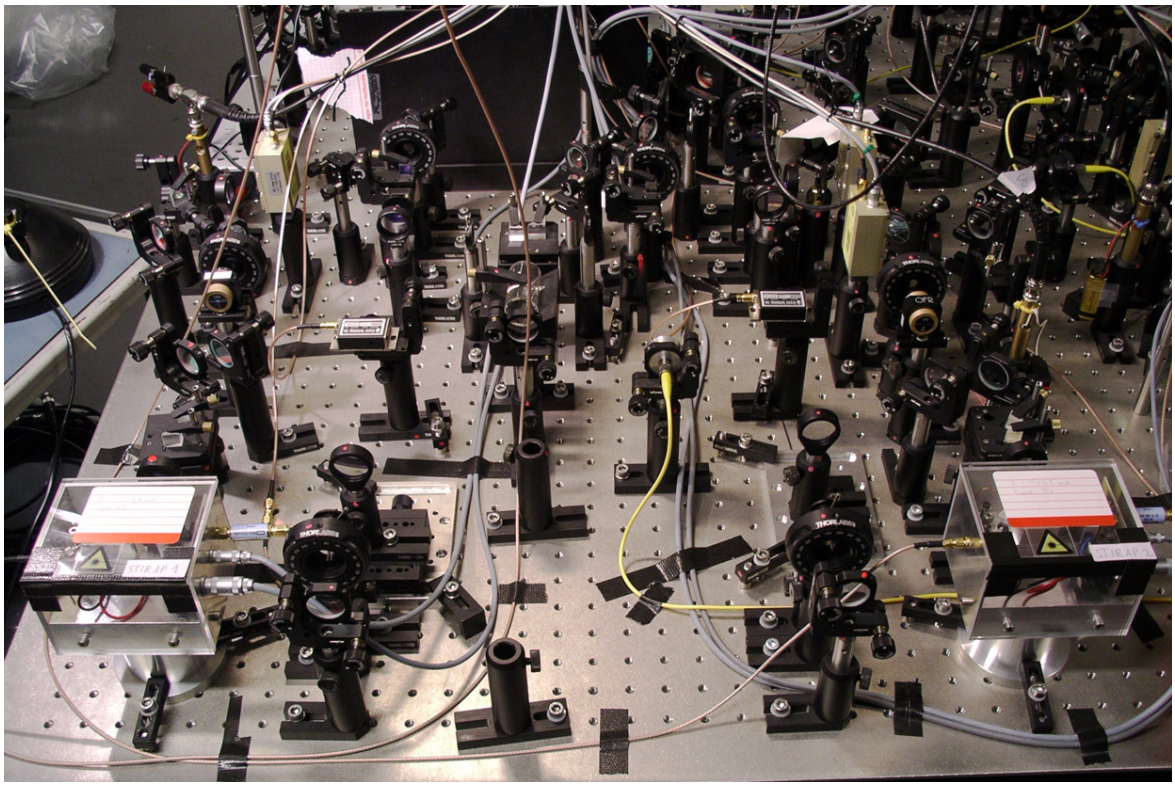

Figure E.1: A picture of the STIRAP laser setup

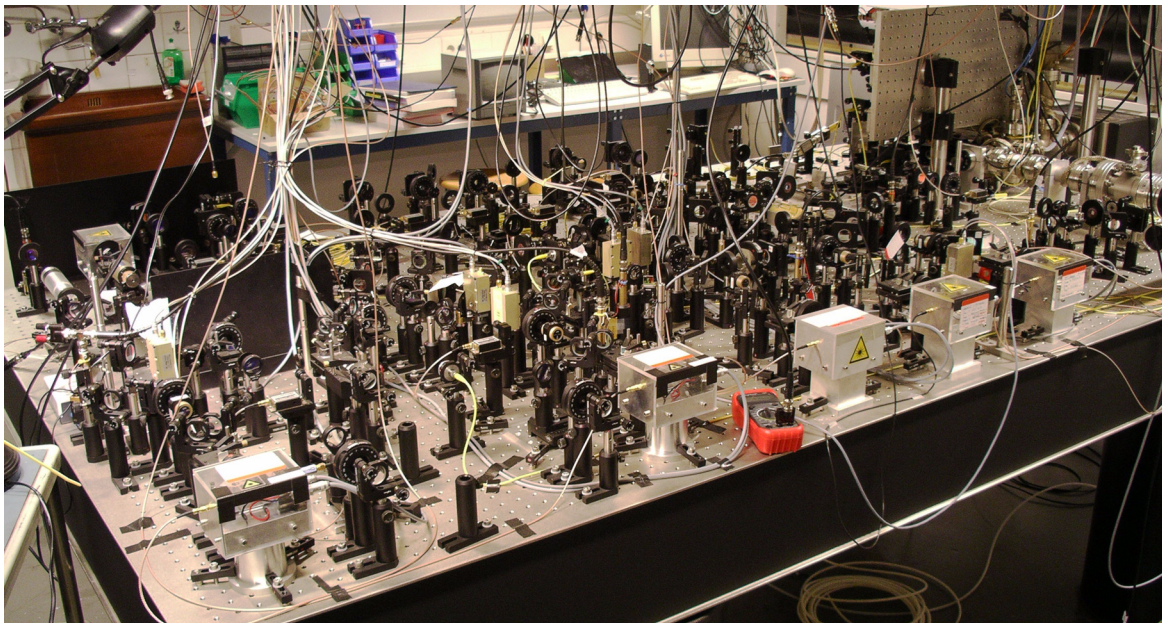

Figure E.2: A picture of the entire experimental setup including the dipole trap laser in the upper left corner, the two STIRAP lasers in the lower left corner, the three D_2 line lasers and the AOMs in the middle and last but not least the vacuum chamber on the right

F Laser Frequencies (Before (red) and After (blue) AOM)

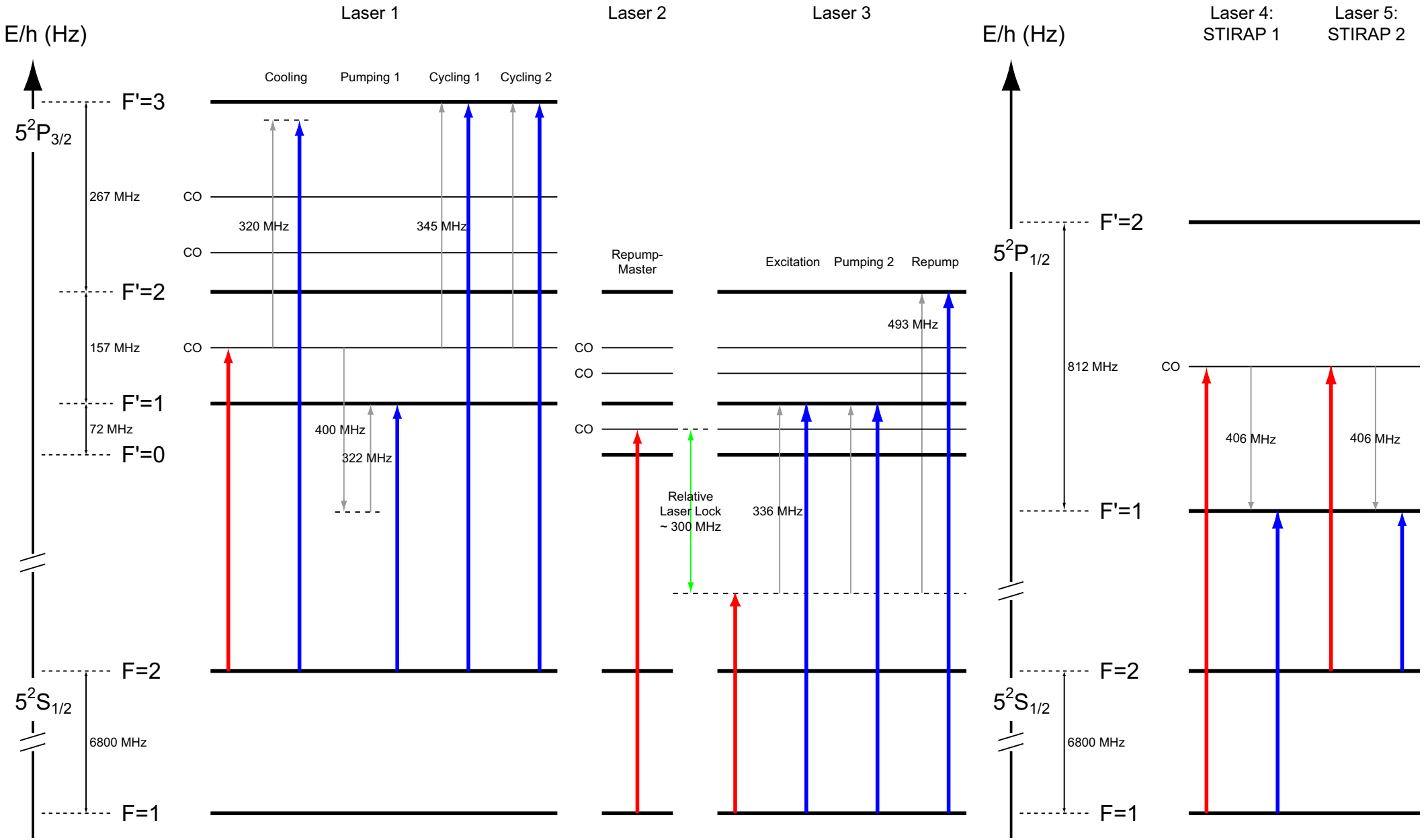

Bibliography

[1] A. Einstein, B. Podolsky, N. Rosen: *Can Quantum-Mechanical Description of Physical Reality be Considered Complete.* Phys. Rev. **47**, 777 (1935)

[2] N. Bohr: *Can Quantum-Mechanical Description of Physical Reality be Considered Complete.* Phys. Rev. **48**, 696 (1935)

[3] E. Schrödinger: *Die gegenwärtige Situation in der Quantenmechanik.* Die Naturwissenschaften **23**, 807-812, 823-828, 844-849 (1935)

[4] D. Bohm: *The Paradox of Einstein, Rosen, and Podolsky.* Quanum Theory. New York: Prentice-Hall, 611-623 (1951)

[5] D. Bohm: *Suggested Interpretation of the Quantum Theory in Terms of "Hidden" Variables*. Phys.Rev. **85**, 166 and 180 (1952)

[6] J.S. Bell: *On the problem of hidden variables in quantum mechanics*. Rev. Mod. Phys. **38**, 447 (1966), Reprint in: *Speakable and Unspeakable in Quantum Mechanics.* Cambridge: Cambridge University Press, 1 (1987)

[7] J.S. Bell: *On the Einstein-Podolsky-Rosen Paradox.* Physics **1**, 195 (1964), Reprint in: *Speakable and Unspeakable in Quantum Mechanics.* Cambridge: Cambridge University Press, 14 (1987)

[8] J.F. Clauser, M.A. Horne, A. Shimony, R A. Holt: *Proposed Experiment to Test Local Hiden-Variable Theories*. Phys. Rev. Lett. **23**, 880 (1969)

[9] S.J. Freedman, J.F. Clauser: *Experimental Test of Local Hidden-Variable Theories.* Phys. Rev. Lett. **28**, 938 (1972)

[10] A. Aspect, P. Grangier, G. Roger: *Experimental Realization of Einstein-Podolsky-Rosen-Bohm Gedankenexperiment: A New Violation of Bell's Inequalities.* Phys. Rev. Lett. **49**, 91 (1982)

[11] A. Aspect, J. Dalibard, G. Roger: *Experimental Test of Bell's Inequalities Using Time Varying Analyzers.* Phys. Rev. Lett. **49**, 1804 (1982)

[12] P.G. Kwiat, K. Mattle, H. Weinfurter, A. Zeilinger, A.V. Sergienko, Y. Shih: *New High-Intensity Source of Polarization-Entangled Photon Pairs.* Phys. Rev. Lett. **75**, 4337 (1995)

[13] G. Weihs, T. Jennewein, C. Simon, H. Weinfurter, A. Zeilinger: *Violation of Bell's Inequality under strict Einstein Locality Conditions.* Phys. Rev. Lett. **81**, 5039 (1998)

[14] M.A. Rowe, D. Kielpinski, V. Meyer, C.A. Sackett, W.M. Itano, C. Monroe & D.J. Wineland: *Experimental violation of a Bell's inequality with efficient detection.* Nature **409**, 791 (2001)

[15] R. P. Feynman: *Simulating Physics with Computers*. Int. J. Theo. Phys. **21**, 467 (1982)

[16] P. Benioff: *Quantum Mechanical Models of Turing Machines That Dissipate No Energy.* Phys. Rev. Lett. **48**, 1581 (1982)

[17] M.A. Nielsen, I.L. Chuang: *Quantum Computation and Quantum Information.* Cambridge: Cambridge University Press (2000)

[18] T. Sleator, H. Weinfurter: *Realizable Quantum Logic Gates.* Phys. Rev. Lett. **74**, 4087 (1995)

[19] J.I. Cirac, P. Zoller: *Quantum Communication with Cold Trapped Ions.* Phys. Rev. Lett. **74**, 4091 (1995)

[20] T.W. Hänsch, A.L. Schawlow: *Cooling of Gases by Laser Radiation*. Opt. Comm. **13**, 68 (1975)

[21] S. Chu, L. Hollberg, J.E. Bjorkholm, A. Cable, A. Ashkin: *Three-dimensional viscous confinement and cooling of atoms by resonance radiation pressure.* Phys. Rev Lett. **55**, 48 (1985)

[22] J. Dalibard, C. Cohen-Tannoudji: *Laser cooling below the Doppler limit by polarization gradients: simple theoretical models.* J. Opt. Soc. Am. B **6**, 2023 (1989)

[23] C. Salomon, J. Dalibard, W.D. Philips, A. Clairon, S. Guellati: *Laser Cooling of Cesium Atoms Below 3 μK.* Europhys. Lett. **21**, 683 (1990)

[24] K. Saucke: *Optische Dipolfalle für Einzelatome.* Dipomarbeit, LMU München (2002)

[25] J. Volz & M. Weber, K. Saucke, Ch. Kurtsiefer, H. Weinfurter. To be published

[26] J. Volz. Private Communication

[27] M. Weber. Private Communication

[28] C. Cohen-Tannoudji, B. Diu, F. Laloe: *Quantenmechanik.* Berlin: Walter de Gruyter (1999)

[29] F. Schwabl: *Quantenmechanik.* Berlin: Springer-Verlag (1998)

[30] G.M. Kalvius: *Physik IV.* München: Oldenburg Wissenschaftsverlag (1999)

[31] H.J. Metcalf, P. van der Straten: *Laser Cooling and Trapping.* New York: Springer-Verlag (1999)

[32] C.S. Adams, E. Riis: *Laser cooling and trapping of neutral atoms*. Prog. Quant. Electr. **21**, 1 (1997)

[33] R. Grimm, M. Weidemüller, Y.B. Ovchinnikov: *Optical Dipole Traps for Neutral Atoms.* Adv. At. Mol. Opt. Phys., arXiv: physics/9902072 (2000)

[34] D. Frese, B. Ueberholz, S. Kuhr, W. Alt, D. Schrader, V. Gomer, D. Meschede: *Single Atoms in an Optical Dipole Trap: Towards a Deterministic Source of Cold Atoms.* Phys. Rev. Lett. **85**, 3777 (2000)

[35] N. Schlosser, G. Reymond, I. Protsenko, P. Grangier: *Sub-poissonian loading of single atoms in a microscopic dipole trap.* Nature **411**, 1024 (2001)

[36] N. Schlosser, G. Reymond, P. Grangier: *Collisional Blockade in Microscopic Optical Dipole Traps*. Phys. Rav. Lett. **78**, 3005 (2002)

[37] V. Gomer, B. Ueberholz, S. Knappe, F. Strauch, D. Frese, D. Meschede: *Decoding the dynamics of a single trapped atom from photon correlations.* Appl. Phys. B **67**, 689 (1998)

[38] R.A. Cline, J.D. Miller, M.R. Matthews, D.J. Heinzen: *Spin relaxation of optically trapped atoms by light scattering.* Opt. Lett. **19**, 207 (1994)

[39] S. Reynaud: *Resonance fluorescence: the dressed atom approach.* Ann. Phys. (France) **8**, 315 (1983)

[40] B.R. Mollow: *Power Spectrum of Light Scattered by Two-Level Systems.* Phys. Rev. **188**, 1969 (1969)

[41] J. Volz: *Kompakte Festkörperlichtquelle für verschränkte Photonen.* Dipomarbeit, LMU München (2000)

[42] C.C. Davis: *Lasers and Electro-Optics.* Cambridge: University Press (1996)

[43] A. Messiah: *Quantenmechanik.* Berlin: Walter de Gruyter (1962)

[44] J.R. Kuklinski, U. Gaubatz, F.T. Hioe, K. Bergmann: *Adiabatic population transfer in a three-level system driven by delayed laser pulses.* Phys. Rev. A **40**, 6741 (1989)

[45] U. Gaubatz, P. Rudecki, S. Schiemann, *K. Bergmann: Population transfer between molecular vibrational levels by stimulated Raman scattering with partially overlapping laser-fields. A new concept and experimental results.* J. Chem. Phys. **92**, 5363 (1990)

[46] T.A. Laine, S. Stengholm: *Adiabatic processes in three-level systems.* Phys. Rev. A **53**, 2501 (1996)

[47] N.V. Vitanov, S. Stengholm: *Population transfer via a decaying state.* Phys. Rev. A **56**, 1463 (1997)

[48] D.A. Steck: *Rubidium 87 D Line Data.* LA-UR-03-8638 (2001)

[49] D.A. Steck: *Sodium D Line Data.* LA-UR-03-8639 (2000)

[50] D.A. Steck: *Cesium D Line Data.* LA-UR-03-7943 (2000)

[51] I. Bergström, C. Carlberg, R. Schuch, eds: *Trapped charged particles and fundamental applications*. Singapore: World Scientific (1995)

[52] P.K. Ghosh: *Ion Traps.* Oxford: Clarendon Press (1995)

[53] D. Prichard, E. Raab, V. Bagnato, C. Wieman, N. Watts: *Light traps using Spontaneous Forces*. Phys. Rev. Lett. **57**, 310 (1986)

[54] E.L. Raab, M. Prentiss, A. Cable, S. Chu, D.E. Pritchard: *Trapping of neutral sodium atoms with radiation pressure*. Phys. Rev. Lett. **59**, 2632 (1987)

[55] A. Migdall, J. Prodan, W. Phillips, T. Bergeman, H. Metcalf: *Observation of Magnetically Trapped Neutral Atoms.* Phys. Rev. Lett. **54**, 2596 (1985)

[56] T. Bergeman, G. Erez, H.J. Metcalf: *Magnetostatic Trapping Fields of Neutral Atoms.* Phys. Rev. A **35**, 1535 (1987)

[57] S. Chu, J.E. Bjorkholm, A. Ashkin, A. Cable: *Experimental Observation of Optically Trapped Atoms*. Phys. Rev. Lett. **57**, 314 (1986)

[58] G.A. Askar'yan: *Effects of the gradient of a strong electromagnetic beam on electrons and atoms*. Sov. Phys. JETP **15**, 1088 (1962)

[59] T. Walker, P. Feng, D. Hoffmann, R.S. Williamson: *Spin-polarized spontaneous-force atom trop.* Phys. Rev. Lett. **58**, 2168 (1992)

[60] M. Greiner: *Magnetischer Transfer von Atomen: Ein Weg zur einfachen Bose-Einstein-Kondensation.* Dipomarbeit, LMU München (2000)

[61] L. Ricci, M. Weidemüller, T. Esslinger, A. Hemmerich, C. Zimmermann, V. Vuletic, W. König and T.W. Hänsch: *A compact grating-stabilized diode laser system for atomic physics.* Opt. Com. **117**, 541 (1995)

[62] U. Schünemann, H. Engler, R. Grimm, M. Weidemüller, M. Zielonkowski: *Simple scheme for tunable frequency offset locking of two lasers.* Rev. Sci. Instrum., **70**, 242 (1999)

[63] *FM Spectroscopy With Tunable Diode Lasers.* New Focus, Inc. (2001)

[64] *Acousto-Optic: application note – modulator model 3000 series.* Crystal Technology, Inc. (1999)

[65] *Integrierte optische modulatoren.* LINOS Photonics (2003)
http://www.linos-katalog.de/pdf/de-08/h08-d-09.PDF

[66] P. Zarda: *Quantenkryptographie*. Diplomarbeit, Universität Innsbruck (1999)

Danksagung

Zum Schluß dieser Diplomarbeit ein paar Dankesworte an alle die zum Gelingen dieser Arbeit beigetragen haben.

Als erstes möchte ich mich bei Martin S. Brandt und Professor Harald Weinfurter bedanken, daß sie mir als TUler diese Arbeit an der LMU ermöglicht haben und mir immer mit Rat zur Seite gestanden haben.

Desweiteren gilt mein besonderer Dank meinen beiden Doktoranden – Jürgen Volz & Markus Weber – für die vielen interessanten Diskussionen, für ihre Hilfe und dass sie mir die Freiheit gelassen haben selbständig zu arbeiten. Und was hätten wir alle ohne Jürgen's Hunger auf Kuchen und seine geniale Überzeugungsgabe für das Kuchenspendieren gemacht.

Vielen Dank an Professor Christian Kurtsiefer für Rat und Unterstützung (insbesondere bei allen Elektronikproblemen) und an Dr. Mohamed Bourennane für die tolle Empfehlung, meine Diplomarbeit an diesem Experiment durchzuführen.

Nicht vergessen darf ich natürlich meinen Nachfolger Daniel Schlenk und meine Vorgängerin Karen Saucke für die tolle Zusammenarbeit an unserem Experiment.

Vielen Dank an Oliver Schulz für seine Hilfsbereitschaft und für viele interessante Gespräche. Viel Glück für die Zukunft und wenn Videorecorder und Salzpyramide einmal vollendet sind musst du sie mir unbedingt zeigen.

Natürlich auch vielen Dank an den Rest der Arbeitsgruppe für die angenehme Atmosphäre: Gerhard Huber, Johannes Schachaneder, Tobias Schmitt-Manderbach, Carsten Schuck, Chunlang Wang, Henning Weier, Patrick Zarda – und an unsere Garchinger – Manfred Eibl, Sascha Gaertner, Nikolai Kiesel, Julia Lau, Christian Schmid und Pavel Trojek. Und auch an die anderen Leute vom Lehrstuhl Hänsch – vielen Dank.

Ausserdem noch vielen Dank an Sabine Seitz und Daniel Dolinsky, dass sie sich ein bisschen um das Englisch in dieser Arbeit gekümmert haben.

Zum Schluß noch vielen Dank an meine Eltern und Freunde, dass sie mir immer zur Seite gestanden und mich aufgebaut haben.